

**IZMIR KATIP CELEBI UNIVERSITY  
GRADUATE SCHOOL OF NATURAL AND APPLIED SCIENCES**

**INVESTIGATION OF THE COOLING SYSTEM EFFICIENCY IN  
ALUMINUM LOW PRESSURE DIE CASTING**

**M.Sc. THESIS**

**Hakan YAVUZ**

**Department of Material Science and Engineering**

**MAY 2019**



**IZMIR KATIP CELEBI UNIVERSITY**  
**GRADUATE SCHOOL OF NATURAL AND APPLIED SCIENCES**

**INVESTIGATION OF THE COOLING SYSTEM EFFICIENCY IN**  
**ALUMINUM LOW PRESSURE DIE CASTING**

**M.Sc. THESIS**

**Hakan YAVUZ**  
**Y160219002**

**Department of Material Science and Engineering**

**Thesis Advisor: Asst. Prof. Dr. Onur ERTUĞRUL**

**MAY 2019**



**İZMİR KATİP ÇELEBİ ÜNİVERSİTESİ**  
**FEN BİLİMLERİ ENSTİTÜSÜ**

**ALUMİNYUM ALÇAK BASINÇLI DÖKÜMDE KULLANILAN SOĞUTMA**  
**SİSTEMİNİN VERİMİNİN ARAŞTIRILMASI**

**YÜKSEK LİSANS TEZİ**

**Hakan YAVUZ**  
**Y160219002**

**Malzeme Bilimi ve Mühendisliği Ana Bilim Dalı**

**Tez Danışmanı: Dr. Öğr. Üyesi Onur ERTUĞRUL**

**MAYIS 2019**



**Hakan YAVUZ**, a M.Sc. student of **IKCU Graduate School Of Natural And Applied Sciences**, successfully defended the thesis entitled “**Investigation Of The Cooling System Efficiency In Aluminum Low Pressure Die Casting**”, which he prepared after fulfilling the requirements specified in the associated legislations, before the jury whose signatures are below.

**Thesis Advisor :**

**Asst. Prof. Dr. Onur ERTUĞRUL**  
İzmir Katip Çelebi University

**Jury Members :**

**Assoc. Prof. Dr. Osman ÇULHA** .....  
Manisa Celal Bayar University

**Asst. Prof. Dr. Ziya Haktan KARADENİZ** .....  
İzmir Katip Çelebi University

**Date of Submission : 29.04.2019**  
**Date of Defense : 23.05.2019**



*To my family,*



## **FOREWORD**

First and foremost, I would like to thank my advisor, Dr. Onur Ertuğrul, for his valuable helps, especially for sharing his experiences in preparing the thesis.

Next, I would like to thank to Mr. Eren Bozkurt who made the experimental study with great care and be a good friend. I would also thank to Mr Erhan Akıncı and Emre Çubuklusu, who are the managers of the CMS R&D Departments and supported us in everything.

Next, I would like to thanks my manager Mr. Samim Özer, who is the manager of the engineering department, for his understanding and support.

And of course, great thanks for my family, my parents Mesrur and Saime Yavuz, my wife Mine Yavuz and my sons Emir and Can Yavuz, for their love.

May 2019

Hakan YAVUZ



## TABLE OF CONTENTS

	<u>Page</u>
<b>FOREWORD</b> .....	<b>vii</b>
<b>TABLE OF CONTENTS</b> .....	<b>ix</b>
<b>ABBREVIATIONS</b> .....	<b>xi</b>
<b>LIST OF TABLES</b> .....	<b>xiii</b>
<b>LIST OF FIGURES</b> .....	<b>xv</b>
<b>ABSTRACT</b> .....	<b>xix</b>
<b>ÖZET</b> .....	<b>xxi</b>
<b>1. INTRODUCTION</b> .....	<b>1</b>
1.1 Aim and Objective of the Thesis .....	1
1.2 Theoretical Background .....	2
1.2.1 Aluminum casting methods .....	2
1.2.1.1 Gravity casting .....	2
1.2.1.2 Horizontal transfer casting .....	4
1.2.1.3 Counter-gravity casting .....	7
1.2.1.4 Centrifugal casting .....	8
1.2.1.5 Pressure-assisted casting .....	8
1.2.1.6 Investment casting .....	9
1.2.2 Low pressure die casting (LPDC) process for automotive industry .....	10
1.2.2.1 Melt preparation .....	11
1.2.2.2 Solidification sequence and cooling channels .....	12
1.2.3 Compressible flow and numerical approaches .....	20
1.2.3.1 Compressibility and compressible flow .....	20
1.2.3.2 Numerical models for compressible internal flow .....	22
1.2.4 Effect of cooling system on material properties and microstructure .....	26
<b>2. EXPERIMENTAL PROCEDURE</b> .....	<b>31</b>
2.1 Experimental Study For Verification .....	31
2.1.1 The experimental setup .....	31
2.1.2 Pressure tests .....	33
2.2 Numerical Study For Verification .....	35
2.2.1 The geometric setup .....	35
2.2.2 Mesh generation .....	37
2.2.3 Setup .....	38
2.2.4 Solver .....	40
2.2.5 Results .....	41
<b>3. RESULTS AND DISCUSSION</b> .....	<b>44</b>
3.1 CFD Study For Cooling Efficiency .....	44
3.1.1 Setup .....	44
3.1.2 Solver .....	45
3.1.3 Flow rates and pressure distributions .....	47
3.2 Casting Simulation Study for the Effect of Cooling System .....	54

3.2.1 Setup .....	56
3.2.1.1 The Geometric Setup.....	56
3.2.1.2 Definition.....	58
3.2.1.3 Optimization .....	60
3.2.2 Results and dicussion .....	60
<b>4. CONCLUSION.....</b>	<b>68</b>
<b>REFERENCES.....</b>	<b>71</b>
<b>CURRICULUM VITAE .....</b>	<b>75</b>

## **ABBREVIATIONS**

<b>CFD</b>	: Computational Fluid Dynamics
<b>LPDC</b>	: Low Pressure Die Casting
<b>RSM</b>	: Reynold Stress Model
<b>SST</b>	: Shear Stress Transport
<b>RMS</b>	: Root Mean Square
<b>DAS</b>	: Dendrite Arm Spacing
<b>SDAS</b>	: Secondary Dendrite Arm Spacing
<b>UTS</b>	: Ultimate Tensile Strenght
<b>HTC</b>	: Heat Transfer Coefficient



## LIST OF TABLES

	<b><u>Page</u></b>
<b>Table 1.1</b> : Alloy composition of typical A356 aluminium alloy [8].....	11
<b>Table 3.1</b> : Design table for numerical experiments. ....	45
<b>Table 3.2</b> : Design table of experimental study for cooling effect on material and mechanical properties.....	56
<b>Table 3.3</b> : Material definitions. ....	58
<b>Table 3.4</b> : Heat transfer coefficients for cooling channel designs. ....	59
<b>Table 3.5</b> : Ranking list according to optimization results.....	60



## LIST OF FIGURES

	<u>Page</u>
<b>Figure 1.3</b> : Level pour method [5].	5
<b>Figure 1.4</b> : Controlled tilt casting [5].	5
<b>Figure 1.5</b> : Roll-over as a casting process [5].	6
<b>Figure 1.6</b> : Roll-over after casting (inversion casting) [5].	6
<b>Figure 1.7</b> : Counter-gravity castings by (a) Conventional low-pressure casting machined using a sealed pressure vessel; (b) Electromagnetic pump in an open furnace [5].	7
<b>Figure 1.8</b> : Vacuum delivery systems to the shot sleeves of pressure die-casting machines (a) horizontal cold chamber [5].	8
<b>Figure 1.9</b> : Squeeze casting [5].	9
<b>Figure 1.10</b> : Investment casting [6].	10
<b>Figure 1.11</b> : Low pressure casting setup [8].	11
<b>Figure 1.12</b> : Directional solidification [8].	12
<b>Figure 1.13</b> : Illustration of ideal unidirectional solidification in a simple shaped casting [8].	13
<b>Figure 1.14</b> : Illustration of undesired non-unidirectional solidification in a simple shaped casting [8].	14
<b>Figure 1.15</b> : Heat transfer between mold and casting metal.	15
<b>Figure 1.16</b> : LPDC process cooling channels.	16
<b>Figure 1.17</b> : Simple compressed air preparation system [16].	17
<b>Figure 1.18</b> : The efficiency of the different cooling types [18].	17
<b>Figure 1.19</b> : Illustration of the nozzle cooling system [19].	18
<b>Figure 1.20</b> : Surface impingement of a single round or slot gas jet [20].	19
<b>Figure 1.21</b> : Average surface heat flux for different flow rates [21].	20
<b>Figure 1.22</b> : Control volume and the flow illustration [23].	21
<b>Figure 1.23</b> : Piping system pressure definitions.	22
<b>Figure 1.24</b> : The comparison of the turbulence models on pressure change along ejector a) SST b) k- $\epsilon$ c) RSM [25].	23
<b>Figure 1.25</b> : The comparison of the turbulence models on pressure change along ejector a) SST b) k- $\epsilon$ c) RSM [26].	24
<b>Figure 1.26</b> : The comparison of the turbulence models on pressure change along ejector [28].	24
<b>Figure 1.27</b> : Secondary dendrite arm spacing as a function of cooling rate for A356 alloy [37].	27
<b>Figure 1.28</b> : Variation of yield stress (a), ultimate tensile strength (b), maximum force (c) and elongation percentage (d) with secondary dendrite arm spacing [37].	27
<b>Figure 1.29</b> : Variation of yield stress (a), ultimate tensile strength (b), Fmax (c) and elongation percentage (d) with cooling rate [37].	28
<b>Figure 1.30</b> : Relationship between DAS and cooling rate[38].	28

<b>Figure 1.31</b> : Effect of DAS on ultimate tensile strength (UTS) [38].	29
<b>Figure 1.32</b> : Effect of cooling rate and solidification time on SDAS [39].	29
<b>Figure 1.33</b> : Optical microstructures of sample 1 (a), sample 2 (b), sample 3 (c), sample 4 (d), sample 5 (e) with different cooling rates [39].	30
<b>Figure 2.1</b> : The experimental setup.	31
<b>Figure 2.2</b> : Technical drawing of the manometer.	32
<b>Figure 2.3</b> : Flowmeter technical drawing	32
<b>Figure 2.4</b> : Cooling channel technical drawing.	33
<b>Figure 2.5</b> : First test pressure from the manometer (3 Bars).	33
<b>Figure 2.6</b> : First test flow result from the flowmeter (104.3 Nm <sup>3</sup> /h).	34
<b>Figure 2.7</b> : Second test pressure from the manometer (5 Bars).	34
<b>Figure 2.8</b> : Second test flow results from the flowmeter (167.1 Nm <sup>3</sup> /h).	35
<b>Figure 2.9</b> : Geometric definition a) CAD data b) selected part for simulation setup.	36
<b>Figure 2.10</b> : Simulation geometric definitions.	36
<b>Figure 2.11</b> : Mesh of the numerical study.	37
<b>Figure 2.12</b> : a)Classification of the mesh quality metrics based on skewness b)Mesh node and element count with quality properties.	38
<b>Figure 2.13</b> : Analysis type.	39
<b>Figure 2.14</b> : Simulation setup for calculations.	39
<b>Figure 2.15</b> : Solver control parameters.	40
<b>Figure 2.16</b> : RMS (root mean square) for momentum and mass.	40
<b>Figure 2.17</b> : RMS for heat transfer.	41
<b>Figure 2.18</b> : RMS for turbulence.	41
<b>Figure 2.19</b> : Cross-section control volume and variables.	42
<b>Figure 2.20</b> : Flow results at gauge pressure 3 bars.	43
<b>Figure 2.21</b> : Flow results at gauge pressure 5 bars.	43
<b>Figure 3.1</b> : Simulation geometry for numerical experiments.	44
<b>Figure 3.2</b> : RMS for momentum and mass.	46
<b>Figure 3.3</b> : RMS for heat transfer.	46
<b>Figure 3.4</b> : RMS for turbulence.	47
<b>Figure 3.5</b> : Inlet area for measurement and velocity magnitude results.	48
<b>Figure 3.6</b> : Outlet areas and velocity vector results.	48
<b>Figure 3.7</b> : Inlet flow rate results according to outlet count.	49
<b>Figure 3.8</b> : Total outlet mass flow results according to outlet count.	50
<b>Figure 3.9</b> : Average outlet mass flow results according to outlet count.	51
<b>Figure 3.10</b> : Inlet flow rate results according to inlet/outlet cross section area ratio.	51
<b>Figure 3.11</b> : Total outlet mass flow results according to inlet/outlet cross section area ratio.	52
<b>Figure 3.12</b> : Pressure distribution for double inlet 6 bar cooling system at maximum and minimum inlet flow rate.	53
<b>Figure 3.13</b> : Average outlet mass flow results according to inlet/outlet cross section area ratio.	54
<b>Figure 3.14</b> : Chill-housing assembly [40].	55
<b>Figure 3.15</b> : a) SDAS change according to distance from cooling chill b) Micro structure from 2.5 mm distance c) Micro structure from 52.5 mm distance [40].	55
<b>Figure 3.16</b> : Design locations for numerical experiments.	56
<b>Figure 3.17</b> : Casting Simulation Geometry.	57

<b>Figure 3.18 :</b> Cooling channel geometries a) 2 outlet b) 8 outlet c) 16 outlet. ....	57
<b>Figure 3.19 :</b> Thermocouple points. ....	58
<b>Figure 3.20 :</b> Temperature depent heat transfer coefficient between mold parts and casting part. ....	59
<b>Figure 3.21 :</b> Cooling channel heat transfer coefficient calculation example.....	59
<b>Figure 3.22 :</b> Thermocouple results from magmasoft.....	61
<b>Figure 3.23 :</b> Optimization design ranks on flow rate vs $A_i/A_o$ . ....	63
<b>Figure 3.24 :</b> Main effect plot for cooling rate.....	63
<b>Figure 3.25 :</b> Main effect plot for SDAS. ....	63
<b>Figure 3.26 :</b> Cooling rate results obtained by simulation software. ....	64
<b>Figure 3.27 :</b> Cooling rate vs SDAS. ....	65
<b>Figure 3.28 :</b> a) Elongation vs SDAS b) tensile strength vs SDAS c) yield strength vs SDAS. ....	65
<b>Figure 3.29 :</b> a) Cycle time vs cooling rate b) fraction of eutectic phase. ....	66
<b>Figure 3.30 :</b> a) Elongation vs cooling rate b) tensile strength vs cooling rate c) yield strength vs cooling rate. ....	66
<b>Figure 3.31 :</b> Flow rate vs cooling rate. ....	67



# **INVESTIGATION OF THE COOLING SYSTEM EFFICIENCY IN ALUMINUM LOW PRESSURE DIE CASTING**

## **ABSTRACT**

In this thesis, the flow rate of air coolers used in low pressure casting method is examined. Low pressure die casting (LPDC) method is used for many types of products. Light alloy wheels, motor housings and pistons are examples of these products. Air-cooling is used to provide directional solidification to avoid casting defects on the casting part. In this study, the flow rate of air-cooling is calculated by using computational fluid dynamics (CFD) methods. After the numerical calculations were confirmed by experimental methods, the affect of the variables on the cooling system flow rate was measured with different numerical experiments by changing the number of cooling inlets, number of cooling outlets and cooling pressure. Results showed that the pressure is the most effective variable on flow rate, Inlet and outlet counts are effective on flow rate. To reduce cycle time of casting and provide energy efficiency inlet and outlet counts must be optimized to have maximum flow rate. The effects of optimized cooling on the microstructure and material properties of the castings were investigated numerically. According to the results, it was observed that optimized cooling designs had better microstructure and material properties.



## **ALÜMİNYUM ALÇAK BASINÇLI DÖKÜM İŞLEMİNDE SOĞUTMA SİSTEMİ VERİMİNİN ARAŞTIRILMASI**

### **ÖZET**

Bu çalışmada, düşük basınçlı döküm yönteminde (ABDY) kullanılan hava soğutucularının, akış hızları incelendi. Alçak basınçlı döküm yöntemi birçok ürün tipi için kullanılır. Hafif alaşım jantlar, motor gövdeleri ve pistonlar bu ürünlere örnektir. Hava soğutma, döküm parçasındaki döküm hatalarını önlemek için, yönlü katılaşma sağlamak amacıyla kullanılır. Bu çalışmada, hava soğutmalarının akış hızı, hesaplamalı akışkanlar dinamiği (HAD) yöntemleri kullanılarak hesaplanmıştır. Sayısal hesaplamalar deneysel yöntemlerle doğrulandıktan sonra, soğutma girişlerinin sayısı, soğutma çıkışlarının sayısı ve soğutma basıncı değiştirilerek, bu değişkenlerin, soğutma sisteminin debisi üzerindeki etkileri farklı sayısal deneylerle ölçülmüştür. Sonuçlar, basıncın debi üzerinde en etkili değişken olduğunu, Giriş ve çıkış sayımlarının debi üzerinde etkili olduğunu göstermiştir. Döküm çevrim süresini azaltmak ve enerji verimliliği sağlamak için giriş ve çıkış sayıları maksimum akış hızına sahip olacak şekilde optimize edilmelidir. Optimize edilmiş soğutmaların, döküm parçaların mikroyapı ve malzeme özelliklerine etkisi numerik olarak incelenmiştir. Elde edilen sonuçlara göre optimize edilmiş soğutma tasarımlarının daha iyi mikroyapı ve malzeme özelliklerine sahip olduğu gözlemlendi.



## **1. INTRODUCTION**

### **1.1 Aim and Objective of the Thesis**

The scope of this thesis is using scientific explanation of the cooling system and numerical methods to calculate the efficiency of the cooling systems. Air and/or water cooling channels are used for LPDC process. Air cooling channels are used for LPDC process in this thesis.

Cooling channels affect many of the properties for Aluminum low pressure die casting process such as microstructure quality, mechanical properties and productability of the casting part. More efficient cooling system means higher quality casting products. In this thesis the effect of the cooling efficiency on material properties are investigated. To understand cooling system efficiency, cooling rate of the casting part and effect of cooling rate on mechanical properties (elongation, tensile and yield strength), micro structure properties (SDAS) and casting quality (fraction of the eutectic phase) are investigated.

Cooling system efficiency could change according a lot of cooling system variable such as cooling system media (air, water, and oil), Cooling system flow rate, coolant temperature and cooling system process parameters. In this thesis, cooling system flow rate investigated according to cooling system parameters that affecting cooling system flow rate, for nozzle air jet cooling system. Cooling system inlet and outlet count and cooling system pressure are accepted as a variable for investigation. The investigation is made for finding a numerical solution for optimized cooling system.

The aim of this thesis is to investigate the flow rate of the cooling systems of Low Pressure Die Casting (LPDC) Method by optimizing the inlet number, outlet number and system pressure in the jet type mold cooling pipe. Optimized results are numerically investigated in order to find best solution for casting proses cooling efficiency. To examine process efficiency for casting process, cycle time for casting process and quality of casting that correlated with variables mentioned above, with different cooling system parameters numerically investigated additionally.

## **1.2 Theoretical Background**

### **1.2.1 Aluminum casting methods**

There is the growing demand for aluminium alloys in automotive industry, because of the unique properties of aluminum such as low density, specific strength, good fatigue and corrosion resistance [1]. Aluminium casting industry has big importance for automotive producers. The low density of Aluminum is a big opportunity for weight reduction which has a big interest from the automotive industry [2]. Twenty years ago about %2 of the stock cars were made of aluminum in Europe, now this amount is over %80 [1]. For instance, a 90 kg weight reduction for automotive industry means 0.43 km/liter less fuel consumption and significant fuel efficiency improvement. According to researches, using aluminum and magnesium instead of steel can reduce the weight of the cars around %50 [2]. So, Aluminium casting industry is growing to meet this demand. There are many different casting methods for automotive industry such as high pressure die casting, low pressure die casting (LPDC), permanent mold casting and sand casting which are best known methods. The method of casting could change according to different criterias. These criterias are related to casting design, mechanical property requirements, physical property requirements, Process requirements and economics [3]. Some of these casting methods are summerized below.

Automotive manufacturers develop car parts, which must be safe, lightweight, meeting environmental laws and gaining competitiveness [4]. One of the main lightweight automotive components is wheels. Light alloy wheels reduce the vehicle weight, and the most used production method for light alloy wheels is LPDC. Light alloy aluminum wheels are more attractive than steel based wheels for automotive industry, cause of their lightness and cost [4].

#### **1.2.1.1 Gravity casting**

Today, gravity casting is the most used method for most of the foundries since this is one of the most economic casting methods. Different types of the gravity casting methods are:

- a. Gravity casting of open mold:** Some casting parts do not need back side finishing as seen in Figure 1.1 (a). In this case, casting can be done using an open mold [5].

- b. Gravity pouring of closed molds:** Generally, molds made of two parts are used in casting processes as shown in Figure 1.1 (b). Sprue starts from top and the end of the sprue is on bottom part. The bottom part (the drag) forms the base of the casting, and the top half (the cope) forms the top of the casting [5].

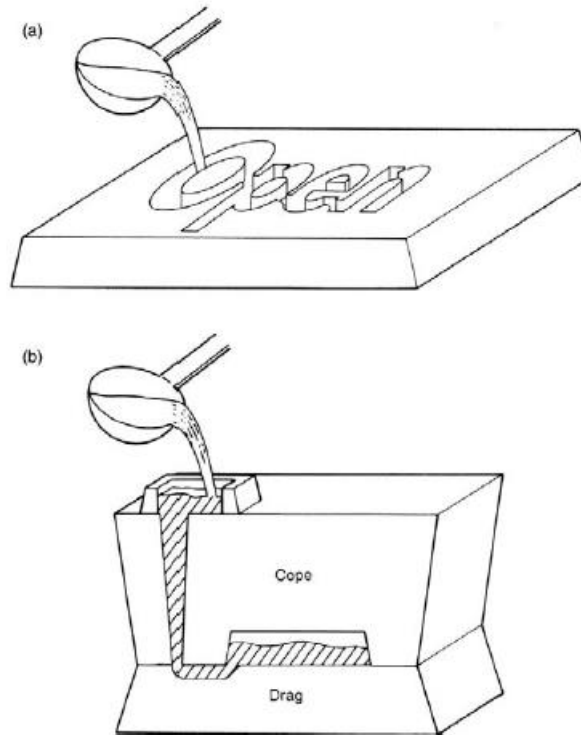


**Figure 1.1 :** (a) An open and (b) a closed mold partially sectioned [5].

- c. Two-stage filling (priming methods):** A lot of trial for two staged filling process have been made over years. For two staged filling first the sprue will be filled after that filling start with runner and gates, etc. (Figure 1.2(a)) [5].
- d. Vertical stack molding:** Molding is done with many molds placed on top of each other. Filling is done from the top (Figure 1.2(c)) [5].
- e. Horizontal stack molding (H process):** The molding is done by means of horizontal molds. The filling starts from the front and fills the casting cavity of each mold one by one (Figure 1.2(b)) [5].

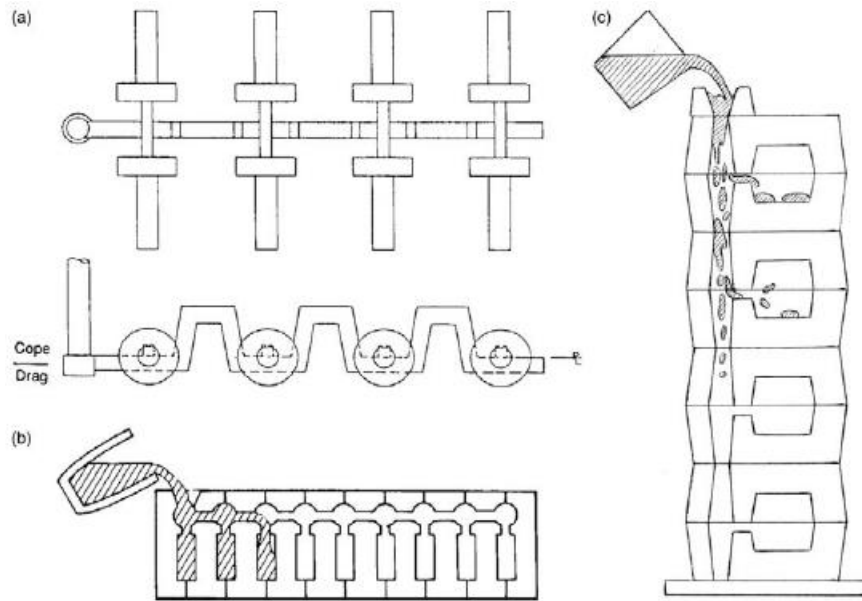


**Figure 1.2 :** (a) Sequential filling for a number of impressions on a pattern plate (b) Sequential filling for horizontal stack molded castings (H Process). (c) Vertical stack molding [5].

#### 1.2.1.2 Horizontal transfer casting

For the solution of the top filling problem, which is a big quality problem in filling of the mold, many studies have been done on horizontal and anti-gravity filling methods. Some of these studies are:

- a. Level pour (side pour):** Level pour method is found by Erik Laid in 1978. With this method high quality cast products have been produced. The working system of the mold is shown in figure 1.3. During the casting of longer parts, quality problems caused by top filling method have been tried to be prevented. In this method, there is a casting runner around the mold that is similar to the water canal and provides filling from both sides. This casting runner can move up and down. Insulation is provided in the areas where the ingates are located which prevents leakages during filling [5].

During filling, the mold is moved slowly downwards with the electric motor. In this way, filling is started from the bottom of the mold. As the filling continues, the water chillers placed under the ingates of the casting system allow the metal to solidify. In this way, while the mold continues to fill, the open slots become solidified. With this filling method, a slow and controlled filling is provided from the bottom up [5].

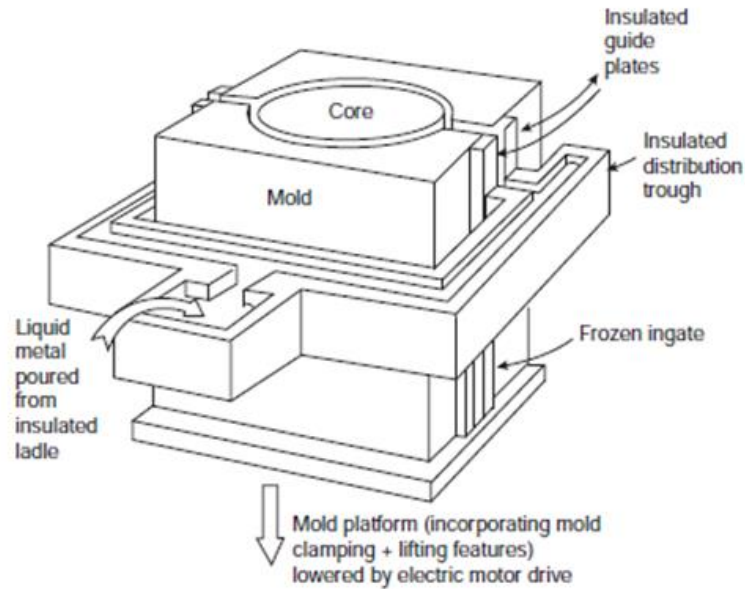


**Figure 1.3 :** Level pour method [5].

- b. Controlled tilt casting:** Controlled tilting casting method provides a more controlled filling. In this filling method, a filling basin is positioned horizontally. The mold is positioned slightly angled with respect to the filling basin (Figure 1.4). If the mold system is tilted in a controlled manner, the filling time and filling speed will be controlled. As a result, a better quality filling will be provided [5].

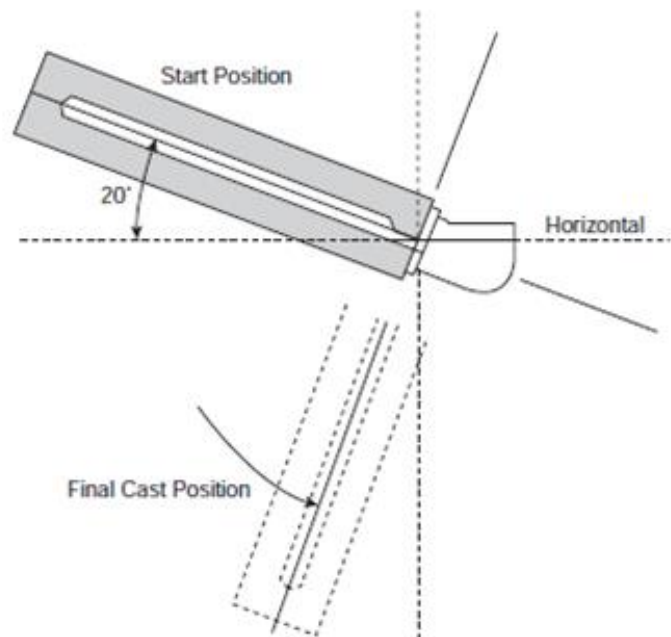


**Figure 1.4 :** Controlled tilt casting [5].

- c. **Roll-over as a casting method:** In general, it is a casting method in which the melting system works together with the mold system. The whole assembled system, during casting, rotates swiftly through  $180^\circ$ . This method is widely used in the investment casting method (Figure 1.5) [5].

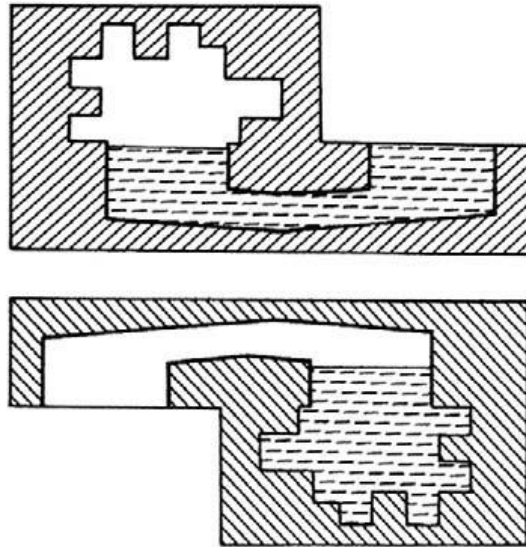


**Figure 1.5 :** Roll-over as a casting process [5].

- d. **Roll-over after casting (inversion casting):** The inversion casting method is not actually a tilting casting method. In fact, it is mostly used to help the solidification. After the normal gravity casting process, the whole assembly is rotated  $180^\circ$ . Thus providing the feeding support to the casting part when the part solidifies at a controlled temperature (Figure 1.6) [5].

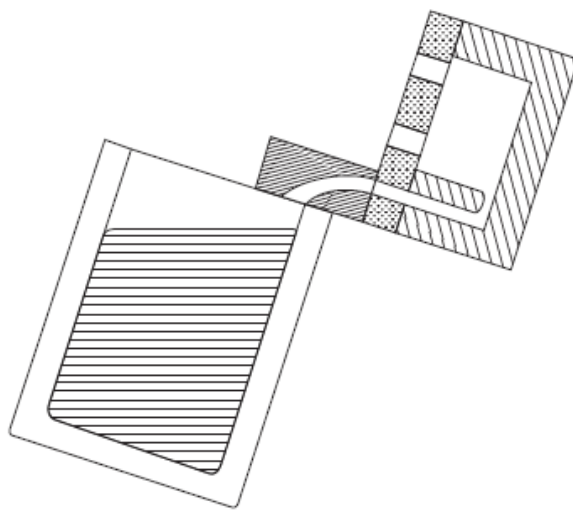


**Figure 1.6 :** Roll-over after casting (inversion casting) [5].

### 1.2.1.3 Counter-gravity casting

“Counter-gravity casting” or in other words “counter-gravity pouring” is developed for to avoid the fundamental problems of gravity casting. Controlled filling parameters let the filling process to be more stable. There are two types of counter-gravity casting [5];

- a. Low pressure die casting (LPDC):** The most widely used method is the low pressure casting method, which provides the liquid metal to rise in a riser tube by pressurizing airtight furnace with dry air or inert gas. (Figure 1.7(a)). LPDC process is popular in wheel production. At chapter 1.2.3 this process will be investigated boardly.
- b. Liquid metal pumps:** The filling method using the pump is one of the most controlled filling methods. Many types of pumps can be filled with liquid metal, and the characteristics of these pumps are evaluated with volumetric flow graphs. The idea of filling with electromagnetic liquid metal pumps is to create flow in riser tubes with magnetic forces, then filling mold cavity with that way (Figure 1.7(b)). The liquid metal pumps will let the flow control to stable filling process [5].

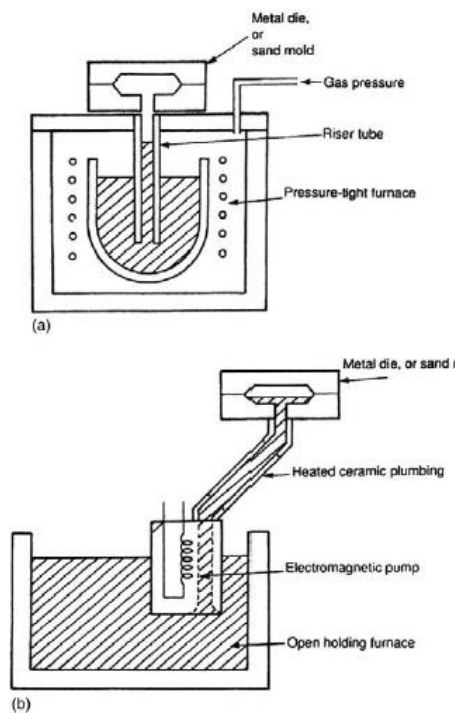


**Figure 1.7 :** Counter-gravity castings by (a) Conventional low-pressure casting machined using a sealed pressure vessel; (b) Electromagnetic pump in an open furnace [5].

#### 1.2.1.4 Centrifugal casting

Casting on a rotating centrifuge table is commonly used for alloys based on Ti and Nb. The melting furnace and rotating table are enclosed in a vacuum chamber. Molds to make shaped castings are placed around the periphery of the centrifuge, and are connected by a spider of radial runners to a central sprue. This is called as centrifuge casting [5].

#### 1.2.1.5 Pressure-assisted casting

It is known that the increase in the pressure in casting methods shortens the solidification time. This has a positive effect on mechanical properties.

The positive effect of the high pressure applied during the casting to the mechanical properties reduces the effect of casting defects caused by fast and turbulent filling on the mechanical properties of high pressure die casting (Figure 1.8). Squeeze casting and counter pressure casting methods do not have as much casting defects unlike high pressure casting. These casting methods have tolerable casting defects. In this case, better mechanical properties can be obtained by compression casting method [5].

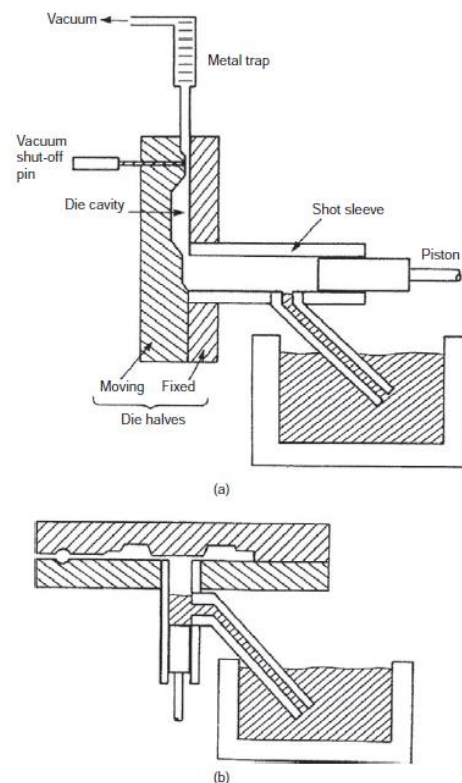


**Figure 1.8 :** Vacuum delivery systems to the shot sleeves of pressure die-casting machines (a) horizontal cold chamber [5].

There are two kinds of squeeze casting method. The squeeze casting method involves forming a semi-solid casting material with a high pressure. In this way the pores in the material can be closed. In addition, high heat transfer between the mold and the casting part, which is formed by high pressure, is ensured to develop in the mechanical properties of the casting material.

There are a lot of casting methods that have much in common with this shaping technique. Their common features are the loading of the liquid metal into the bottom half of an open die or mold, and the subsequent closing of the die or mold so as to displace the liquid into the extremities of the cavity (Figure 1.9).

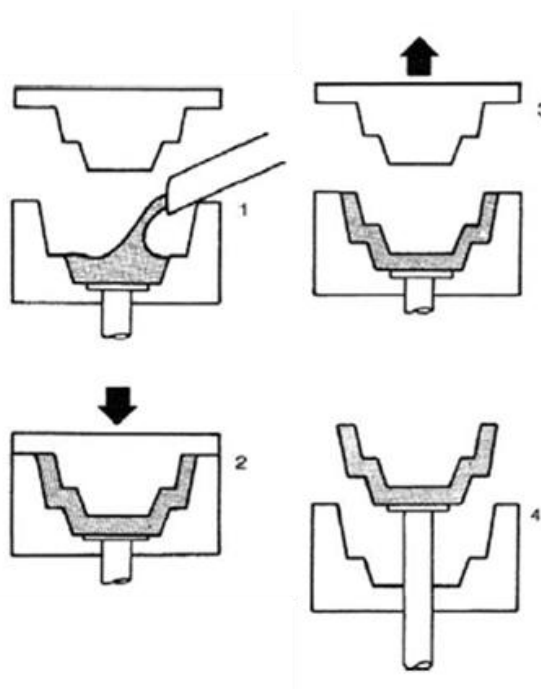


**Figure 1.9 :** Squeeze casting [5].

#### **1.2.1.6 Investment casting**

The investment casting method is mainly used in the production of special and complex parts for the aviation and biomedical sector. Filling method is not a very good method in terms of casting quality. It is one of the casting methods using ceramic mold. The models are made of wax before and this model is immersed in liquid ceramic. Once the liquid ceramic is solidified, ceramic is placed in an oven and the wax is removed by heating. The filling is made into the casting cavity formed in the ceramic (Figure 1.10) [6].

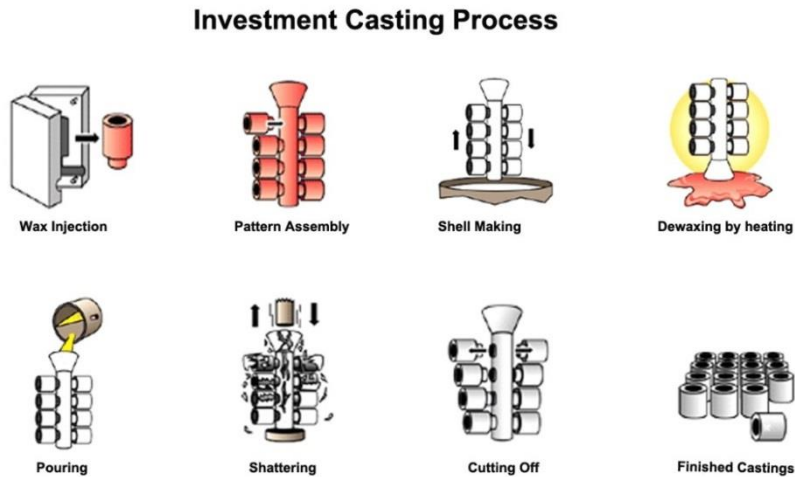


**Figure 1.10 : Investment casting [6].**

### **1.2.2 Low pressure die casting (LPDC) process for automotive industry**

LPDC is a casting process that filling sequence is applied against gravity. Mold material can be either sand or metal. Low-pressure die casting (LPDC) process is the most used production method for light alloy wheel production [7] since it helps to produce high quality parts and have low cost production. The LPDC machine has two main components; the mold, cooling system and moving parts, like pistons which are connected to mold parts to open and close mold casting cavity, are placed above the machine construction. These are molding parts of the LPDC Machine. The riser tubes, which provide liquid metal flow towards to mold, placed under the molding parts and connected to the holding furnace. The holding furnaces are the pressure vessels that are generally electrically heated.

Process starts with pressure increase in the holding furnace. Dry air or nitrogen gases are sent by pressurization system into the holding furnace. Holding furnaces are the airtight and the pressure increase according to pressurization system pressure which is set by casting operators. With increasing pressure molten metal rises in the riser tubes through mold cavity. At the end of the riser tubes, there is a casting gate which is connected to mold cavity. The molten metal comes from the casting gate through the mold cavity. The pressure increase until mold cavity completely filled with molten metal. After filling sequence completed, solidification sequence starts. With mold and cooling systems, the molten metal solidifies until the casting gate and the pressure reduce when time comes which casting operator set. Then the mold opens

and the solidified casting part is removed from the mold. Figure 1.11 shows schematic of the simple LPDC setup.

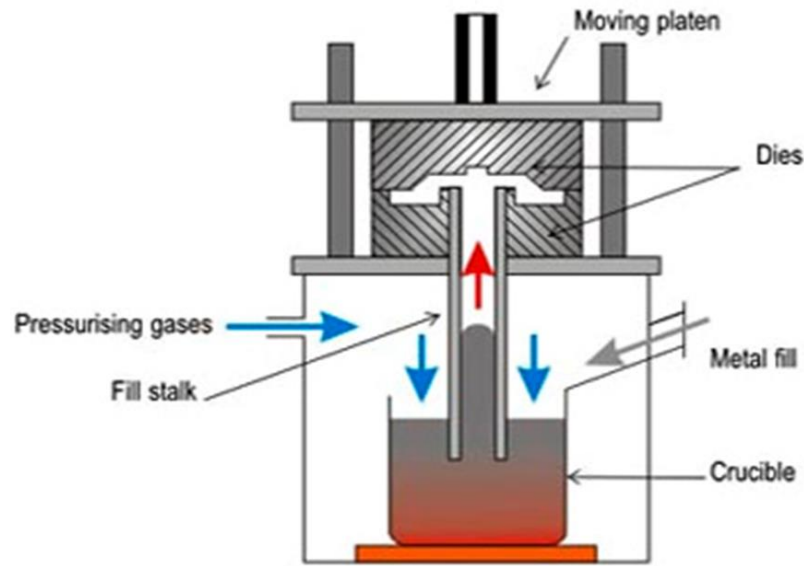


**Figure 1.11 :** Low pressure casting setup [8].

### 1.2.2.1 Melt preparation

Melt preparation is the first stage of the casting process. A356 (AlSi7Mg) is generally used aluminium alloy for light alloy casting wheels (Table 1.1).

**Table 1.1 :** Alloy composition of typical A356 aluminium alloy [8].

	Elements							
	Si	Fe	Cu	Mn	Mg	Zn	Ti	Al
Composition (%)	6.5-7.5	0.50	0.25	0.35	0.25-0.45	0.35	0.25	Balance

Aluminum ingots are melted in shaft type melting furnaces. There are two type ingots for this operation. They are the primary aluminium ingots that come from aluminium ingot production company which makes aluminium ingots from ore and secondary aluminium ingots that comes from internal sources that remelting aluminium scraps and chips. After melting process completed, liquid aluminium is poured into ladels.

Melt treatment process follow the melting process. Three treatments are needed before the casting process. They are degassing, fluxing and alloy addition. The short descriptions of these treatments are summarized below.

**Degassing** – The molten aluminum has a very high hydrogen gas solubility which can be absorbed from the humid environment in ambient air. The hydrogen gas dissolved in the aluminum alloy can then result in gas pores in the casting products. Therefore, the molten metal must be degassed [8].

**Fluxing** – "Fluxing" is a common term used in the casting process to describe the addition of chloride or fluoride-based salt. Cleaning of the metal is achieved by the addition of the flux salt which reacts with the non-metallic closures in the melt. This reaction then forms a cluster called slag, which can be separated from the melt [8].

**Alloy addition** – Three main types of aluminium master alloy [8].

**Al-Mg:** To have required mechanical properties Mg is added to A356 Aluminum alloy [8].

**Al-Sr:** Strontium is added to have fatigue strength for aluminium silicon alloy. Strontium affects eutectic structure as a modifier to have globular structure [8].

**Al-TiB:** Titanium boride is a nucleation enhancer for A356 alloy. Titanium boride added to A356 alloy to have finer microstructure. Finer microstructure causes higher mechanical properties. In addition, Titanium boride increases fluidity of aluminium silicon alloy [8].

### 1.2.2.2 Solidification sequence and cooling channels

Solidification begins after mold cavity is completely filled. In order to obtain the desired mechanical properties and the shape, solidification must be controlled. For wheel casting, to avoid shrinkage porosity, directional solidification must be provided with controlled process parameters [9]. Figure 1.12 shows the desired solidification direction for aluminium alloy wheel casting.

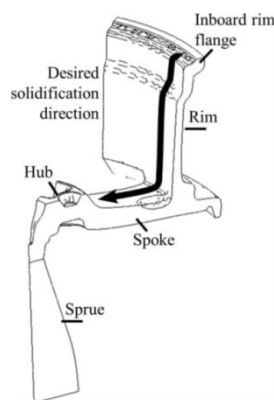


**Figure 1.12 :** Directional solidification [8].

Macro or shrinkage porosity generally occurs when directional solidification is not achieved, which causes the encapsulation of the liquid in situations [7]. Shrinkage porosity occurs due to the density change between liquid and solid phases. This porosity will not vanish, but if desired directional solidification is reached, shrinkage porosity will be at the sprue where the casting defects not important for final product.

The main cause of shrinkage porosity is based on physical changes that occur during solidification. Due to the difference in density between the solid and the liquid state of the casting material, shrinkage of 7% occurs in volume. As a result, if the solidification cannot be achieved in a directional manner, pores are formed in the casting material. Directional solidification means removal of the reduced volume by liquid metal during solidification. The liquid metal to complete the decreasing volume is called "feeding". If sufficient feeding is not achieved during casting, discontinuities and pores are formed in the casting part [8].

With directional solidification, desired feeding can be provided. Figure 1.13 is an example of casting geometry where desired directional solidification may occur. As the thickness of the section and the mass of the casting parts increases, the solidification time increases. As can be seen in Figure 1.13, the solidification time at point A is less. At the points B and C the solidification time is longer. In this case, after the solidification has started at point A, it provides the feeding effect provided by point C, the absence of casting cavity in the point B.

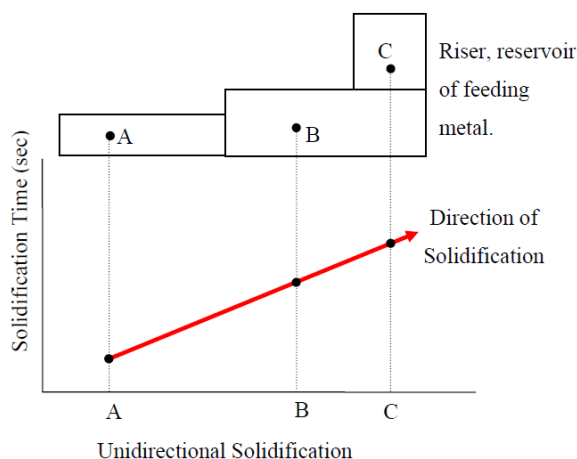


**Figure 1.13 :** Illustration of ideal unidirectional solidification in a simple shaped casting [8].

An example of non-directional solidification is the cast geometry, which can be seen in Figure 1.14. It can be seen in Figure 1.14 that the point of solidification of point A is greater than point B. As a result, when solidification begins at point A, there will be no feeding effect to cover the volume change caused by shrinkage. Because the B point is already solidified; the point A will not have enough liquid metal to feed point A. Result of this situation, at point A, shrinkage porosity may occurs.

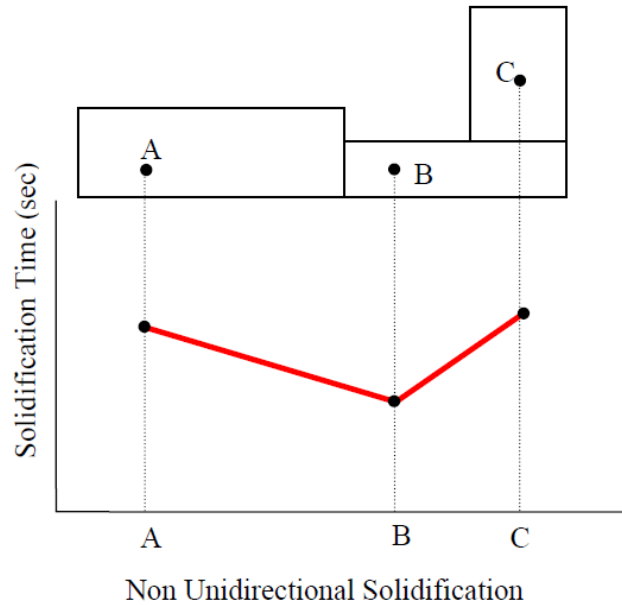


**Figure 1.14 :** Illustration of undesired non-unidirectional solidification in a simple shaped casting [8].

To make directional solidification; solidification of the metal must be controlled with air or/and water cooling channels which are assembled to the die structure. There are a lot of cooling channels which work with predetermined parameters [10]. The parameters of the cooling sequence can be applied as time controlled or/and temperature controlled. The cooling channels which are using the forced air can be controlled by mold temperature, the flowrate in the piping system, or the cooling time that cooling channel active [11]. The cooling channels are not effective on cast part directly, but effective on mold surfaces, to change mold temperature locally. To obtain directional solidification in a low pressure die casting, cooling channels are changed local die temperatures [10]. Equation 1.1 shows the heat transfer between contact interfaces. Figure 1.15 illustrates heat transfer phenomena between mold and molten metal.

$$Q = H \times A \times \Delta T \quad (1.1)$$

Where;

$Q$  = thermal energy (watt)

$h$  = Heat transfer coefficient ( $\text{W/m}^2 \cdot \text{K}$ )

$A$  = Contact area ( $\text{m}^2$ )

$\Delta T$  = Temperature differences between interfaces which heat transfer occurs ( $T_1 - T_2$ ) (K)

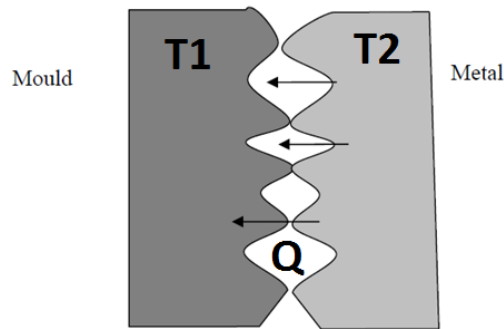


**Figure 1.15 :** Heat transfer between mold and casting metal.

According to the equation, for Figure 1.15, if  $\Delta T$  is higher, heat transfer will increase from molten metal to mold. If the  $\Delta T$  close to 0, heat transfer will be close to 0. As we know, molten metal will be hot, so to increase heat transfer, or in other word to make faster solidification mold must be cooler. Cooling channels make mold interface cooler, therefore if cooling channels are opened at the right time and the duration of the cooling sequence is enough for solidification, directional solidification will occur.

In addition, cooling channels have significant effect on cooling rate. Also, the mechanical properties of the casting will improve more because of the higher cooling rate [12]. Cooling rate is the average temperature change for unit time for solidification. The refinement of metal structures changes with the solidification rate, and thus, has an important role on mechanical properties of the casting [13]. To reach directional solidification and maximize cooling rate, the efficiency of the cooling channels must be maximized, and cooling time must be optimized. This thesis focused on the efficiency of the cooling channels with optimizing flow rate and the effect of the cooling rate on mechanical properties and material properties.

In LPDC process of wheel production, generally air or/and water cooling is used for cooling the mold. In wheel casting, different types of cooling channels are used for LPDC Process, as shown in Figure 1.16.

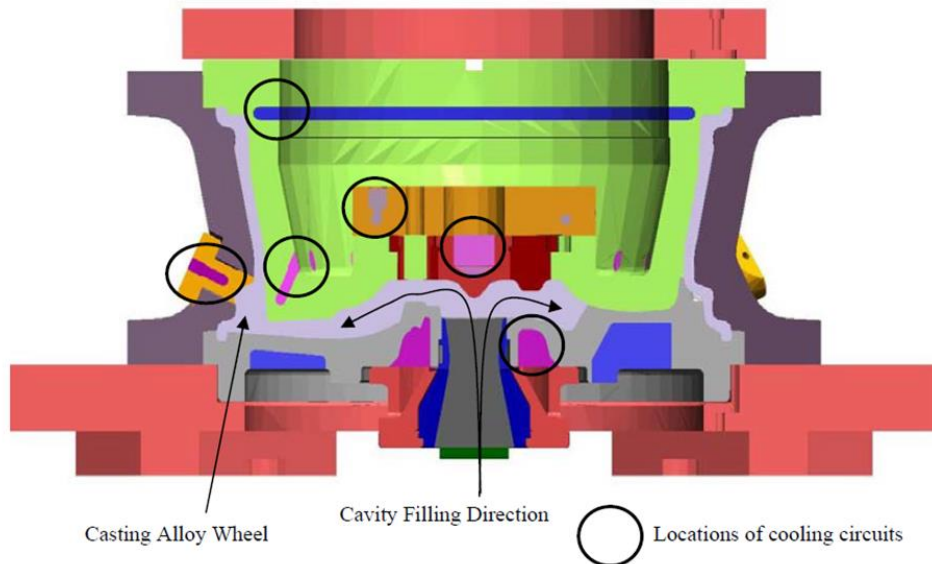


**Figure 1.16 :** LPDC process cooling channels.

In order to obtain directional solidification and high cooling rate for cooling design, locations and efficiency must be optimized. Cooling channels with forced coolant is the fast and effective method to change temperature gradient of the casting. Cooling channels for LPDC casting are nozzle type cooling. Compressed air flows through pipeline. At the end of the pipe line there is a nozzle system, from which the air goes out and impinges the mold outer surface. Impinging jet has an excellent heat transfer properties that widely used in heating and cooling applications [15]. In order to understand nature of this cooling type, literature research made on compressed flow, nozzle cooling and numerical methods for compressed flow.

LPDC air cooling channels are working with compressed air systems. After the compressor, dryer and filter systems prepare the air for the usage. Pipelines let the compressed air flow through the collectors and valves [16]. Figure 1.17 shows simple compressed air preparation system. The cooling channels set to be on, then valves let the compressed air goes through nozzle and air goes out with high velocity. This high velocity air causes impingement air jet to the mold wall and mold will be cooled.

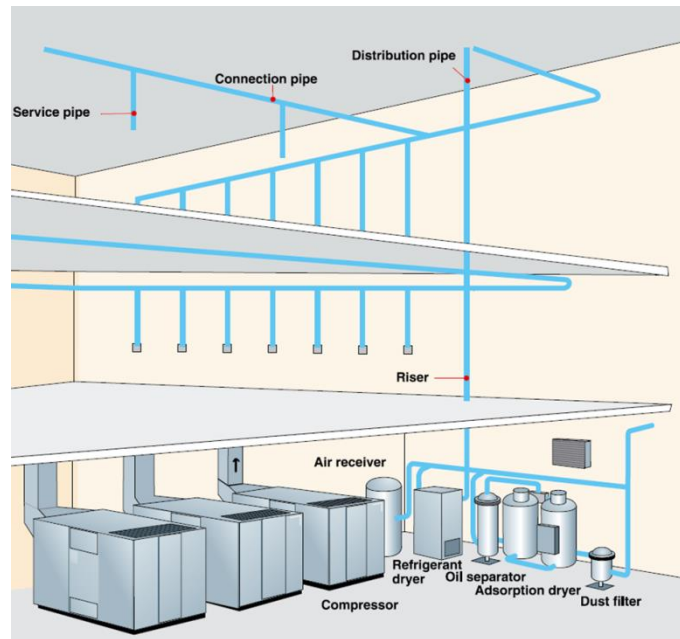


**Figure 1.17 :** Simple compressed air preparation system [16].

Liquid or gas flow is a heating, cooling and fluid distribution solution for industrial applications. A typical piping system contains different sizes of pipes connected to each other by various piping connecting system to guide fluid flow, valves control the flow rate, and pumps pressurize piping system with fluid [17].

Different cooling systems and their cooling efficiencies are summarized in Figure 1.18. When low cooling capacity is needed, air-cooling, which has slow flow properties to remove heat from hot surface, is widely used. The cooling performance can be increased with larger cooling surface area or higher flow rate for cooling air through the hot surface [18].

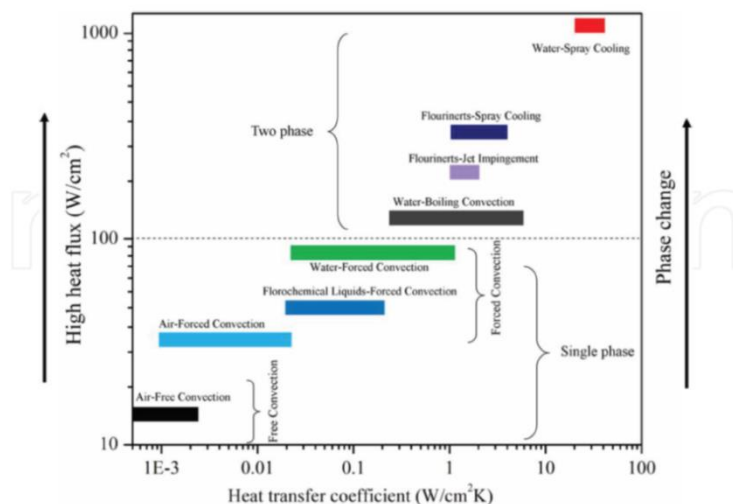


**Figure 1.18 :** The efficiency of the different cooling types [18].

An impingement cooling system is sequenced nozzle array to make heat transfer with impact on a surface that needs cooling or heating. Nozzle system can be separated as two class as a submerged jet or a free jet. If the fluid has the same density with surrounding environment then the jet is called as “submerged”. If the fluid has a different density with surrounding environment then the jet is called as “free” [19]. Figure 1.19 is the illustration of the nozzle system which is used for LPDC process.

The nozzle system has the impinged jet that causes a large amount of heat and mass transfer. So, nozzle cooling systems have many industrial usages for heating and cooling applications, e.g. drying of paper, cooling of photovoltaic cells, deicing of aircraft wings, annealing of metals, heat exchangers in automotive and aeronautical applications, cooling in grinding process or cooling of gas turbine blades [19].

Pressurized air comes from the piping system as illustrated in Figure 1.19. Due to the high pressure inside the pipe, the air exits the nozzle tip at high speed and impact to the mold surface. The flow in the pipe is defined as an internal compressible flow.

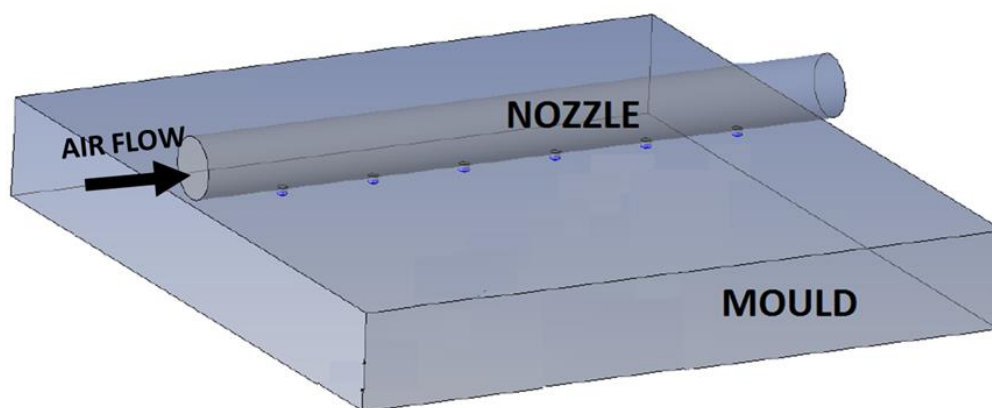


**Figure 1.19 :** Illustration of the nozzle cooling system [19].

Heat transfer due to impact of air from nozzle depends on many parameters such as the distance to the cooled surface, the distance between the nozzles and the geometry of the nozzle affect the heat transfer. As shown in Figure 1.20, gas jets are typically discharged into a quiescent ambient from a round nozzle of diameter  $D$  or a slot (rectangular) nozzle of width  $W$ . Near the nozzle exit the jet flow is turbulent and has a uniform velocity profile. However, at longer distance between nozzle exit and impact surface, momentum exchange between the jet and the ambient causes the free boundary of the jet to protect homogenous velocity profile with changing the center of the flow. Downstream of the center flow, the velocity profile is not homegenous

over the all flow cross section and the maximum velocity decreases with increasing length between the nozzle exit and the impact surface. If the surface that jet impacted is not effective on flow properties, this condition is called as a “free jet”.

Within the stagnation or impingement zone, flow properties be affected by target surface and the velocity decrease at normal axis ( $z$ ) and will increase transvers axes ( $r$  or  $x$ ). However, when flow continues from nozzle exit to impact surface, momentum of flow affected by not moving environment and in the stagnation zone, flow changes and returned to decelerating wall jet. Hence, at longer  $r$  or  $x$  lengths, velocity vectors parallel to the surface and the velocity magnitude changes from decay zone to wall jet velocity. The velocity profiles of the wall jets are defined by zero velocity at both the impact zone and free surfaces [20]. According to this, boundaries that near the wall and ambient areas that have no momentum, flow has 0 m/s velocities. Velocity profiles has local maximum at the center and losses energy when distance increases as shown in Figure 1.20.

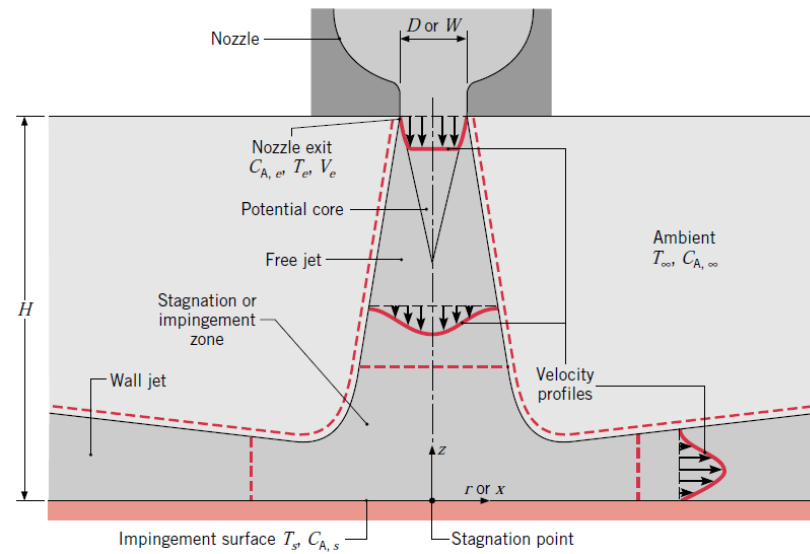


**Figure 1.20 :** Surface impingement of a single round or slot gas jet [20].

In this study, the shape of impact or nozzle type will not be examined. If the flow rate increases, the amount of coolant used will increase. Thus, heat transfer between cooling air and mold wall calculated according to flow rate.

According to Hosain et al. [21], at the constant temperature wall that jet impacted, 5 different flow rates shows different heat flux from the wall surface. Also, heat flux and the flow rate are almost linear and increasing with each other, as shown in Figure 1.21.

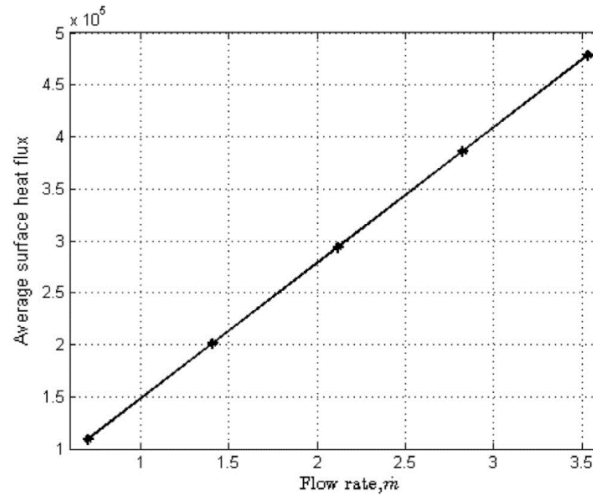


**Figure 1.21 :** Average surface heat flux for different flow rates [21].

As a result, in this research, the effect of pressure, outlet number and inlet number on the flow rate is numerically investigated with assuming that heat transfer would increase with the increase of flow rate.

### 1.2.3 Compressible flow and numerical approaches

High cooling efficiency means lower flow rate, less machinery investment (e.g. piping and pumps) and has good protection on the lifetime of the production tool and even on the quality of the product [21]. Engineering research on heat transfer is important for thermal studies. The demand for the energy sources is increasing rapidly. Thermal systems with high efficiency of the cooling systems are important for energy saving [22]. Therefore, many experimental and numerical studies on compressible flow are made. In the following captions, literature is given in view of these studies.

#### 1.2.3.1 Compressibility and compressible flow

The compressibility of the fluids is simply the amount of change in the fluid density of the pressure change. Gases are, in general, very compressible. On the other hand, liquids have limited compressibility. According to gas dynamics, pressure and temperature changes important for compressible fluid flow [23].

General assumptions for compressible flow;

- The gas is continuous, the motion of the molecules are individual.
- Chemical changes are not considered.
- The gas obeys the perfect gas laws.

- The specific heats at constant pressure and constant volume are both constant.
- The gravitational forces are negligible.
- The magnetic and electrical effects are negligible.
- The effect of viscosity is negligible

Results of these assumptions, the variables are velocity, pressure, density and temperature. As a result, compressible flow can be derived by applying the following principles:

- Conservation of mass
- Conservation of momentum
- Conservation of energy
- Equation of state

Numerical solutions, consider these principles. For example, Figure 1.22 is simple illustration of the control volume. According to conservation laws, differences between rates mass enter control and rate mass leaves control volume equals to rate of increase of mass of fluid in control volume.

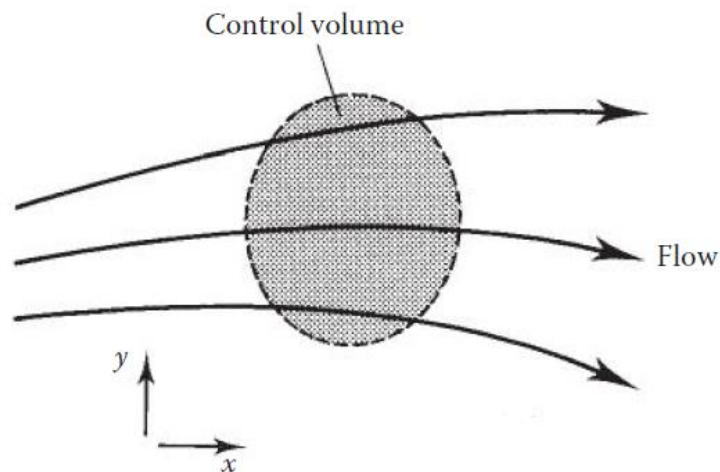


**Figure 1.22 :** Control volume and the flow illustration [23].

The pipe flow of the air until the nozzle is a compressible internal flow. There are different computational models on internal flows for complex geometries. Because of this, there is not enough discussion about approximations or stability of the models on compressible flow problems [24]. Thus, numerical models for calculation of the compressible internal flow must be investigated in different studies.

### 1.2.3.2 Numerical models for compressible internal flow

The numerical solution of the compressible flow for gases can be calculated with ideal gas law. Thus, numerical solution material must be an ideal gas. For ideal gases, the density is a function of pressure. So if the pressure increases, gas density will increase. To calculate density change, pressure level of the system must be defined as shown in Figure 1.23. Manometers measure the static pressure if there is a flow in the pipe. When the system measured with manometer, system static pressure can be defined as a measured pressure for simulation. After the definition of the system, simulation model must be defined.

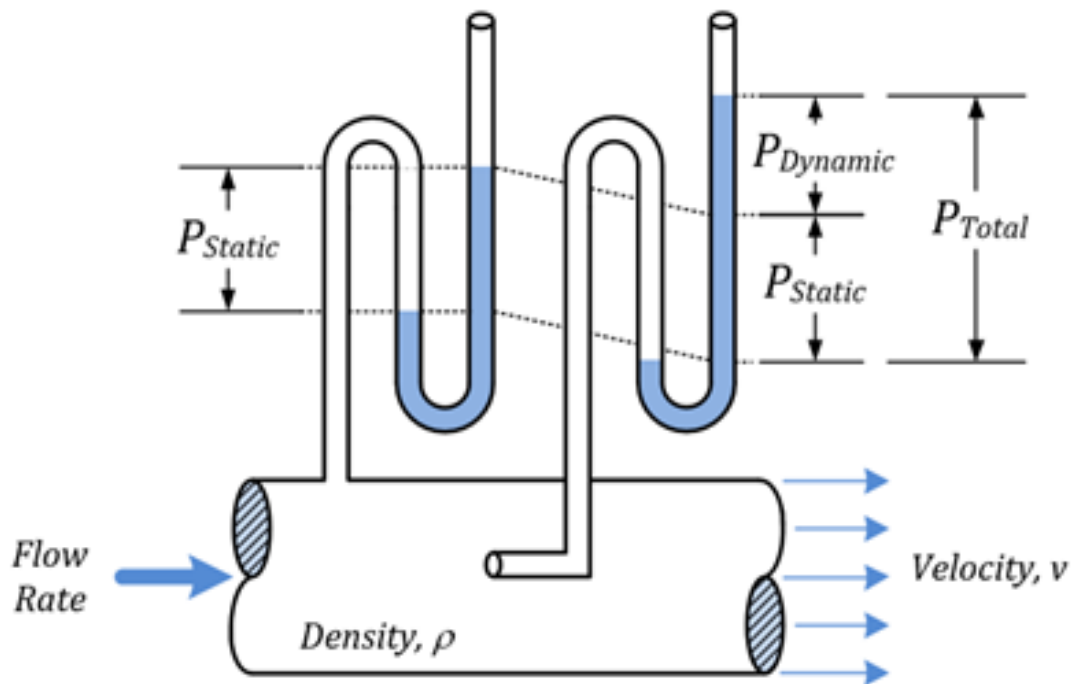


**Figure 1.23 :** Piping system pressure definitions.

As mentioned before; mass, momentum and energy effective on compressible flow. So, Total energy equation must be used for simulation model. These are known areas for the numerical solution of the compressible flow. But the turbulence model for compressible flow model is still being discussed.

Generally used turbulence models are k- $\epsilon$ , Reynold Stress Model (RMS) and Shear Stress Transport (SST). Models, which are calibrated for the type of flow, are more accurate results according to other models [25].

According to Federico Mazzelli, to decide best turbulence model for flow modeling, different models must be tested according to the specific operating condition. For

Mazelli's study, the SST model shows the best performance at low motive pressures. The RSM model shows as good as SST model, but the model suffers from numerical stiffness and convergence problems that make its use improper as shown in Figure 1.24 [25].

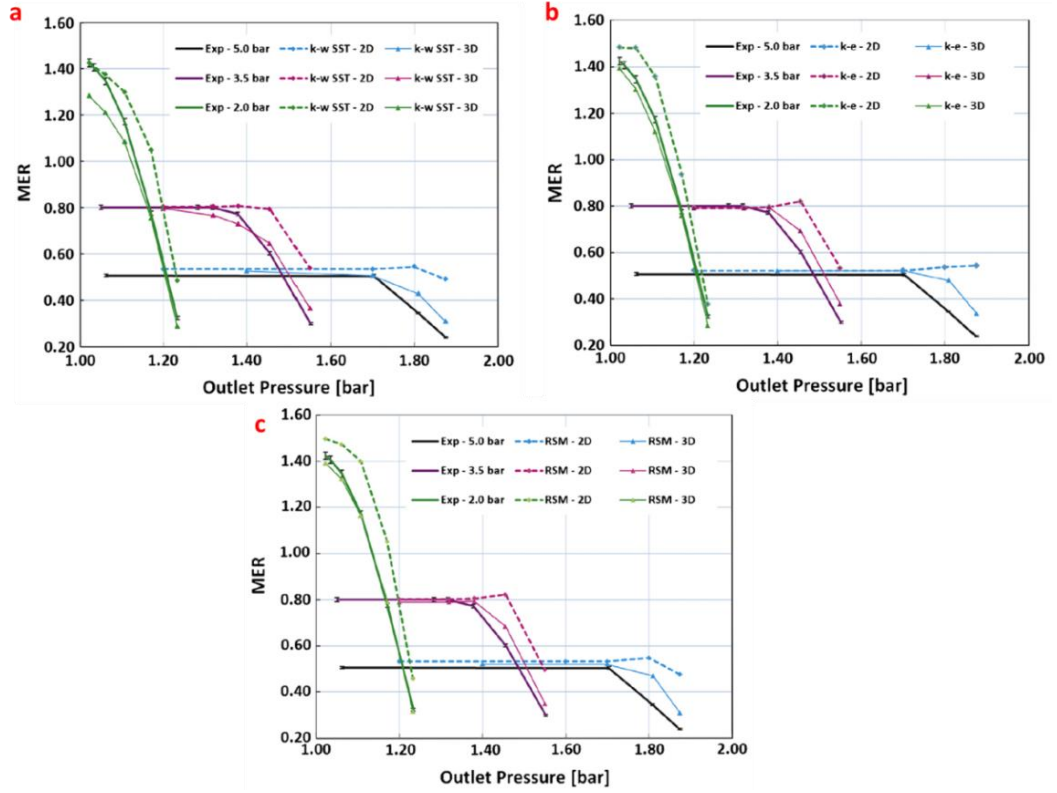


**Figure 1.24 :** The comparison of the turbulence models on pressure change along ejector a) SST b) k-ε c) RSM [25].

According to A. Hemidi [26], even though the k-ε turbulence model showed best results, the SST or other models must be considered for different design conditions (Figure 1.25).

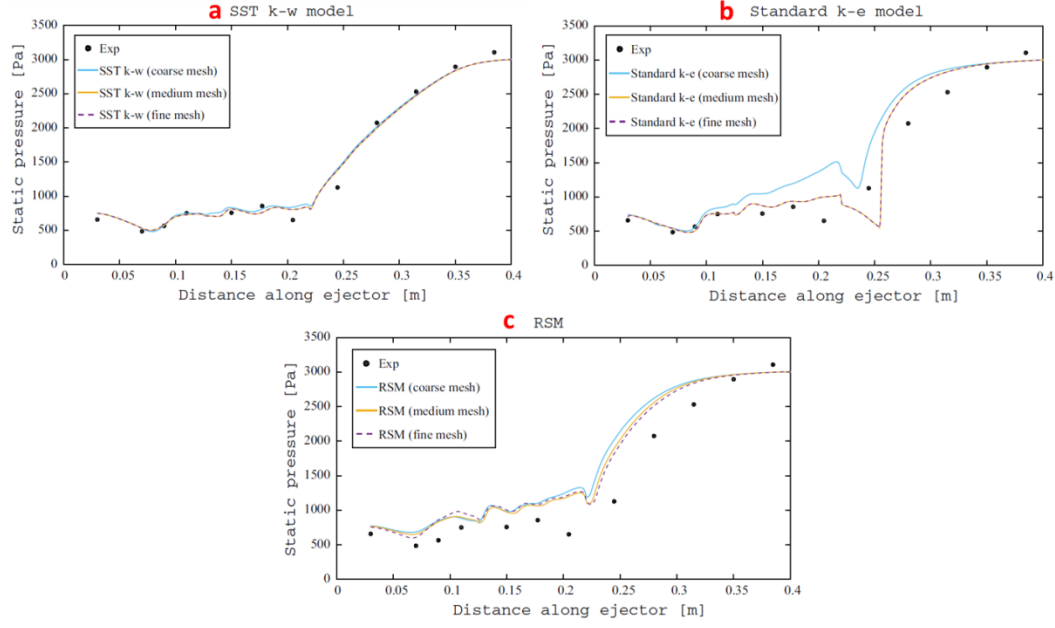


**Figure 1.25 :** The comparison of the turbulence models on pressure change along ejector a) SST b) k- $\epsilon$  c) RSM [26].

According to G. Besagni [27], good agreement with the experiment results belongs to SST model for local and global flow calculations. As a result, SST model is the best way to the prediction of the parameters according to other models.

According to S. Croquer [28], at high Reynolds number k- $\epsilon$  shows best match to experimental results with a deviation of less than 1%. But simulation time three times longer than SST model. So for low Reynolds number SST model is the over all best turbulence model for compressible flow simulation (Figure 1.26).

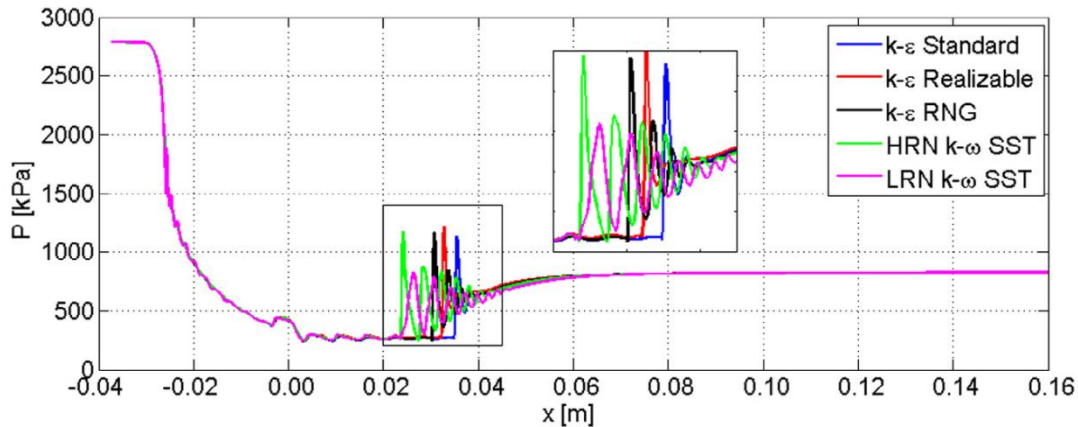


**Figure 1.26 :** The comparison of the turbulence models on pressure change along ejector [28].

There are many comparison works in the literature for SST turbulence model. According to the literature research for impingement air jet studies, SST model has better results as summarized below:

- Experimental and numerical investigations made about the nozzle system that impingement air jet through flat plate show that SST model have best predictions for the fluid flow and heat transfer characteristics [29].
- According to optimization results, between accuracy and the computational cost, the SST turbulence model is optimum turbulence model for impingement air jet problems [30;31].
- According to study of Panumadu et al., SST model have good prediction for laminar to turbulent flow transformation for short distance between the nozzle and plate surface condition. SST model is the best suitable model for modeling the jet impingement phenomenon [32].
- With the maximum relative error is 13.58%, the results showed that the SST model is the best for impingement air jet numerical problem [33].
- For local nusselt number prediction results, the qualitative comparison show that SST model is much better over all agreement with experimental results compared to k- $\epsilon$  model [34].
- Comparison between different turbulent models clearly demonstrates that SST turbulence model performed better than others. Including the computational cost, the SST turbulence model was also optimum turbulence model [35].

Thus, SST model choosen for numerical investigation. As a results simulation setup, has air ideal gas for density calculation, total energy equation for solution, and SST model for flow calculation. Simulation type will be transient.

After model definition is completed, we must choose the right boundary conditions, which are very important for simulation setup. Generally, boundary conditions are defined by measured or calculated values. Simple simulation has an inlet, outlet and wall boundary conditions as in this numerical study. The temperature of the air and the piping system are assumed as the same. The heat transfer between the piping system and the air accepted as an adiabatic. Thus wall boundary condition must be an adiabatic. The inlet and outlet boundary conditions are defined as a pressure inlet and

outlet. Pressure inlet boundary condition is defined according to measurement results from manometer. The pressure outlet boundary condition has been accepted as open to the atmosphere. Thus, the pressure value for outlet boundary condition equals to 0 atm.

Solver schemes are defined as numerical methods for solving differential equations. Upwind scheme are used for many study for the numerical solution of the compressible internal flow [26;28;29;30;32;34;35]. Thus upwind scheme was used for calculation of mass, energy and turbulence differences. Even though the upwind scheme is not particularly accurate, it is physically correct. Thus there appears to be a trade off between accuracy and stability. Using the upwind scheme, solutions are better behaved and bounded [36]. As a result upwind scheme is not most accurate solution, but the most stable scheme for solution.

#### **1.2.4 Effect of cooling system on material properties and microstructure**

Cooling systems affect the casting directional solidification with changing solidification as mentioned at chapter 1.2.2.2. Changing solidification time also affects the cooling rate. The cooling rate has significant importance for microstructure and mechanical properties. In this section, the research of the effect of the cooling rate on material properties summarized.

The physical and mechanical properties of aluminum castings may be classified as;

- Cooling rate; it is one of the most important variables affecting the physical and mechanical material properties during solidification [3].

According to research of M. O. Shabani and A. Mazahery; secondary dendrite arm spacing (SDAS); Using image analysis techniques, it is obtained by examining microstructure photographs taken on different casting parts. The variation of SDAS with cooling rate (R) is presented in Figure 1.27 [37]. According to Figure 1.27; cooling rate affecting SDAS. At higher cooling rates; SDAS will be finer.

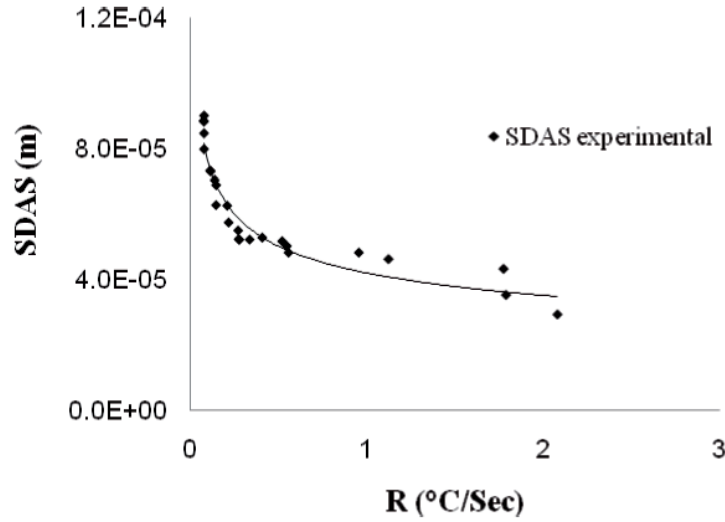


**Figure 1.27 :** Secondary dendrite arm spacing as a function of cooling rate for A356 alloy [37].

According to this research; SDAS is affecting mechanical properties shown as Figure 1.28. Measurements showed that; microstructures with fine dendrite structure have better mechanical properties than coarse ones [37].

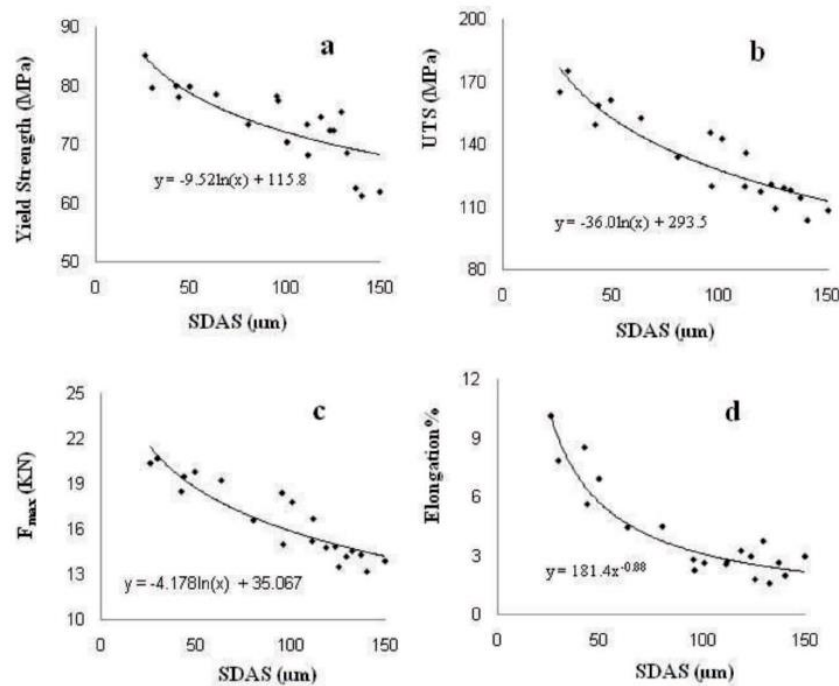


**Figure 1.28 :** Variation of yield stress (a), ultimate tensile strength (b), maximum force (c) and elongation percentage (d) with secondary dendrite arm spacing [37].

According to these results; M. O. Shabani and A. Mazahery generated a numerical model for calculation of the mechanical properties which is also shown in Figure 1.29.

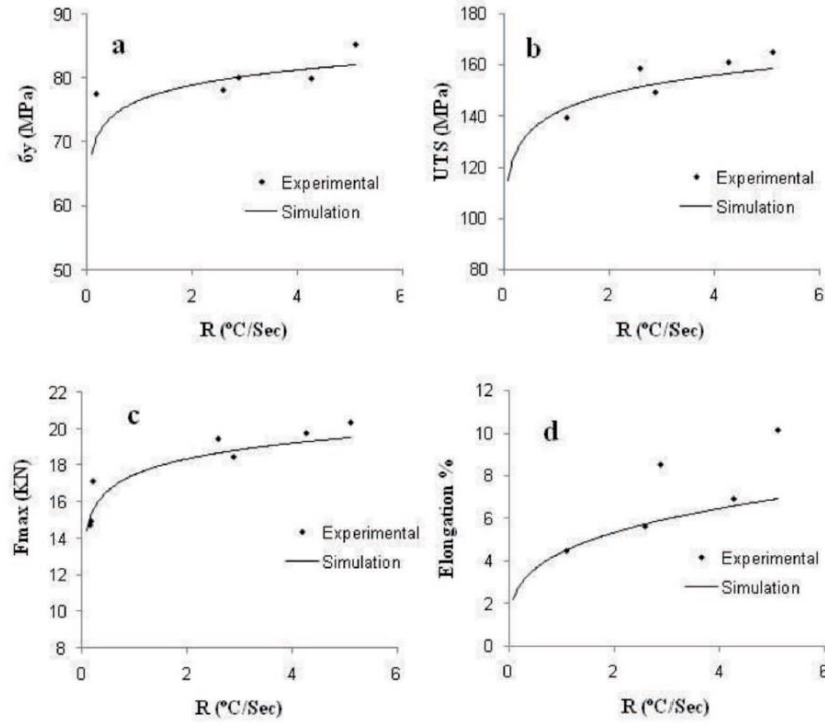


**Figure 1.29 :** Variation of yield stress (a), ultimate tensile strength (b), Fmax (c) and elongation percentage (d) with cooling rate [37].

L.Y. Zhanga and his colleagues are explained these conditions as follows;

The solidification rate has a significant effect on the formation of microstructure and mechanical properties. The higher cooling rate and the shorter the solidification time results in the finer the microstructure formed. And accordingly, better mechanical properties were obtained. In addition, it increases the formation of solid solution and causes the formation of metastable phases. [38]. Figure 1.30 shows the relationship between DAS and cooling rate.

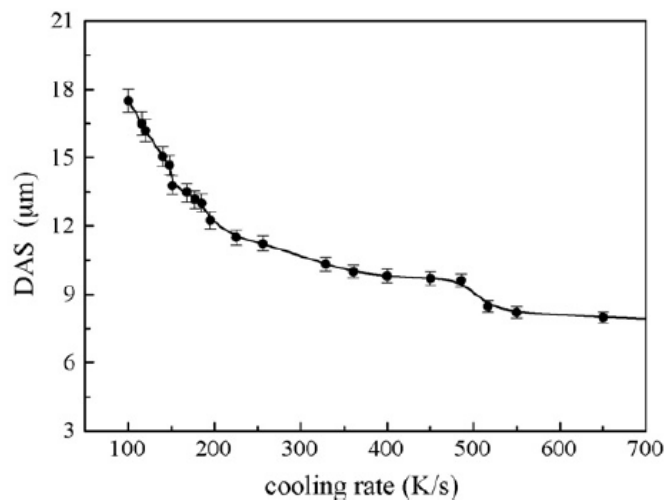


**Figure 1.30 :** Relationship between DAS and cooling rate [38].

According to Figure 1.31 DAS affects the ultimate tensile strength directly. According to Zhanga et al., microstructure of A356 has finer  $\alpha$ -aluminum and eutectic phases at higher cooling rate. Because of this; with finer DAS; this microstructure has higher micro hardness which means better mechanical properties.

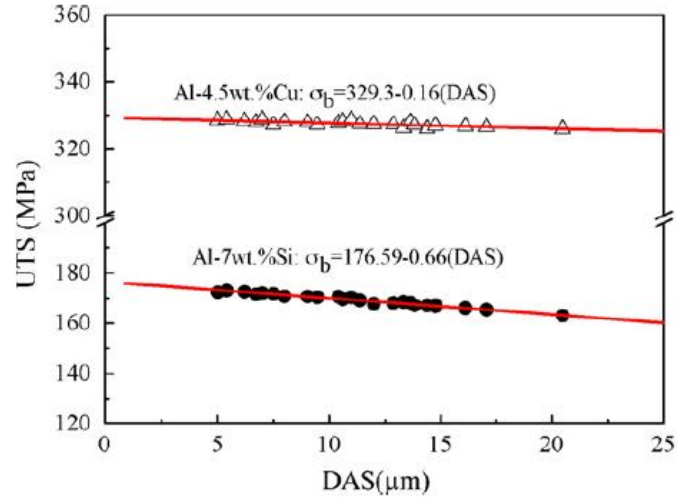


**Figure 1.31 :** Effect of DAS on ultimate tensile strength (UTS) [38].

R. Chen and his colleagues have worked on the effect of cooling rate on the microstructure. They work on microstructure and solidification time as a process parameter (Figure 1.32) [39].

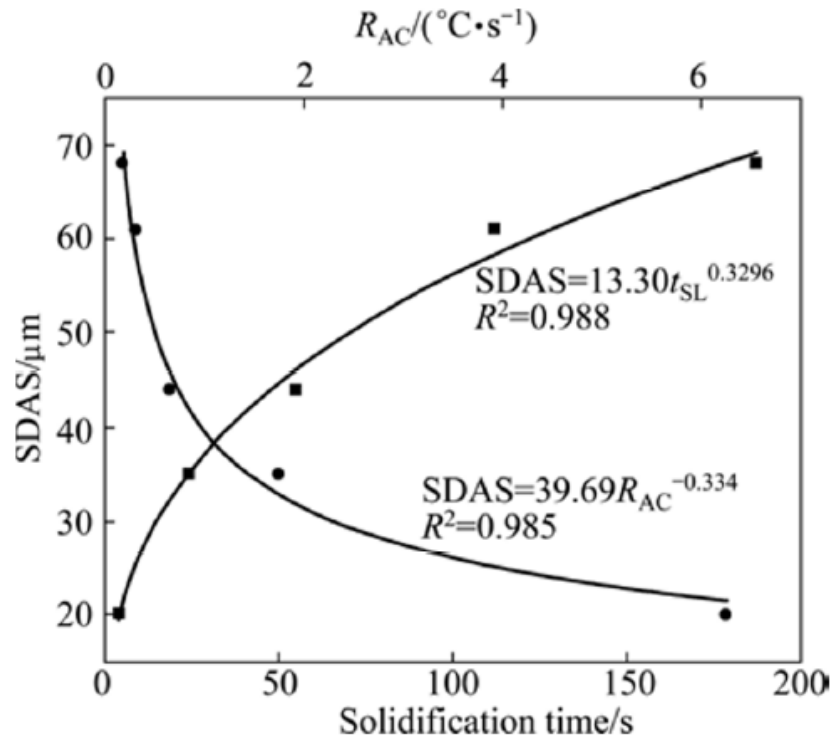


**Figure 1.32 :** Effect of cooling rate and solidification time on SDAS [39].

According to Chen's study; with increasing cooling rate, the primary  $\alpha(\text{Al})$  dendrite nucleation temperature, eutectic reaction temperature and solidus temperature shift to lower temperatures, resulting in a larger undercooling both for  $\alpha(\text{Al})$  and eutectic. The secondary dendritic arm spacing (SDAS) is very sensitive to cooling rate and an increase of cooling rate from 0.19 to 6.25  $^{\circ}\text{C/s}$  decreases SDAS from 68 to 20  $\mu\text{m}$  (Figure 1.33) [39].

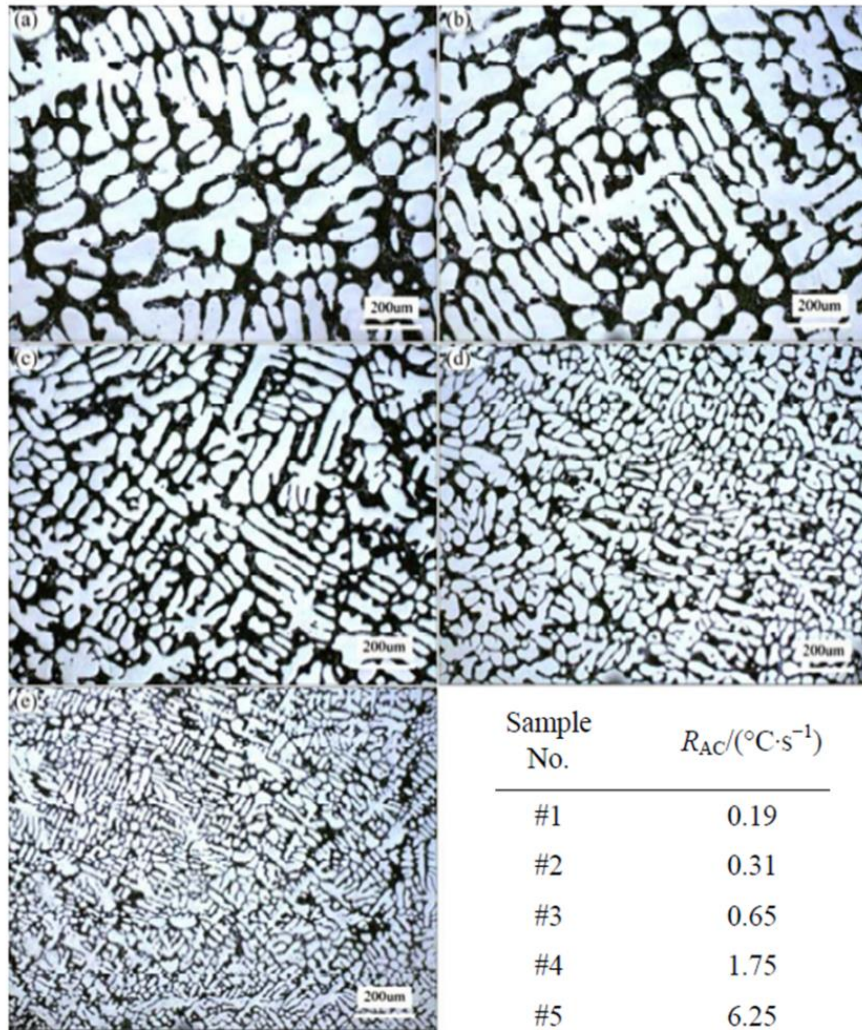


**Figure 1.33 :** Optical microstructures of sample 1 (a), sample 2 (b), sample 3 (c), sample 4 (d), sample 5 (e) with different cooling rates [39].

## **2. EXPERIMENTAL PROCEDURE**

The experimental procedure contains two stages. In the first stage, pressure tests were carried out, and numerical studies were confirmed and the simulation model was determined in accordance with the pressure test results. In the second stage, the effect of the variables determined for air-cooling on the cooling performance is calculated by using the determined model. Finally, the validity of the results obtained from the model was confirmed with the experimental study (pressure test results).

### **2.1 Experimental Study For Verification**

#### **2.1.1 The experimental setup**

The experimental setup (cooling system) used for experimental studies consists of five parts as shown in Figure 2.1. These are;

1. Manometer
2. The service unit
3. Pipeline
4. Flowmeter
5. Cooling channel

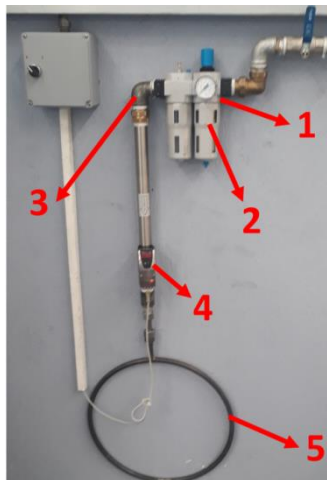


**Figure 2.1 : The experimental setup.**

The type of the manometer used in the experiments was MA-50 which shows the pressure values between 0 and 16 bars. The product number of the Festo product is 356759. The product technical drawing can be seen in Figure 2.2. The flowmeter is the testo 6642. At the Figure 2.3, the technical drawing of the flowmeter can be seen. The flow was measured as Nm<sup>3</sup>/h using the flowmeter.

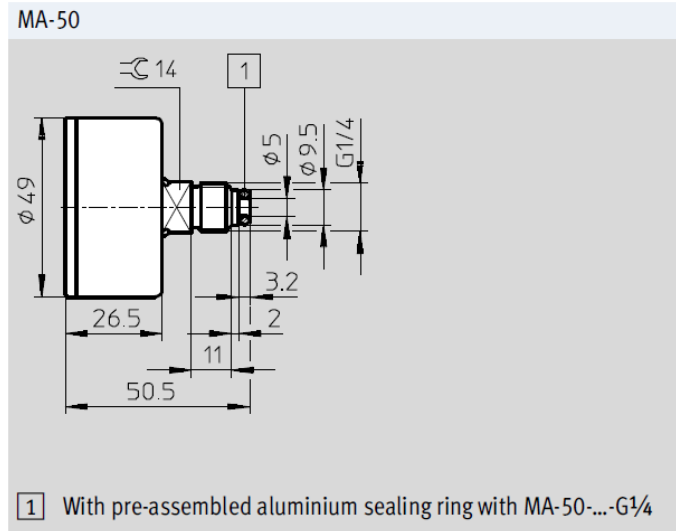


**Figure 2.2 :** Technical drawing of the manometer.

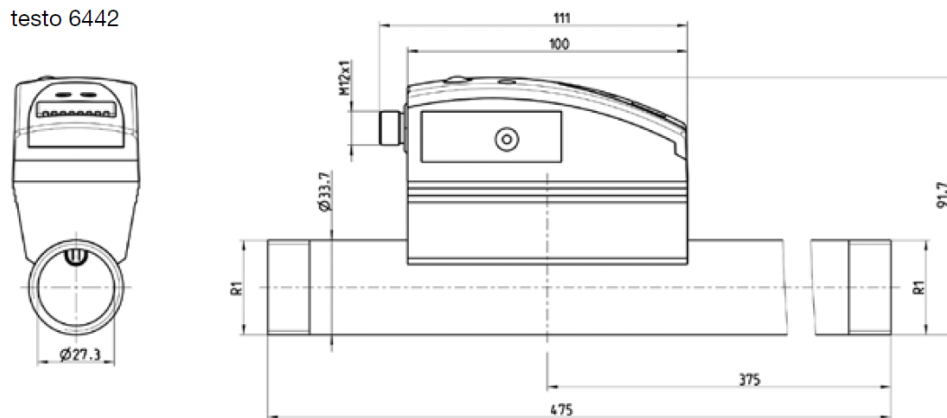


**Figure 2.3 :** Flowmeter technical drawing

The design of the cooling channel can be seen at Figure 2.4. Cooling channel is produced by pipe bending technique. Cooling channel is made by pipe with a hydraulic diameter of 13 mm and a wall thickness of 1.5 mm, which is curled to inner diameter 434 mm, and the outer diameter to 466 mm. 16 holes of 2 mm diameter were drilled at equal intervals on the pipe. The same hydraulic diameter as the cooling pipe and 50 mm long air inlet are welded to the pipe.

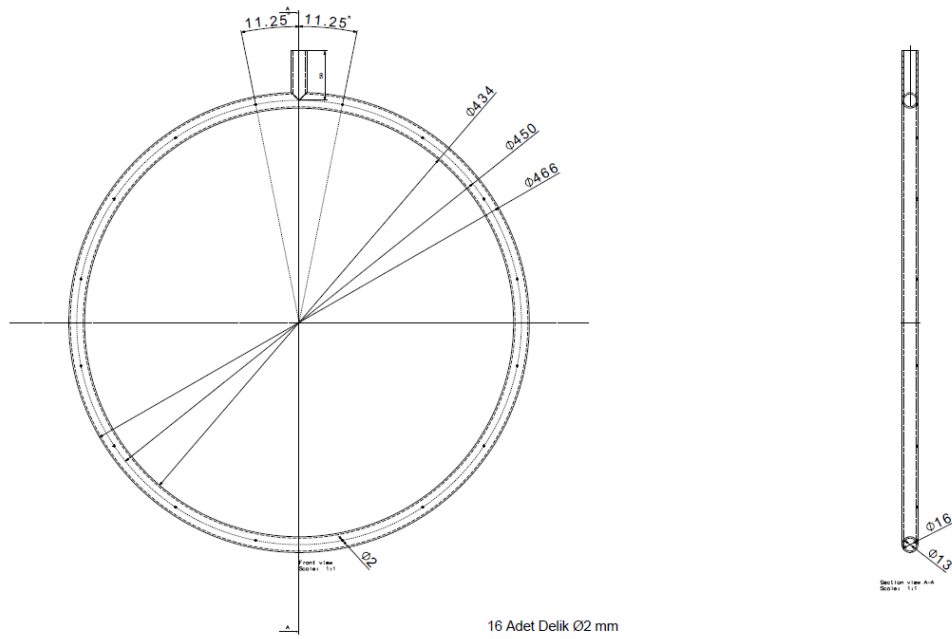


**Figure 2.4 :** Cooling channel technical drawing.

This cooling channel is connected to the flowmeter, and the flowmeter is connected to the pipeline. The manometer is used for adjusting the pressure of the air entering the pipeline. The pressure regulator (festo 194706 LRS-1/8-D-7-I-MINI) was used to adjust the pressure according to the pressure gauge.

### 2.1.2 Pressure tests

The first experiment was performed with an average pressure. Test pressure was determined as three bars. The inputs and outputs obtained from the experiment can be seen in Figure 2.5 and 2.6.



**Figure 2.5 :** First test pressure from the manometer (3 Bars).



**Figure 2.6 :** First test flow result from the flowmeter (104.3 Nm<sup>3</sup>/h).

The second experiment was carried out with a higher pressure. The system pressure was determined as five bars. Test inputs and outputs are shown in Figures 2.7 and 2.8.



**Figure 2.7 :** Second test pressure from the manometer (5 Bars).



**Figure 2.8 :** Second test flow results from the flowmeter (167.1 Nm<sup>3</sup>/h).

The flow rate for the test setup, which was previously mentioned, was measured as 104.3 Nm<sup>3</sup>/h at the gauge pressure of the system at three bars; it was measured as 167.1 Nm<sup>3</sup>/h at the gauge pressure of the system at five bars. Based on these results, data were obtained for numerical analysis model and verification.

## **2.2 Numerical Study For Verification**

The numerical study was done using the CFX V16.2 Computational Fluid Dynamics (CFD) software included in the Ansys Workbench 18.2 programme.

Numerical studies consist of five main sections. In this section of the study, after the test results are obtained, the identification works are summarized below separately, under these five sections. Finally, the results of the simulation and the results obtained from the experiments were compared.

### **2.2.1 The geometric setup**

Catia V5 R2016 was used to define geometric definition of the problem. Figure 2.9 shows the definition boundaries, geometrically.

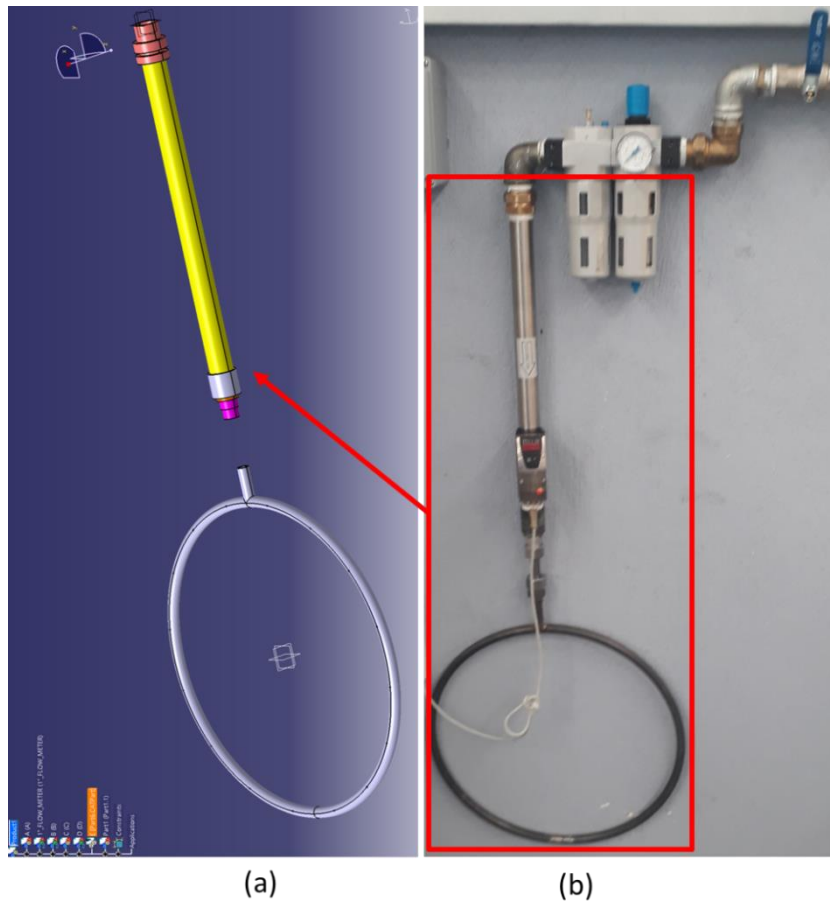


**Figure 2.9 :** Geometric definition a) CAD data b) selected part for simulation setup.

To simplify the problem, only the gaps in which the air is located have been defined, the non-fluid regions are not defined in the simulation geometry. The regions indicated in Figure 2.10 are made for the mesh and identification sections in the problem.

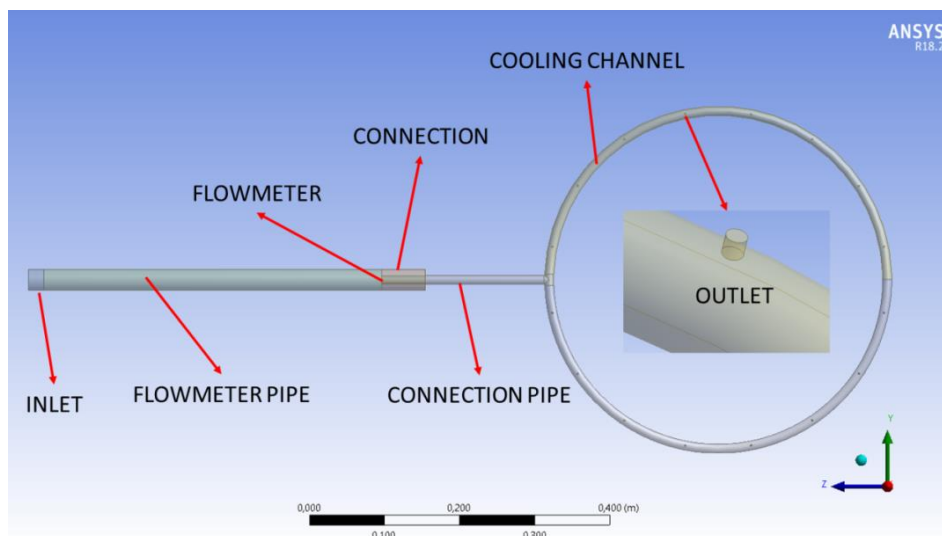


**Figure 2.10 :** Simulation geometric definitions.

### 2.2.2 Mesh generation

The “meshing” is of great importance in the identification of the simulation. In simulations where air flow is simulated, the use of hexagonal elements is recommended since hexagonal elements provide faster resolution with lower mesh elements and nodes. As mentioned earlier, the simulation geometry is divided into several cylindrical parts in order to be able to form hexagonal elements. Figure 2.11 is showing mesh with sectioned and zoomed locations.

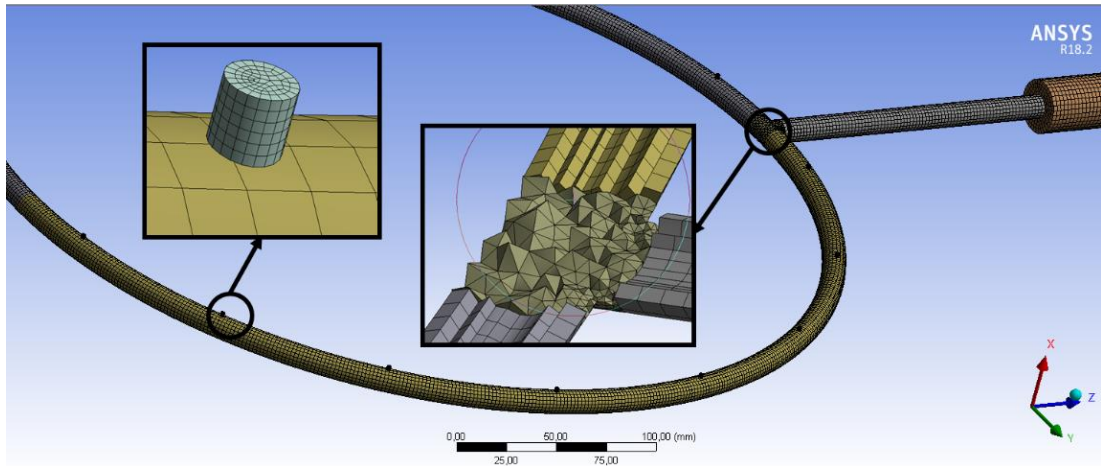


**Figure 2.11** : Mesh of the numerical study.

The mesh was made with 92.297 nodes and 87.634 elements. Two important criteria were determined in the mesh control. First, the skewness should be below 84%, the result obtained is a maximum of 81%. Secondly, the orthogonal quality should be above 18%, which is a minimum of 18.9%. Definition according to ANSYS can be seen in Figure 2.12(a). These values can be seen for our simulation in Figure 2.12(b).



**Figure 2.12 :** a)Classification of the mesh quality metrics based on skewness b)Mesh node and element count with quality properties.

After the criteria for required mesh properties are met, the setup section was started to identify the problem.

### 2.2.3 Setup

In the setup section, it is better firstly to determine whether the work is done in a transient or steady state. For the steady state definition, the timestep will be determined by the simulation software. However, the total simulation time and timestep are determined by the user in the transient definition. For the simulation setup, the steady state simulation was ignored. The timestep is set to 1E-05sec (0.01 ms). In the simulations performed, it was observed that a balanced state was created for the flow rates before 50 ms. However, the total simulation time was set at 100 ms since the results were desired to be more accurate. Figure 2.13 shows these parameters.

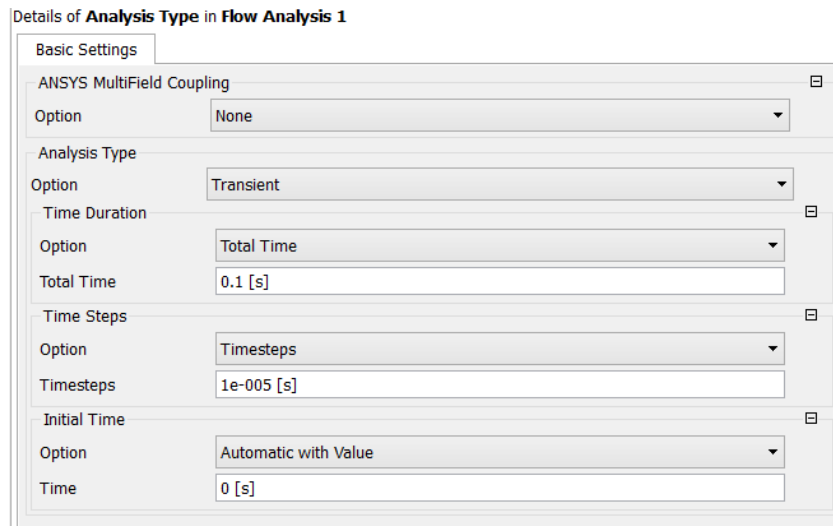


**Figure 2.13 : Analysis type.**

Simulation setup parameters can be seen at Figure 2.14. Since the simulation for the compressive flow is needed, the material in the simulation was selected as “Air Ideal Gas”. Total energy calculations are used in nozzle simulations. Shear stress transport (SST) turbulence model is considered suitable for simulation as mentioned at section 1.5.2. For initial condition, the system is completely static (no movement) and the system temperature is 25 °C (298.15 K).

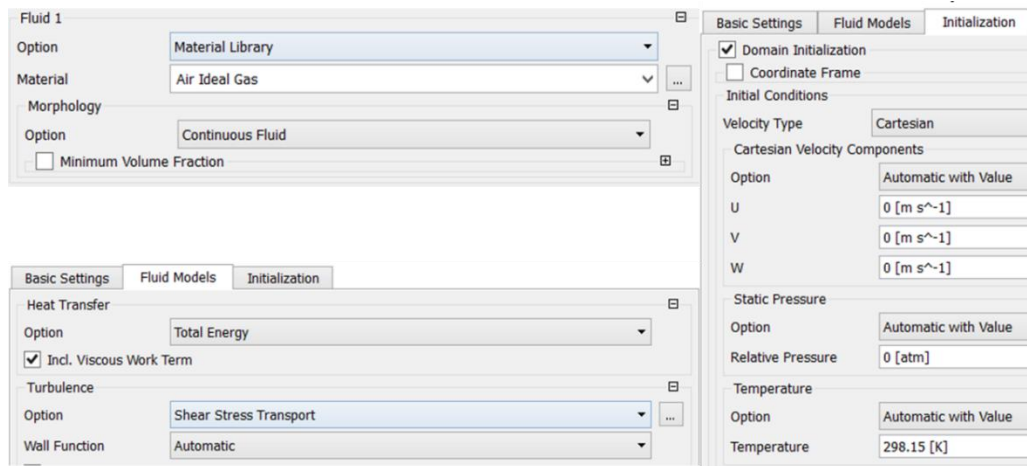


**Figure 2.14 : Simulation setup for calculations.**

When the control of the simulation applied as shown in Figure 2.15, the use of high-speed compressed nozzle systems is described as Upwind, First Order Backward Euler, and First Order, as the appropriate resolution configuration. Convergence value 1E-6 was taken to ensure the accuracy of the results. The information obtained about convergence will be shared in the following sections.

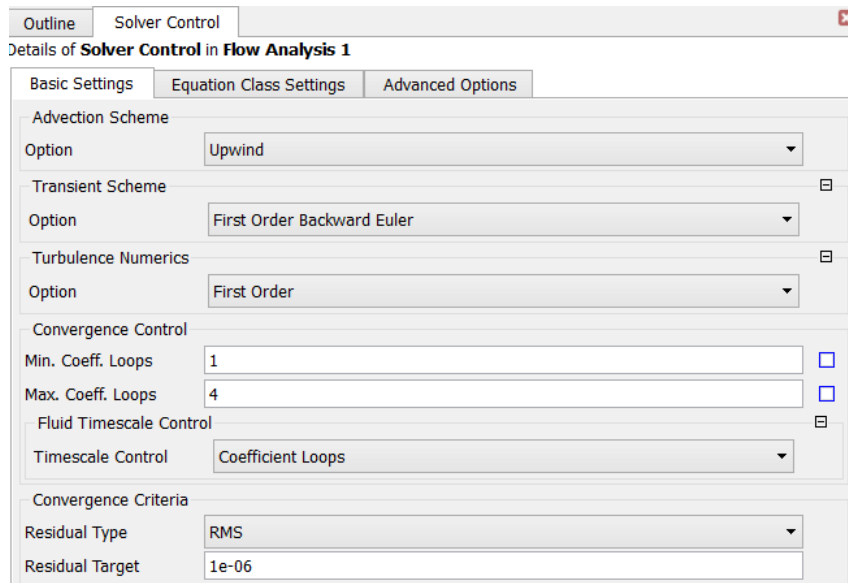


**Figure 2.15 :** Solver control parameters.

## 2.2.4 Solver

Total time of the first verification simulation solution lasted 1 day, 7 hours and 10 minutes for the simulation study. And the other designs simulations lasted about one month. The convergence values for momentum and mass, heat transfer and turbulence are shown below in Figures 2.16, 2.17 and 2.18, respectively. At the end of the simulation, the desired convergence values were obtained.

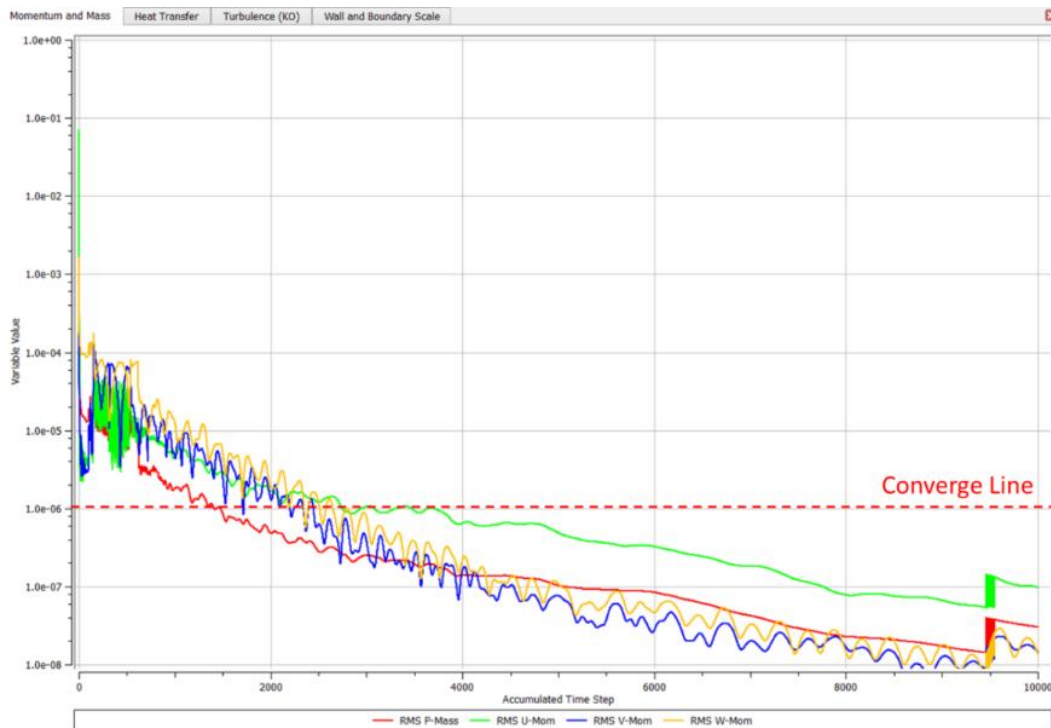


**Figure 2.16 :** RMS (root mean square) for momentum and mass.

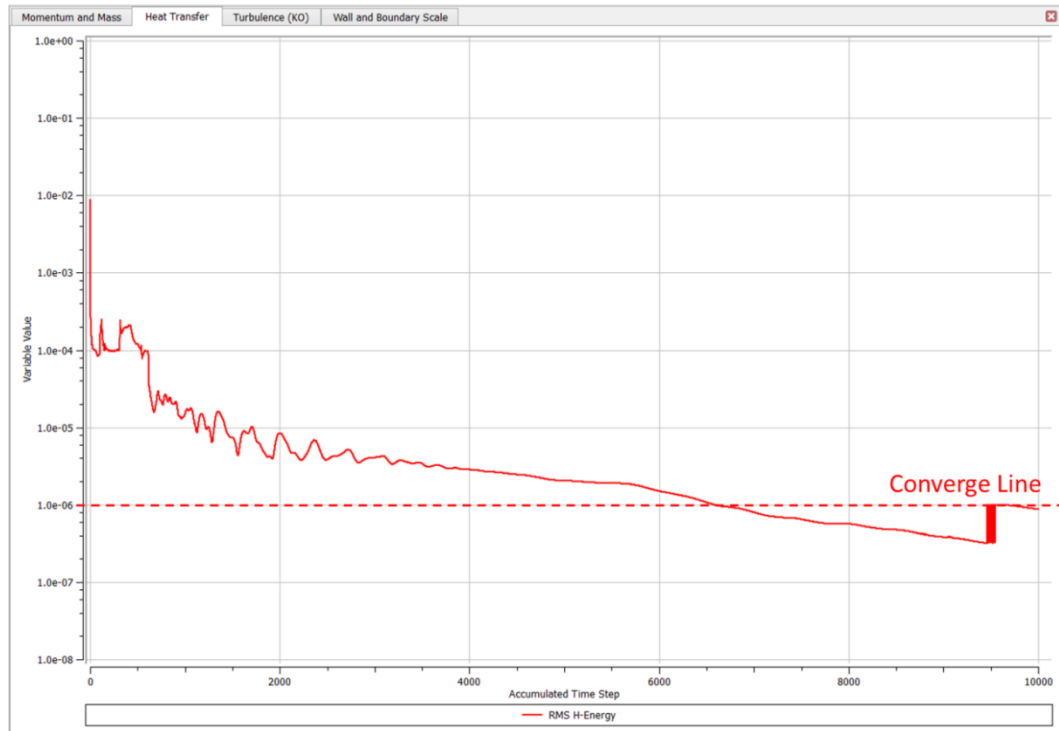


**Figure 2.17 : RMS for heat transfer.**



**Figure 2.18 : RMS for turbulence.**

## 2.2.5 Results

The actual flow is the amount of volume flowing through the cross-sectional area in unit time. The normal flow is the amount of volume flowing through the cross-

sectional area, in unit time, which is equal to the volumetric value of air at the temperature of 0 °C and the pressure of 1.01325 bars. When calculating the actual flow for the geometry seen in Figure 2.19, the pipe cross-sectional area is multiplied by the gas velocity in the section. Equation 2.1 shows this situation. According to ideal gas equation, when the temperature and pressure is changed, the volume of gas will be changed. Equation 2.2 shows this as an equation. Figures 2.20 and 2.21 are calculated from the simulation results with equations 2.1 and 2.2.

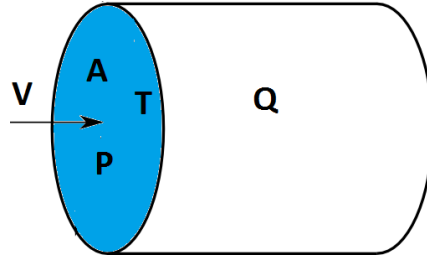


**Figure 2.19 :** Cross-section control volume and variables.

V: Velocity (m/s)

A: Cross-Section Area (m<sup>2</sup>)

T: System Temperature (K)

P: System Gauge Pressure (Bar)

Qa: Flow (m<sup>3</sup>/h)

Tn: Normal Temperature (0 °C = 273.15 K)

Pn: Normal Pressure (1.01325 Bar)

Qn: Normal Flow (Nm<sup>3</sup>/h)

$$Q_a = V \times A \quad (2.1)$$

$$\frac{Q_1}{Q_2} = \frac{(P_2 \times T_1)}{(P_1 \times T_2)} \Rightarrow Q_n = \frac{(P \times T_n)}{(P_n \times T)} \times Q_a \quad (2.2)$$

According to the results seen in Figures 2.20 and 2.21, when the system pressure is 3 bars, the flow rate is 107.4 Nm<sup>3</sup>/h, and when the system pressure is at 5 bars, the flow rate is 167.8 Nm<sup>3</sup>/h. According to the test measurements, as previously mentioned, when the system pressure is at 3 bars, the flow rate is 104.3 Nm<sup>3</sup>/h and the system pressure is at 5 bars, the flow is 167.1 Nm<sup>3</sup>/h. When these results were compared, it was found that the maximum deviation was around 3%. If the deviation

value is below 5%, the simulation model can be considered as appropriate. According to the comparison, simulation model can be used for evaluation of the effects of different variables on cooling efficiency.

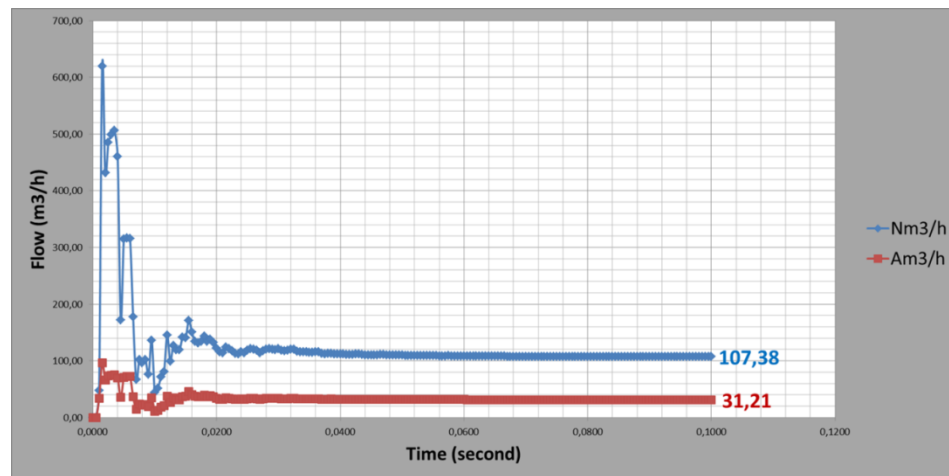


**Figure 2.20 :** Flow results at gauge pressure 3 bars.

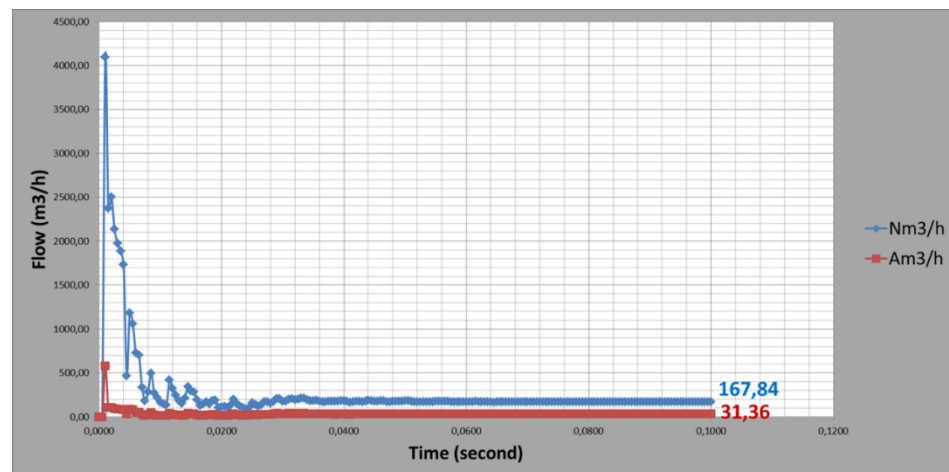


**Figure 2.21 :** Flow results at gauge pressure 5 bars.

### 3. RESULTS AND DISCUSSION

#### 3.1 CFD Study For Cooling Efficiency

##### 3.1.1 Setup

After the numerical model was verified, the variables affecting cooling efficiency were examined. After that, it was decided to design an experiment with three variables. These variables were inlet number, outlet number and the system pressure. The number of inlets and outlets are changed and used for simulation geometry which is shown at Figure 3.1.

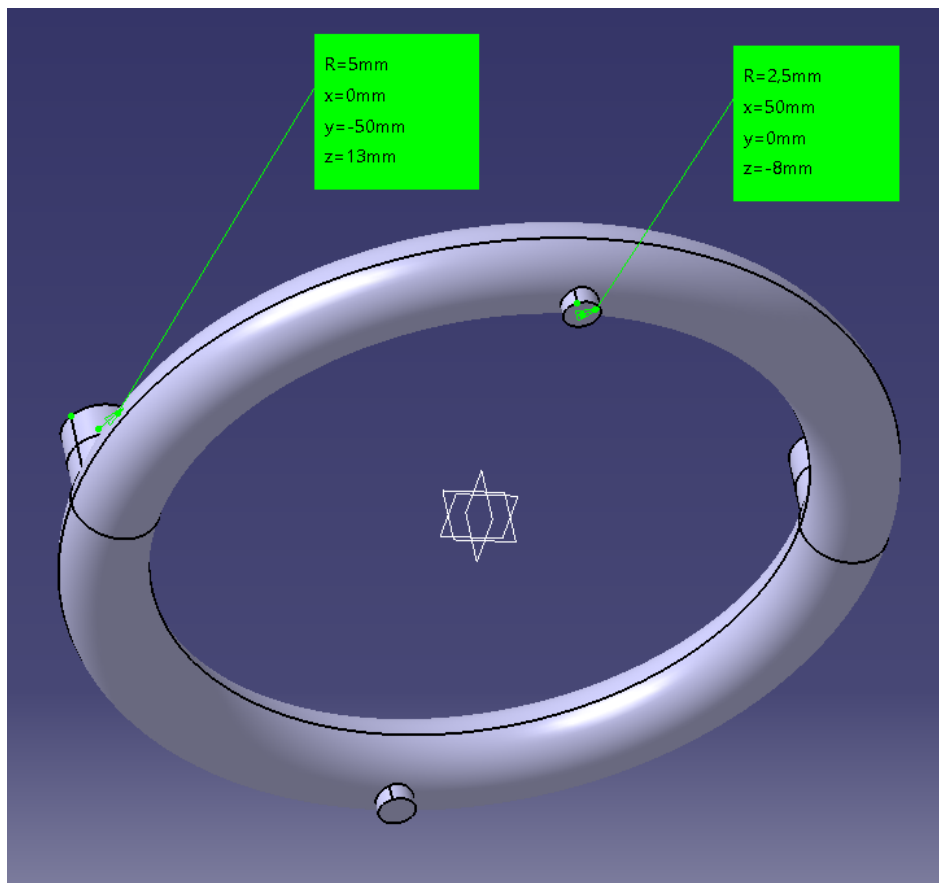


**Figure 3.1 :** Simulation geometry for numerical experiments.

Table 3.1 shows the experimental design. Also, the total inlet area ( $A_i$ ), total outlet area ( $A_o$ ) values and the ratio between these areas are affected by these design variables as can also be seen in Table 3.1. A total of 24 numerical tests were

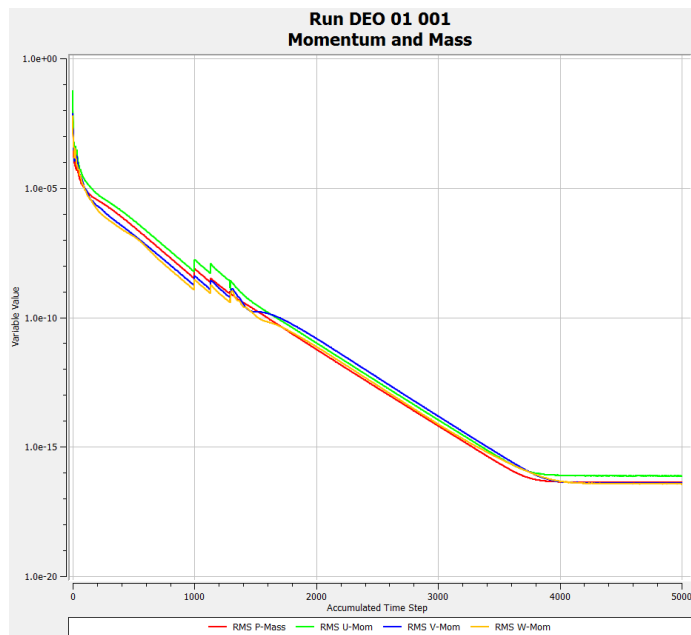
performed and the results of  $A_i/A_o$  and  $A_o/A_i$  were discussed. For all simulations; solution time lasted around 1 day for each, and with pre-post time total simulation time to have results lasted more than 1 month.

**Table 3.1 :** Design table for numerical experiments.

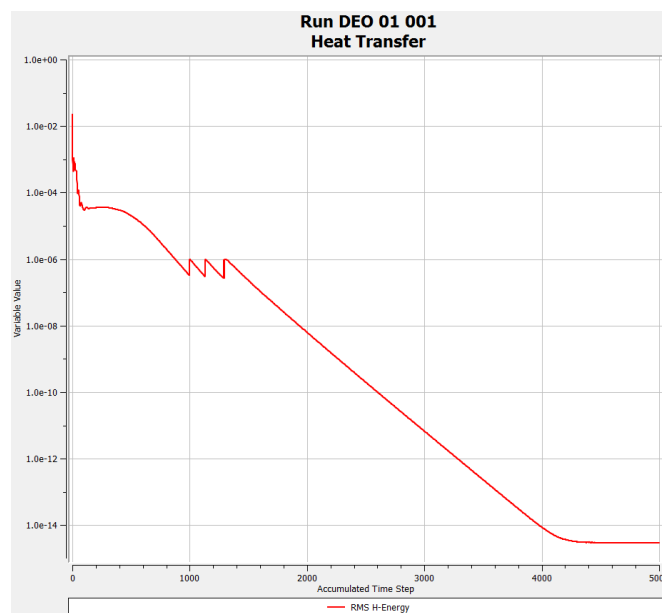
Inlet_Count	Outlet_Count	Pressure (Bar)	Total Inlet Area (m2)	Total Outlet Area (m2)	Di/Do	Do/Di
1	2	2	7,85E-05	3,93E-05	2,00	0,50
1	2	6	7,85E-05	3,93E-05	2,00	0,50
1	4	2	7,85E-05	7,85E-05	1,00	1,00
1	4	6	7,85E-05	7,85E-05	1,00	1,00
1	8	2	7,85E-05	1,57E-04	0,50	2,00
1	8	6	7,85E-05	1,57E-04	0,50	2,00
1	12	2	7,85E-05	2,36E-04	0,33	3,00
1	12	6	7,85E-05	2,36E-04	0,33	3,00
1	16	2	7,85E-05	3,14E-04	0,25	4,00
1	16	6	7,85E-05	3,14E-04	0,25	4,00
1	20	2	7,85E-05	3,93E-04	0,20	5,00
1	20	6	7,85E-05	3,93E-04	0,20	5,00
2	2	2	1,57E-04	3,93E-05	4,00	0,25
2	2	6	1,57E-04	3,93E-05	4,00	0,25
2	4	2	1,57E-04	7,85E-05	2,00	0,50
2	4	6	1,57E-04	7,85E-05	2,00	0,50
2	8	2	1,57E-04	1,57E-04	1,00	1,00
2	8	6	1,57E-04	1,57E-04	1,00	1,00
2	12	2	1,57E-04	2,36E-04	0,67	1,50
2	12	6	1,57E-04	2,36E-04	0,67	1,50
2	16	2	1,57E-04	3,14E-04	0,50	2,00
2	16	6	1,57E-04	3,14E-04	0,50	2,00
2	20	2	1,57E-04	3,93E-04	0,40	2,50
2	20	6	1,57E-04	3,93E-04	0,40	2,50

### 3.1.2 Solver

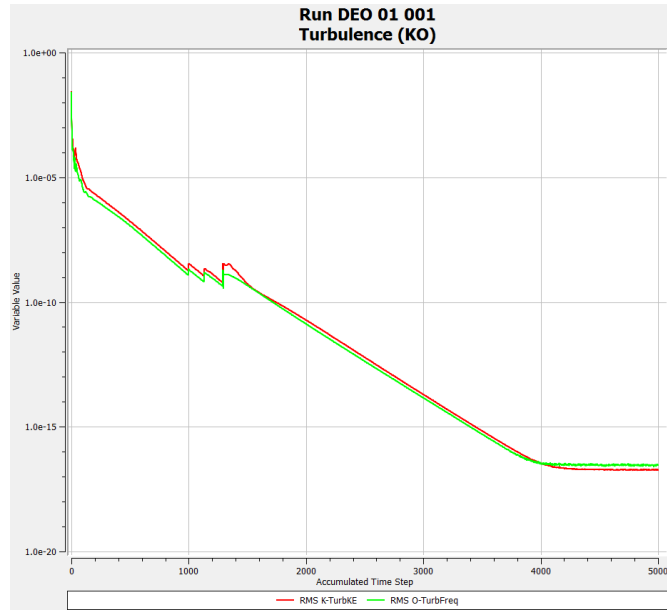
The convergence values for momentum and mass, heat transfer and turbulence are shown below in Figures 3.2, 3.3 and 3.4, respectively. At the end of the simulation, the desired convergence values were obtained.



**Figure 3.2 : RMS for momentum and mass.**



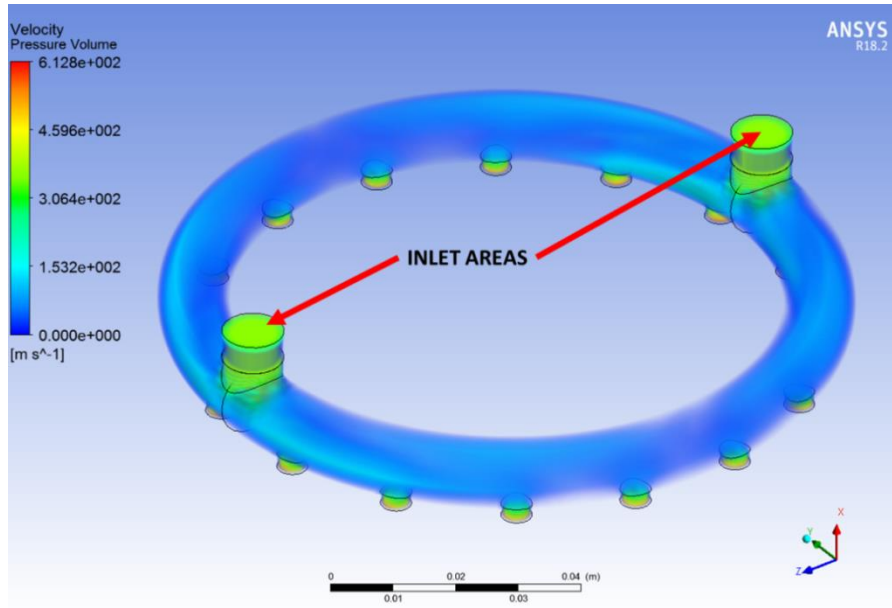
**Figure 3.3 : RMS for heat transfer.**



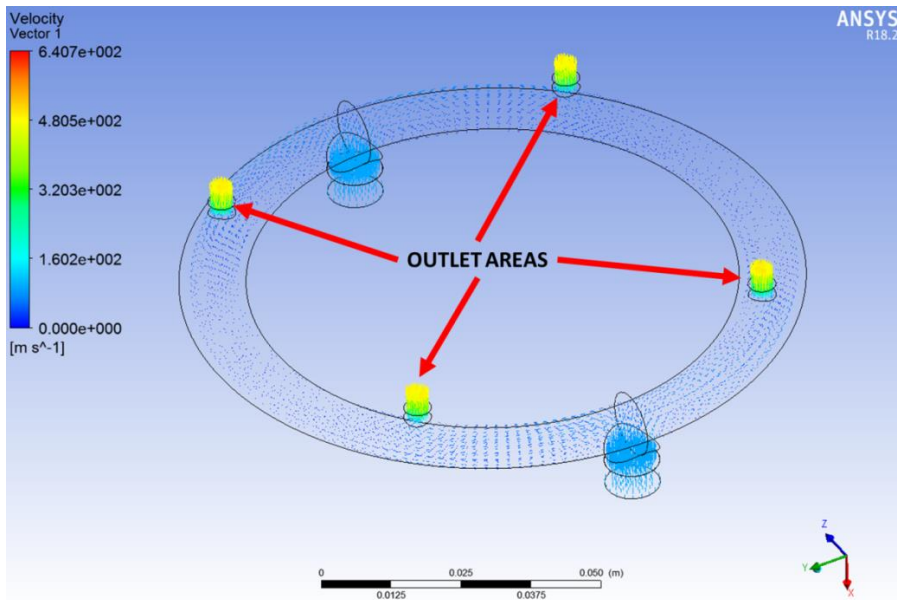
**Figure 3.4 : RMS for turbulence.**

### 3.1.3 Flow rates and pressure distributions

Figures 3.5 and 3.6 show the inlet and outlet areas for measurements. Flow rate results are taken from inlet area. The velocity results are multiplied by inlet surface area to find actual flow rate (equation 3.1). After that, normal flow rate is calculated according to equation 3.2. However, the outlet boundary condition was open to atmosphere. Therefore, mass flow result is chosen for outlet boundary conditions. The mass flow results are chosen directly from simulation results. The results are compared with the outlet number, and inlet/outlet cross section area ratios as summarized below.



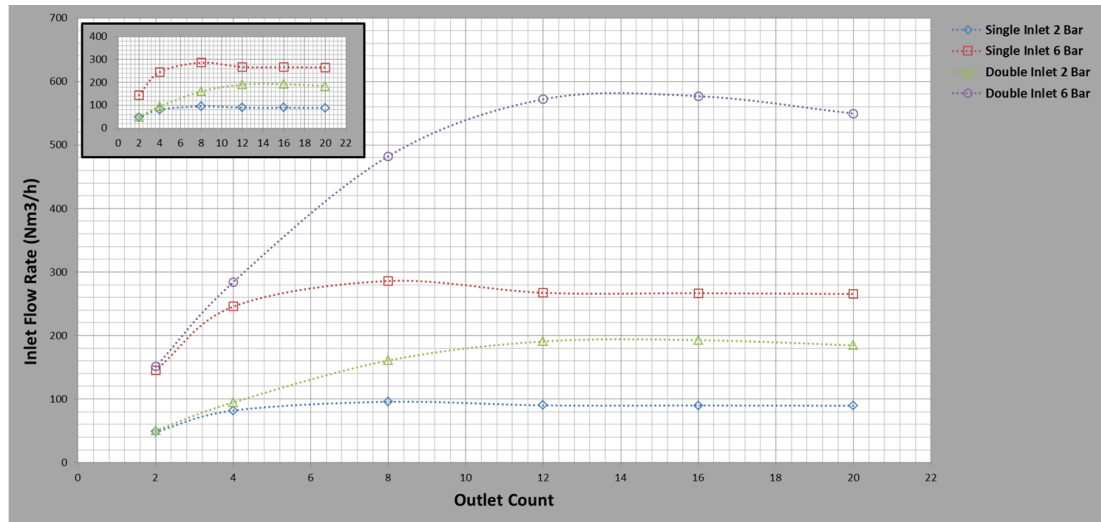
**Figure 3.5 :** Inlet area for measurement and velocity magnitude results.



**Figure 3.6 :** Outlet areas and velocity vector results.

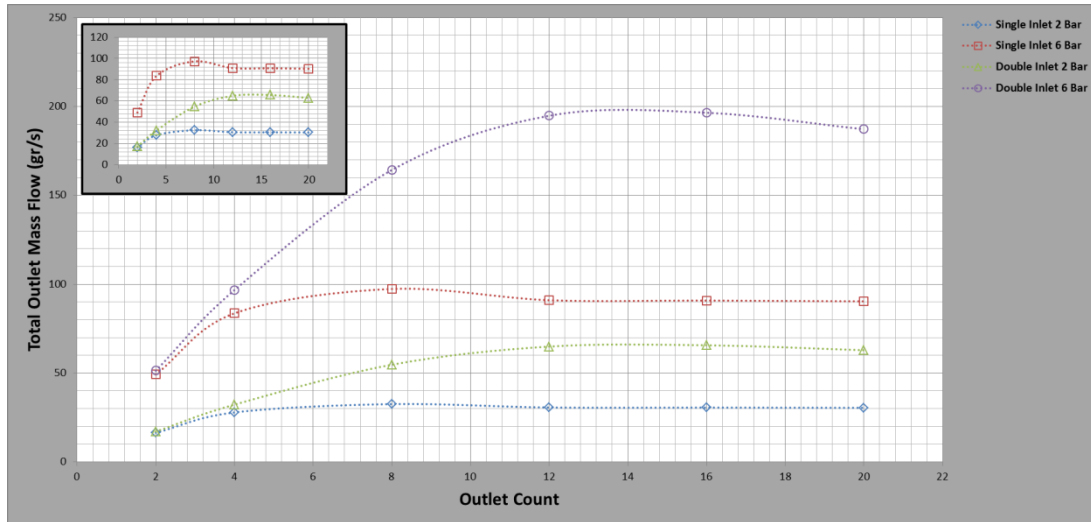
According to Figure 3.7, the highest flow rate values were obtained by 6 bar pressure and double inlet cooling type. Second best values were obtained by 6 bar pressure and single inlet cooling type. The results show that the pressure of the cooling system is more important than other two parameters. Increasing the outlet count, after reaching a peak point, causes the flow rate to drop. These peak points are different for single and double outlet but same for different system pressure values. At Figure 3.7, for single inlet simulation, the results of the flow rate reaches the peak point at cooling system for 8 outlets, however flow rate decreases for cooling system having

12 outlets. For double inlet cooling systems, according to flow rate results, peak point is for cooling system having 16 outlets. When these results are examined, it was seen that the number of inlets and outlets also has an effect on the flow rate. According to these results, if the number of inlet is doubled, the outlet number is doubled with higher flow rate. For this situation, the following comments can be made; more outlet use may be possible if the number of inlet is increased.



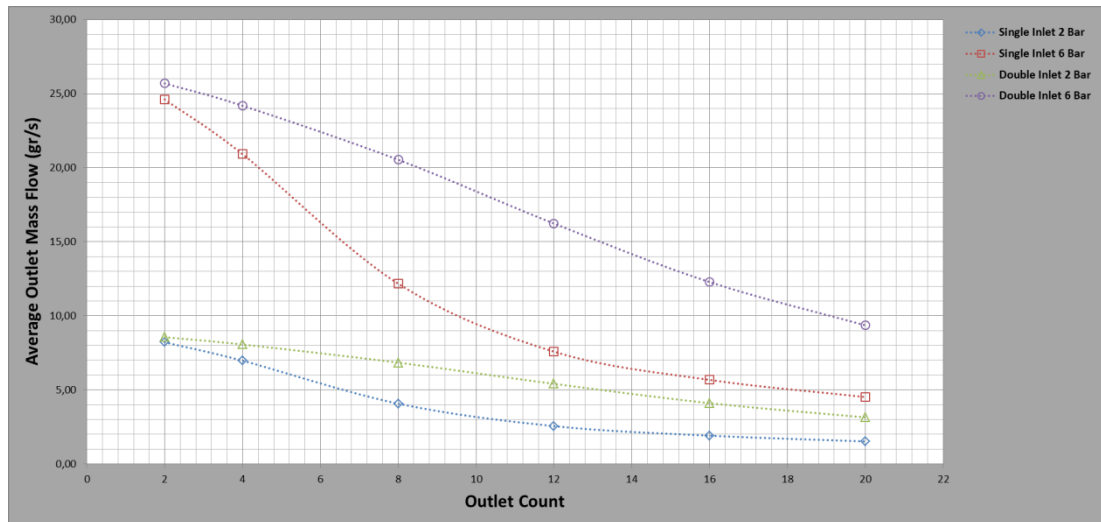
**Figure 3.7 :** Inlet flow rate results according to outlet count.

Figure 3.8 shows total outlet mass flow vs. outlet count results which are similar to inlet flow rate results. Total outlet mass flow results are more important for this study since higher coolant mass flow means more effective cooling. Both total outlet mass flow and inlet flow rate results show that system pressure is has a big influence on cooling efficiency. The number of outlet changes mass flow and flow rate, and the system has a peak point. For both inlet flow rate and total outlet mass flow results for single inlet and 2 bar cooling systems is nearly the same. So, it can be said that the effect of pressure is higher than the inlet and outlet numbers according to this situation. And after the peak points, the flow rate and the mass flow results do not change much. This indicates a stabilization in the mass flow characteristics after a certain number of outlet in the cooling system.



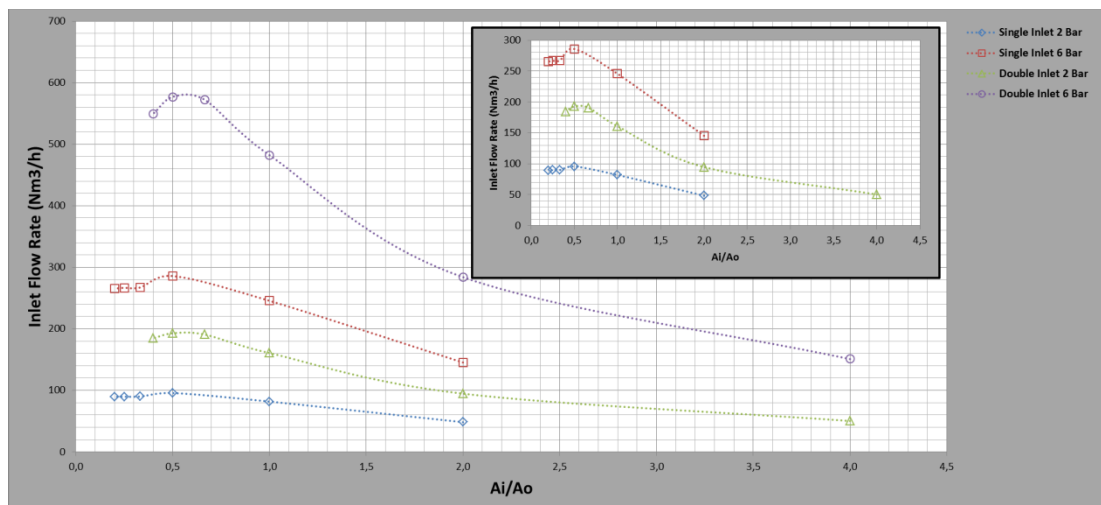
**Figure 3.8 :** Total outlet mass flow results according to outlet count.

Figure 3.9 shows the average outlet mass flow results which is equal to total mass flow results divided by outlet number. Also, it can be accepted as mass flow for each nozzle. Here, the mass flow from all nozzles was assumed to be equal. As the number of outlet increases, average outlet mass flow decreases. At higher system pressure, average outlet mass flow is high as parallelly. So, the number of the outlets has a negative effect on average outlet mass flow, yet system pressure has a positive effect on average outlet mass flow. These results are important for cooling efficiency because if the number of outlets increases, the average mass flow for each outlet is reduced. According to this assumption, the total mass flow rate is the result of multiplying the average outlet mass flow and outlet number. So, the decrease in the total mass flow rate is normal after a certain number of outlets. Because the average mass flow after a threshold point will be so low that the total mass flow will begin to drop. These results can explain the peak points in Figure 3.7 and Figure 3.8. As a result, the number of inlet and outlet affects the flow rate and mass flow directly. Considering that the change of both quantities interacts with one another, the ratio of the total cross-sectional areas of the inlets and outlets ( $A_i/A_o$ ) will be a variable affecting the mass flow and flow rate. And this ratio is considered as a performance parameter for cooling design in order to define cooling flow rate peak point.



**Figure 3.9 :** Average outlet mass flow results according to outlet count.

In order to see the effect of the ratio between the total inlet cross-sectional area and the total outlet cross-sectional area ( $A_i/A_o$ ), the Figure 3.10 and 3.11 are examined to compare it to the inlet flow rate and total outlet mass flow. The graphs show that the results have same shape for both total outlet mass flow and inlet flow rate. Every result shows that around 0.5  $A_i/A_o$  ratios has a peak point for both results. So 0.5, which is an  $A_i/A_o$  value, is acceptable for the maximum efficiency point for cooling channels in this study. At that point flow rate is maximum for total inlet flow rate and outlet mass flow. But the Figure 3.10 and 3.11 show that values that under 0.5, not have so much different flow rate. But higher values for  $A_i/A_o$  are showing too much reduced mass flow and flow rate results at figures. In this case, the  $A_i / A_o$  ratio should be close to and below 0.5 for the more efficient cooling system.



**Figure 3.10 :** Inlet flow rate results according to inlet/outlet cross section area ratio.

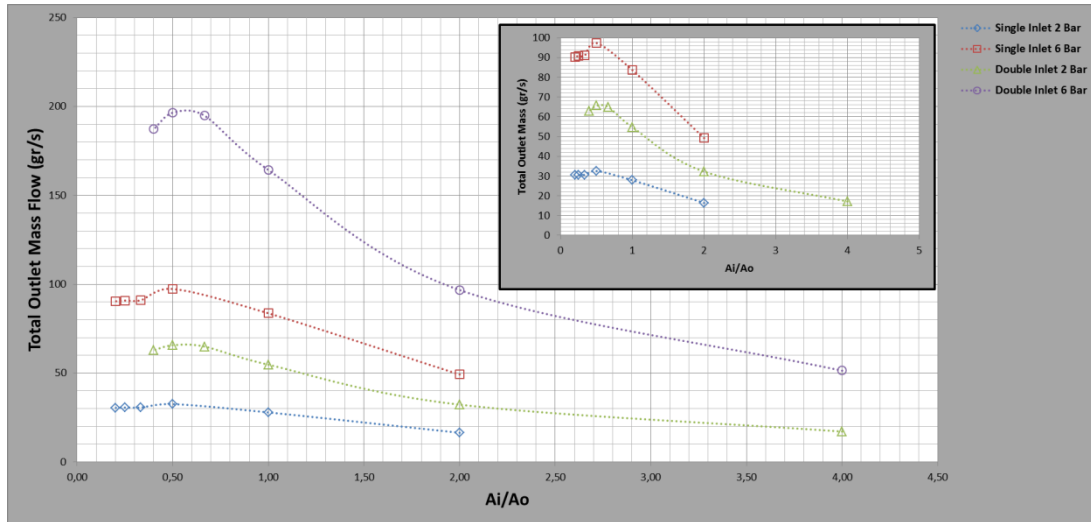


**Figure 3.11 :** Total outlet mass flow results according to inlet/outlet cross section area ratio.

As can be seen in Figure 3.12, for the maximum and minimum flow rates, the piping systems have a different pressure values. Figure 3.12 shows that the 6 bar system pressurized and double inlet cooling system. The cooling system with a maximum flow rate has 16 outlets and the  $A_i/A_o$  ratio is 0.5. The cooling system with the minimum flow rate has 2 outlets and the  $A_i/A_o$  ratio is 4. As understood from these results, due to the small number of outlets, air is compressed inside and increases the pressure. As a result of this, as shown in Figure 3.9 before, although the air flow rate from each nozzle is high with a high mass flow rate, the total flow rate is low. If the pressure is low, both the mass flow rate and the flow rate will decrease and the air density will decrease too. The optimum results were achieved when the  $A_i/A_o$  ratio was around 0.5 in the cooling systems of this study. As can be seen in the simulation results of Figure 3.12, pressure is distributed nearly homogeneously in the cooling systems. This indicates that the outlet number actually affects the pressure inside the cooling system. Because the system works with pressure in two stages. First, the pressure in the collector sends compressed air into the cooling system. Then, due to the increased pressure in the cooling system, the air starts to flow out and this creates a flow according to pressure difference between ambient and cooling channel. The air moves from the high pressure to the low pressure. The greater the pressure difference, the greater the flow rate. The cooling system must be between the collector pressure and the ambient pressure. If the system pressure is too high, the flow rate will decrease as the collector will have a low pressure difference between the cooling system and collector. Likewise, if the pressure is low, a high amount of

air will come from the collector and the flow towards the environment will be reduced. But this drop in flow will have less impact that shown in Figure 3.10 and Figure 3.11 before. Therefore, the cooling system pressure must be balanced with the correct  $A_i / A_o$  ratio.

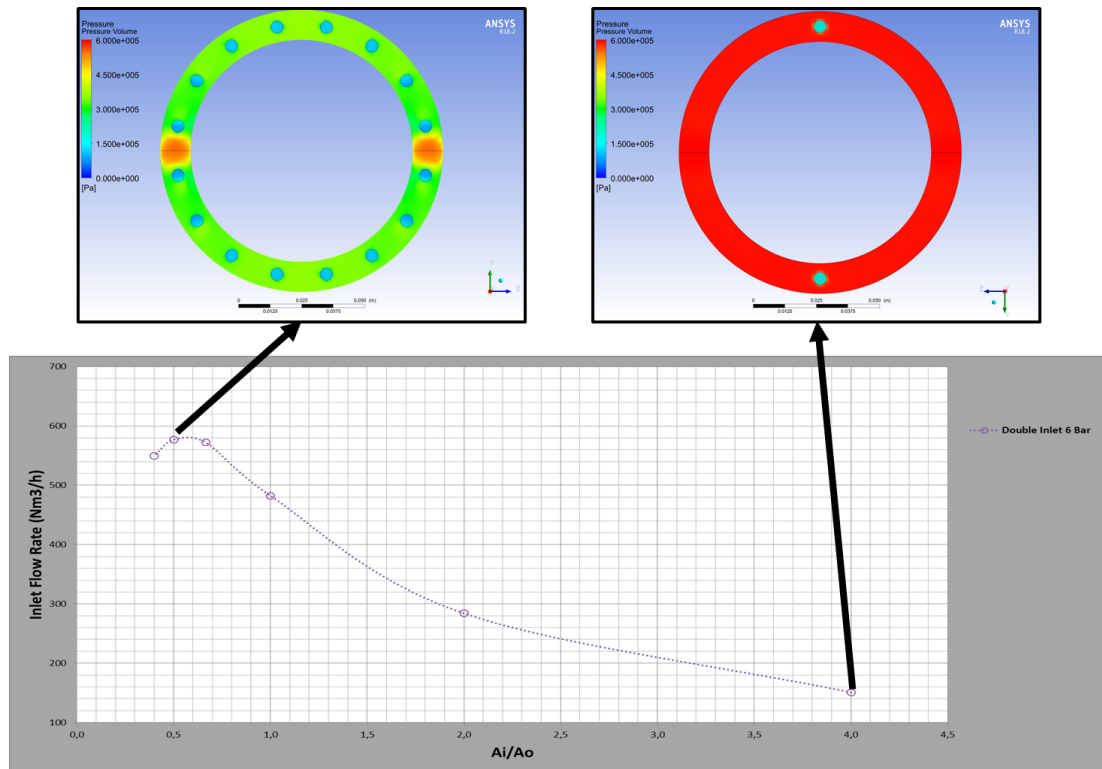


**Figure 3.12 :** Pressure distribution for double inlet 6 bar cooling system at maximum and minimum inlet flow rate.

Figure 3.13 shows the average outlet mass flow results according to inlet/outlet cross section area ratio. It shows that  $A_i/A_o$  ratio gives nearly the same results for double and single inlet results. This means that both system pressure and  $A_i/A_o$  ratio together can explain the average outlet mass flow. The results show that higher  $A_i/A_o$  ratio results in higher mass flow for each nozzle. Previously, we explained that the  $A_i/A_o$  must be around 0.5. But it is a same optimization problem for cooling systems. As mentioned before, air moves from high pressure area to low pressure area. To make cooling system pressure higher,  $A_i/A_o$  ratio should be higher. Decreasing the number of outlets increases the  $A_i/A_o$  ratio. Because it reduces the  $A_o$  denominator. That is a system as shown in Figure 3.12. As can be seen in Figure 3.13, there will be a high flow rate in each nozzle. But since the number of nozzles is low, the total flow rate will be low. Therefore, to increase the total flow rate in the cooling system, instead of reducing the number of outlets (nozzles), increasing the

number of the inlets will be more logical since using more inlets increases  $A_i$  numerator. In order to reach the maximum flow rate,  $A_i/A_o$  should be an optimization value which is found as 0.5 for this study.

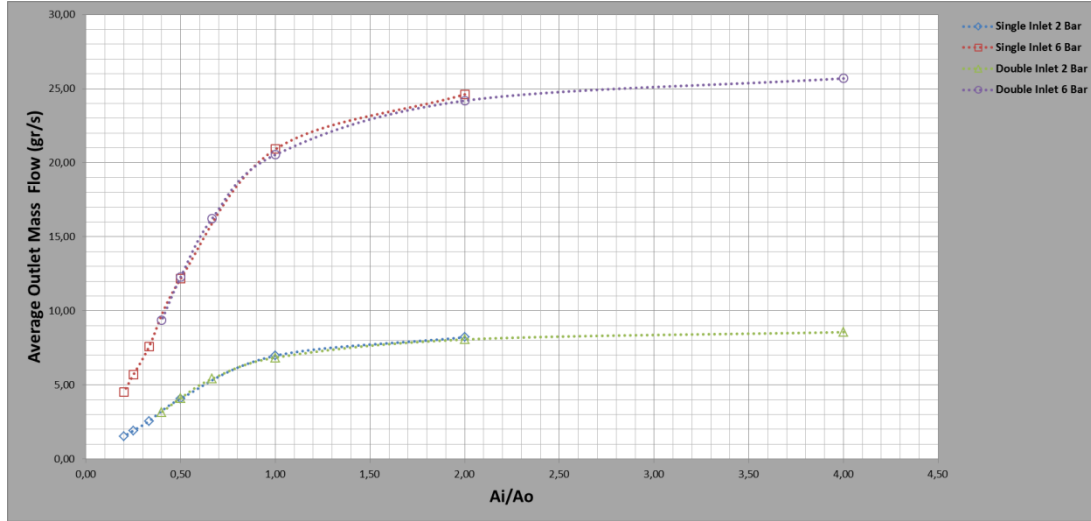


**Figure 3.13 :** Average outlet mass flow results according to inlet/outlet cross section area ratio.

However, only cooling efficiency is not enough to explain mold cooling system design parameters. Because the design of the mold cooling systems are most effective on casting quality and production cost. So the effect of the cooling system design must be defined as a casting part mechanical, material properties and additional cycle times.

### 3.2 Casting Simulation Study for the Effect of Cooling System

In recent years; there are more works on heat transfer and cooling channels. One of them is the study of Velluvakkandi et al. [40], which is about developing an effective die cooling technique for casting solidification. In order to calculate heat transfer and effect of cooling systems, dense fused silica mold and copper chill assembled each other which is shown in Figure 3.14. In that study, SDAS measurement results and distance from cooling chill were investigated as shown in Figure 3.15(a). Thermocouple results were used for heat transfer calculations, and the experiments were made for microstructural investigation as shown in Figure 3.15(b-c). According to results that shown at Figure 3.15 cooling is effective on SDAS results. Velluvakkandi is used numerical studied in the Msc. thesis. So cause similarity, for numerical experiments, Velluvakkandi's numerical studies used as a reference.

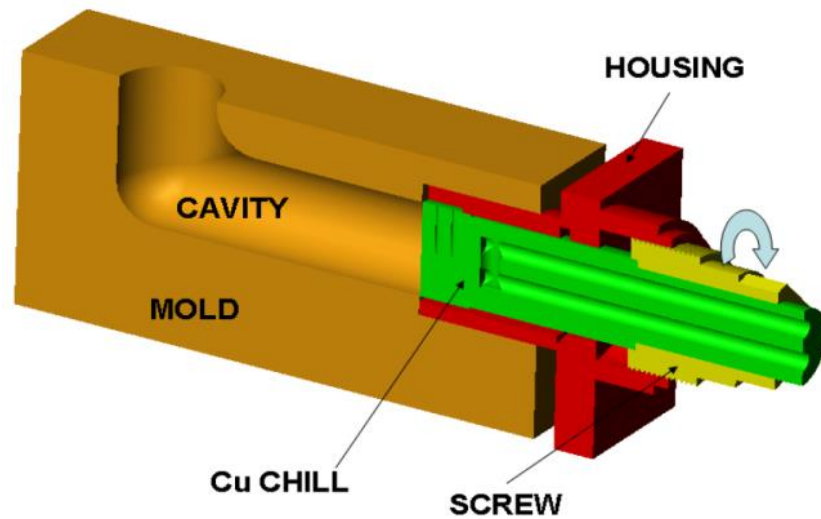


**Figure 3.14 :** Chill-housing assembly [40].

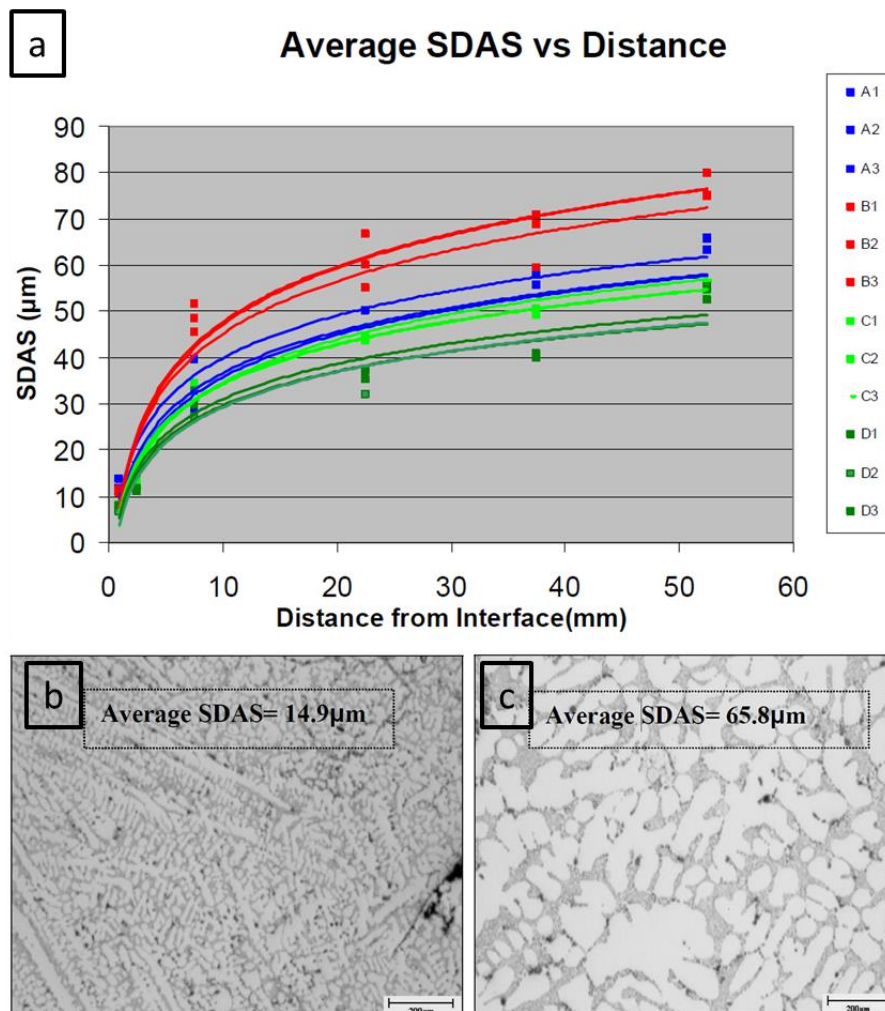


**Figure 3.15 :** a) SDAS change according to distance from cooling chill b) Micro structure from 2.5 mm distance c) Micro structure from 52.5 mm distance [40].

Experimental design is given in Table 3.2 as maximum and minimum inlet flow rates are chosen (from d1 to d8) from Figure 3.16 for each cooling system that classified according to inlet number and the system pressure. To calculate cooling effect on material and mechanical properties, MagmaSoft V5.4 software was used. In this chapter, these numerical experiments is described.

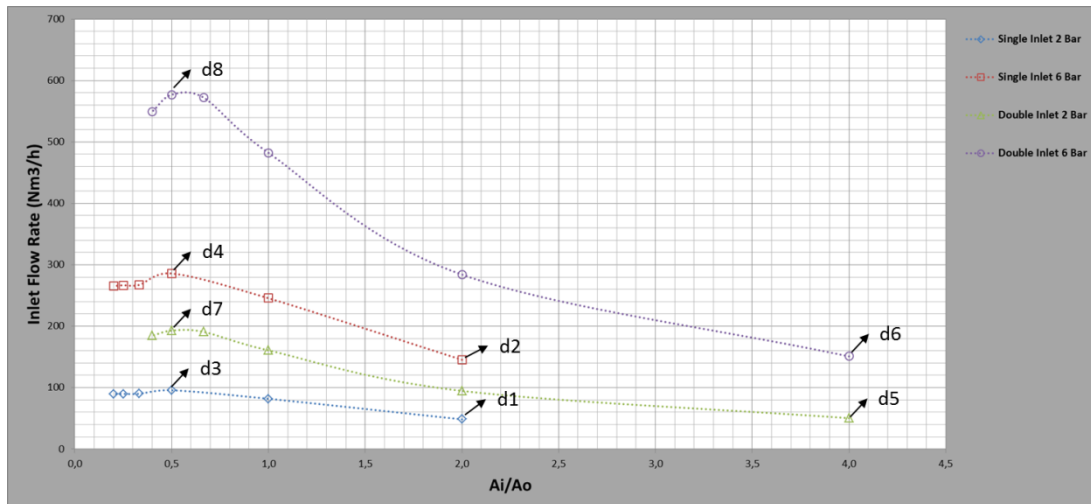


**Figure 3.16 :** Design locations for numerical experiments.

**Table 3.2 :** Design table of experimental study for cooling effect on metarial and mechanical properties.

Design	Inlet_Count	Outlet_Count	Pressure (Bar)	Ai/Ao	Inlet Flow (Nm³/h)
d1	1	2	2	2,00	48,35
d2	1	2	6	2,00	145,40
d3	1	8	2	0,50	95,65
d4	1	8	6	0,50	285,90
d5	2	2	2	4,00	50,26
d6	2	2	6	4,00	150,90
d7	2	16	2	0,50	192,80
d8	2	16	6	0,50	577,00

### 3.2.1 Setup

#### 3.2.1.1 The Geometric Setup

The geometry of the cooling channel that was used for flow rate calculations is shown in Figure 3.17. According to this geometry, the system, which was shown in Figure 3.14 before, is not suitable for this study. So, referring to Figure 3.14, the geometry shown in Figure 3.17 is defined in the MagmaSoft casting simulation software.

Ceramic mold covers the aluminium casting part. Under ceramic mold and casting part, there is a copper chill connected to cooling channels. Cooling channels defined as three different geometries because there are 2, 8 and 16 outlets for different cooling channels as shown in Table 3.2. Figure 3.18 (a-c) shows these geometries. These geometries were defined as parametric geometry for optimization setup. Here, inlet number was not considered for simulation geometry. Flow calculation can't do with Magmasoft for cooling channel as a part of simulation solver. But it can be done with Magmasoft before simulation. This calculation technic will be explain following sections. So, the inlets of the cooling were negligible for this simulation. Mesh is done with 2M elements.

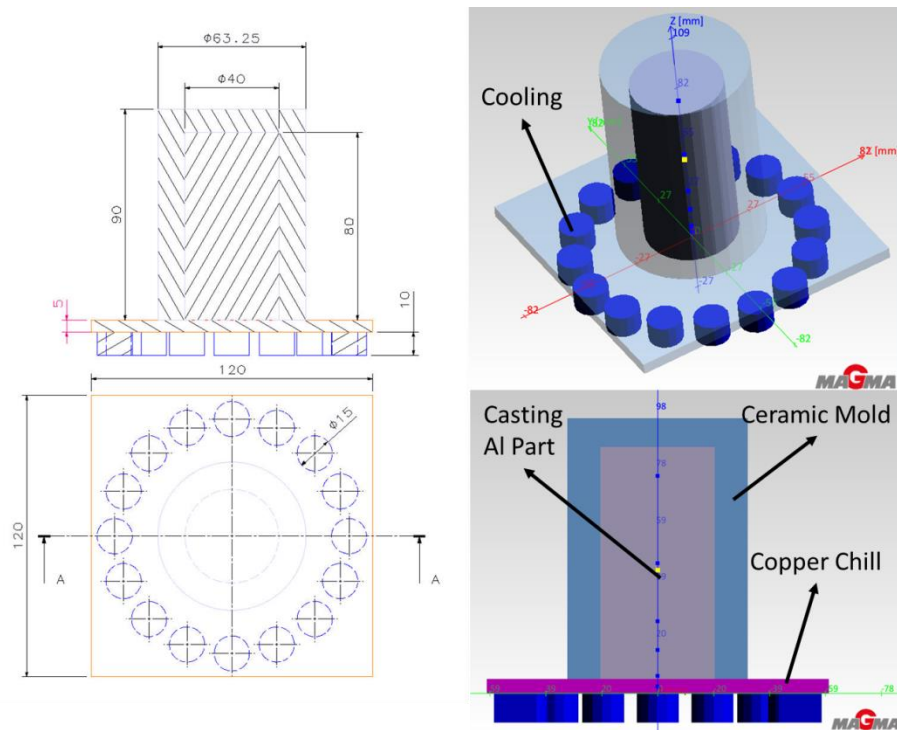


**Figure 3.17 :** Casting Simulation Geometry.

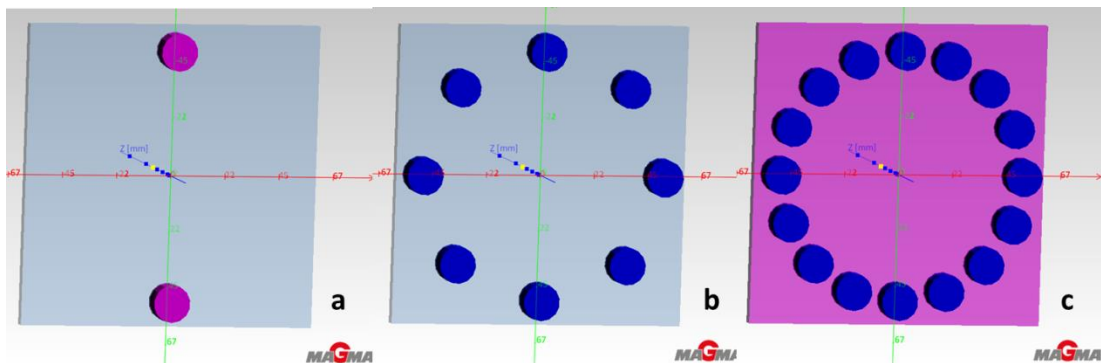


**Figure 3.18 :** Cooling channel geometries a) 2 outlet b) 8 outlet c) 16 outlet.

In order to control the temperature change, two thermocouple points were added to the geometry as shown in Figure 3.19. One of them was at the center of the chill plate, and the other was at the center of the casting part and had 4 mm distance from plate.

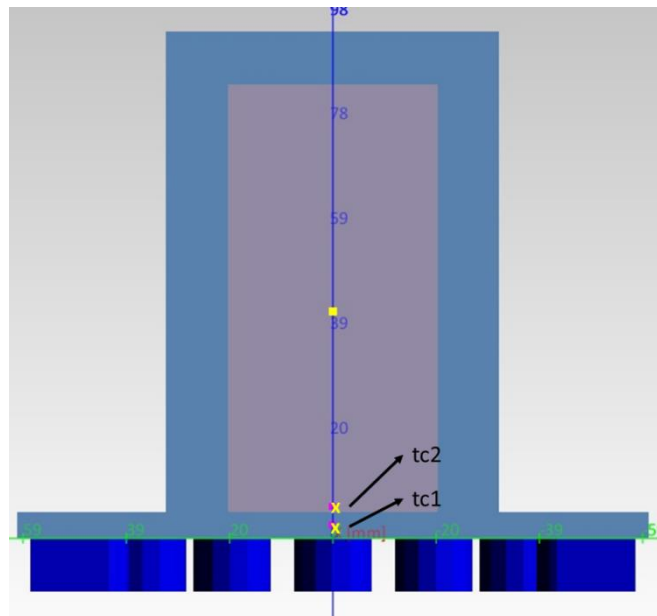


**Figure 3.19 :** Thermocouple points.

### 3.2.1.2 Definition

A definition for casting simulation has 3 steps.

- a. **Material Definition:** Material definitions are shown at table 3.3. Initial temperatures are included.

**Table 3.3 :** Material definitons.

Part	Material	Initial Temperature °C
Casting Part	AlSi7Mg	650
Mold	Insulation	450
Chill	Copper	450
Cooling	Air	20

- b. **Heat Trasfer Definitions:** There are two defitions for heat transfer. The first one is between the casting part and mold parts (mold and chill); second one is between the chill and cooling channels. Magmasoft heat transfer definition for mold parts and casting parts is shown in Figure 3.20. It is a temperature dependent heat transfer coefficient that varies between liquidus temperature (613°C) and solidus temperature (542 °C).

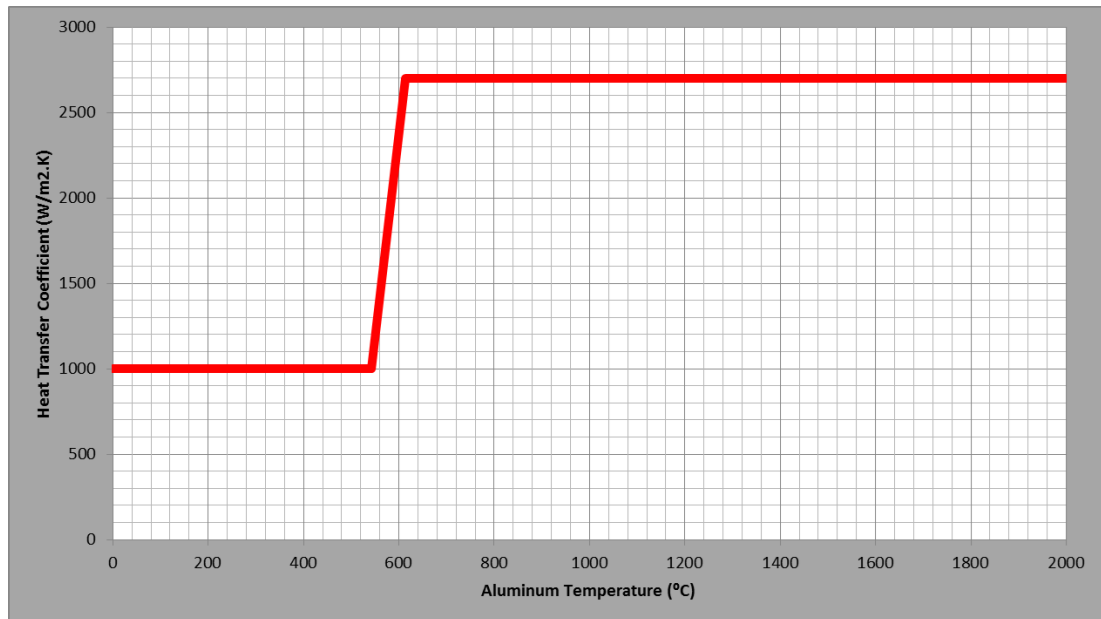


**Figure 3.20 :** Temperature depent heat transfer coefficient between mold parts and casting part.

The heat transfer coefficients of the cooling channels are defined according to Magmasoft heat transfer calculation for cooling channels. Example definition for design 1 is shown in Figure 3.21 and all heat transfer definitions for casting simulation are summarized in Table 3.4.

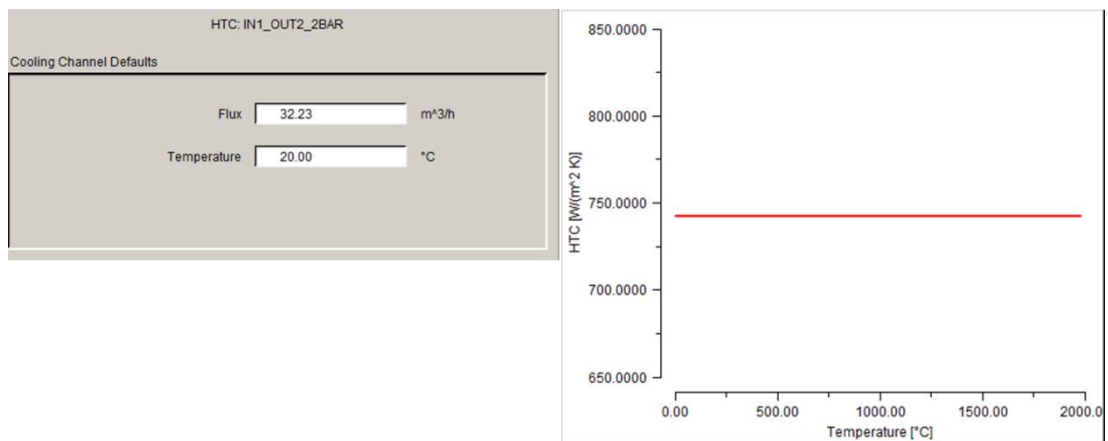


**Figure 3.21 :** Cooling channel heat transfer coefficient calculation example.

**Table 3.4 :** Heat transfer coefficients for cooling channel designs.

Design	Inlet_Count	Outlet_Count	Pressure (Bar)	Ai/Ao	Inlet Flow (Nm³/h)	Average Inlet Flow (Nm³/h)	HTC (W/m².K)
d1	1	2	2	2,00	48,35	24,18	741,95
d2	1	2	6	2,00	145,40	72,70	1764,97
d3	1	8	2	0,50	95,65	11,96	430,20
d4	1	8	6	0,50	285,90	35,74	1007,00
d5	2	2	2	4,00	50,26	25,13	764,80
d6	2	2	6	4,00	150,90	75,45	1818,01
d7	2	16	2	0,50	192,80	12,05	432,90
d8	2	16	6	0,50	577,00	36,06	1014,12

Boundary condition for environment is defined according to Magmasoft database. So definition of heat transfer completed with this definitions.

**c. Proses Definition:** Process definition is made without filling sequence. Only the solidification sequence defined.

### 3.2.1.3 Optimization

According to this definition, optimization is made on 8 designs which are shown at Figure 3.16 and table 3.2 before. The optimization is defined for;

- Maximize cooling rate
- Minimize SDAS
- Maximize mechanical properties (elongation, tensile and yield strength)
- Minimize solidification time (or cycle time)
- Minimize fraction of eutectic phase

At results section optimization results will be discussed.

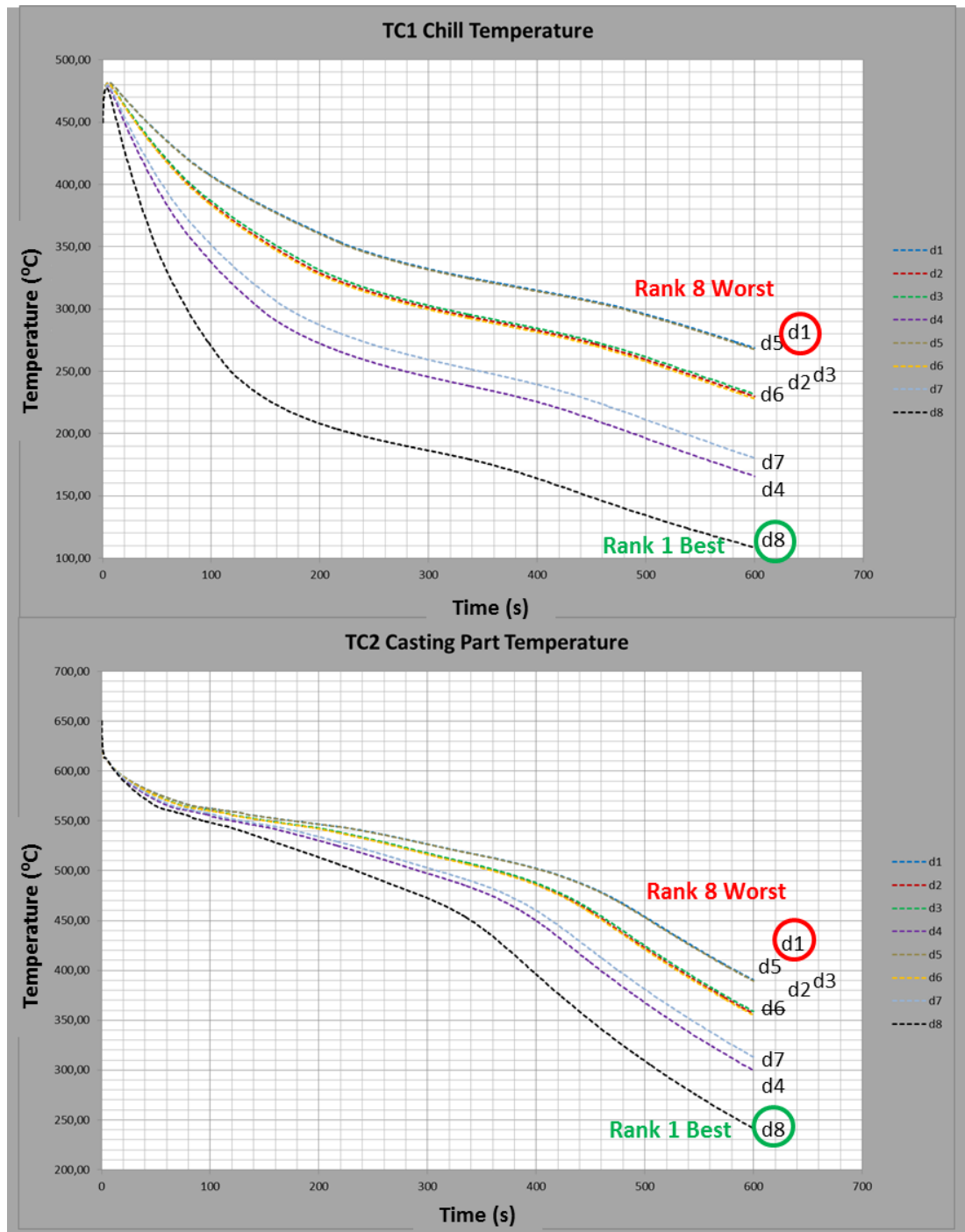
### 3.2.2 Results and discussion

Results for optimization are summarized in Table 3.5. Designs are ranked showing from the best design to the worst design according to optimization parameter that mentioned above at chapter 3.2.1.3.

**Table 3.5 :** Ranking list according to optimization results.

Rank	Design	Inlet_Count	Outlet_Count	Pressure (Bar)	Ai/Ao
1	d8	2	16	6	0,5
2	d4	1	8	6	0,5
3	d7	2	16	2	0,5
4	d6	2	2	6	4
5	d2	1	2	6	2
6	d3	1	8	2	0,5
7	d5	2	2	2	4
8	d1	1	2	2	2

Temperature results for thermocouple points (cooling curves) are shown in Figure 3.22. Thermocouple results show that from the best design to the worst design ranking is right. Lower temperature results, that mean better cooling efficiency, are at the same rankings. So thermocouple results have confirmed the results of the simulation.



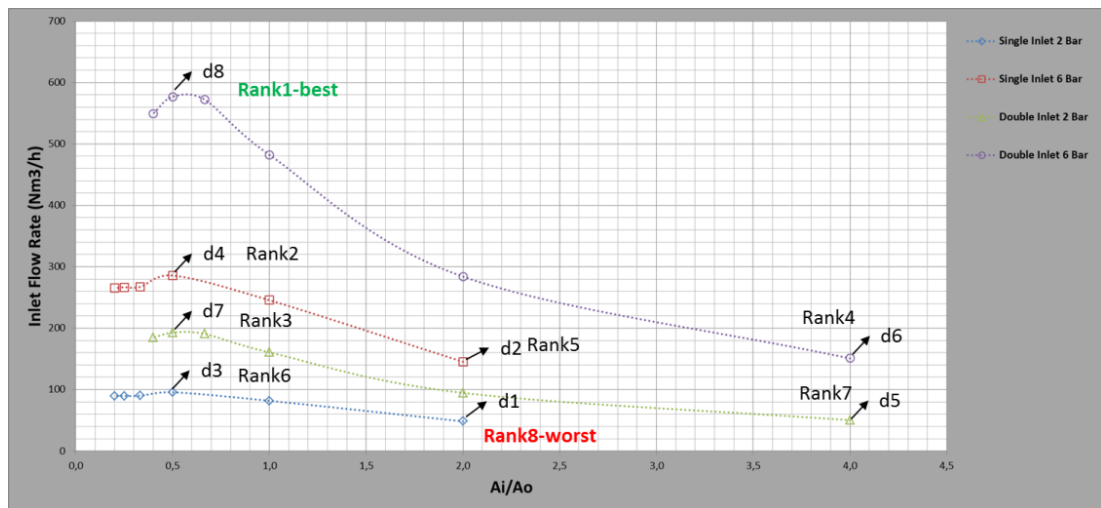
**Figure 3.22 :** Thermocouple results from magmasoft.

Figure 3.23 shows the location of the candidates at inlet flow rate vs  $A_i/A_o$  graph. Results show that inlet flow rate have a significant effect on optimization parameters. When designs are sorted from top to bottom, it is the same as optimization ranking. So, it can be said that inlet flow rate is very effective on the cooling efficiency.

Figures 3.24 and 3.25 show main effect plots vs. cooling rate and SDAS for all designs, respectively. Main Effects Plot is used when you have multiple factors. The

points in the plot are the raw data means of the response variable at the various levels of each factor, with a reference line drawn at the grand mean of the response data. So the main effects plot is used for comparing magnitudes of main effects. Here, cooling rate and SDAS are inversely proportional. It is also parallel with the literature studies [37;41]. According to the literature, the cooling rate defines the solidification behaviour during casting. And, one of the key property the solidification behaviour affects is the secondary dendrite arm spacing (SDAS) which has a direct influence on the mechanical properties of the cast part [37;41]. In the study of Q-Z. Dong et al. [41], they have studied the possibility of predicting the mechanical properties of Al alloys with the change of cooling rates by the help of the simulation software. As a result, the SDAS values found by the experimental study and simulations are quite similar with small differences, and therefore change in mechanical properties such as tensile strength, elongation and hardness values are again only 0.01-4.98%. In the study of Shabani and Mozeheri [37], the secondary dendrite arm spacing (SDAS) is tried to be expressed as a function of solidification time. According to the obtained SDAS-cooling rate and cooling rate-mechanical property graphs, SDAS decreases and mechanical properties enhances with increasing cooling rate (R). As a result, the predictions of mechanical properties shows acceptable agreement with the experimental results obtained using thermocouples.

For our study, main effects on cooling rate and SDAS couldn't be found from Figure 3.24 and 3.25. But inlet and outlet numbers have positive effect on cooling rate. But somehow, inlet and outlet area ratio ( $A_i/A_o$ ) has negative effect on cooling rate. Pressure and inlet flow have positive effect on cooling rate. Same variables affect SDAS results are the opposite. As can be seen from the figure, the flow rate affects mostly the cooling rate and SDAS. According to main effect plots, we must use more outlets and inlets with 0.5  $A_i/A_o$  ratio at higher pressure level to have higher cooling rate.



**Figure 3.23 :** Optimization design ranks on flow rate vs Ai/Ao.

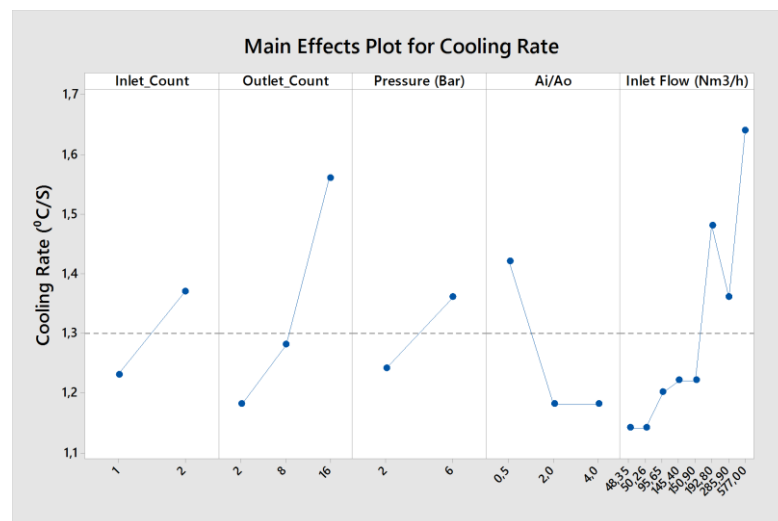


**Figure 3.24 :** Main effect plot for cooling rate.

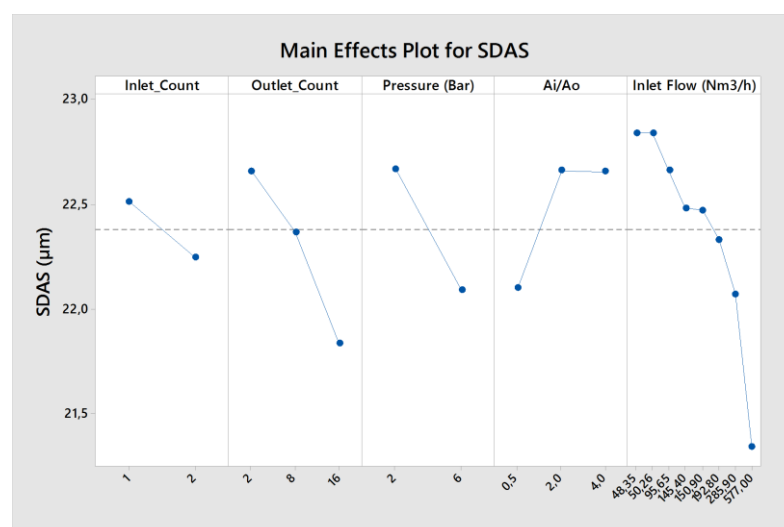


**Figure 3.25 :** Main effect plot for SDAS.

Figure 3.26 shows cooling rate results obtained by MagmaSoft. At the same scale, design 8 is very high cooling rate according to others. Design 4 and design 7 mean higher cooling rate too. But other designs are have nearly same cooling rate. However, the cooling rate decreases as it moves away from the cooling zone. Therefore, this work only applies to areas close to the cooling zone.

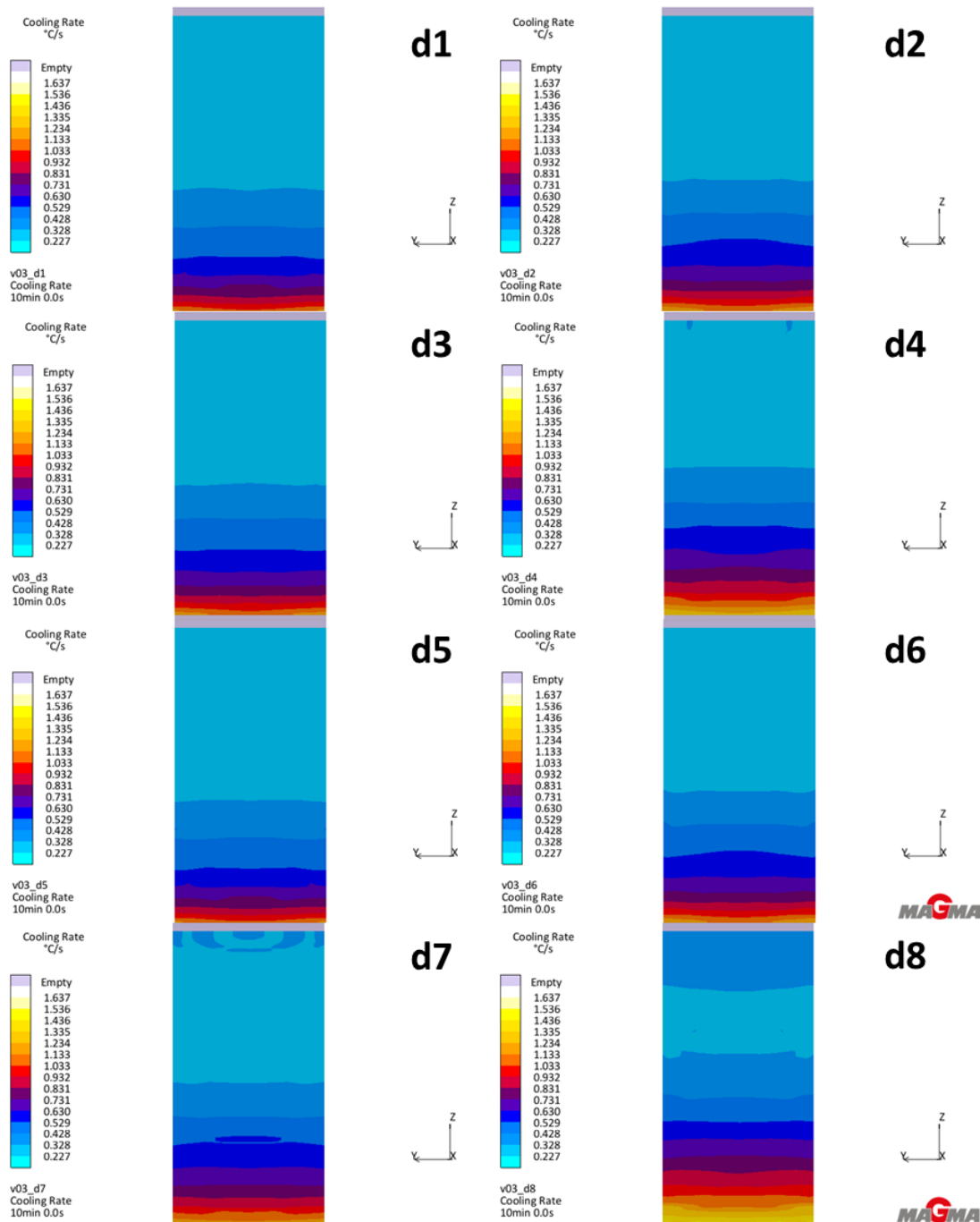


**Figure 3.26 :** Cooling rate results obtained by simulation software.

Figure 3.27 shows the relationships between cooling rate and SDAS. According to literature research, at higher cooling rate which means more effective cooling, makes

microstructure finer. According to Figure 3.27; at higher cooling rate we can have finer SDAS microstructure. The results are consistent with the literature review. So effective cooling makes better SDAS length at higher cooling rates.

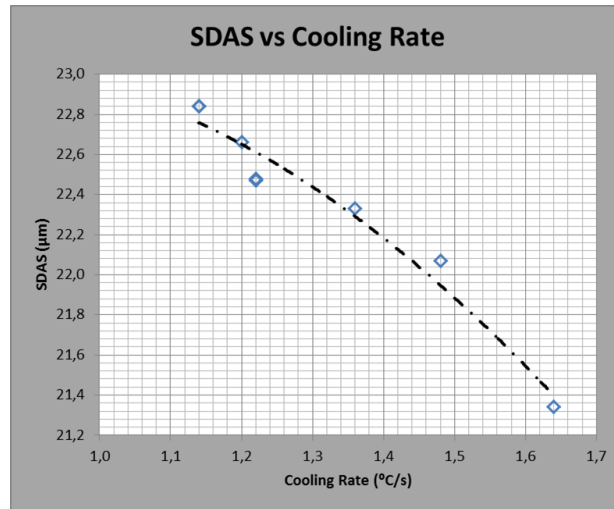


**Figure 3.27 :** Cooling rate vs SDAS.

As mentioned at chapter 1.2.4 finer microstructure has an effect on mechanical properties. The relationship between SDAS and mechanical properties is shown at Figure 3.28. According to L.Y. Zhanga study [38] which is shown in Figure 1.31 the relationship between mechanical properties and SDAS is linear and inversely proportional like as Figure 3.28.

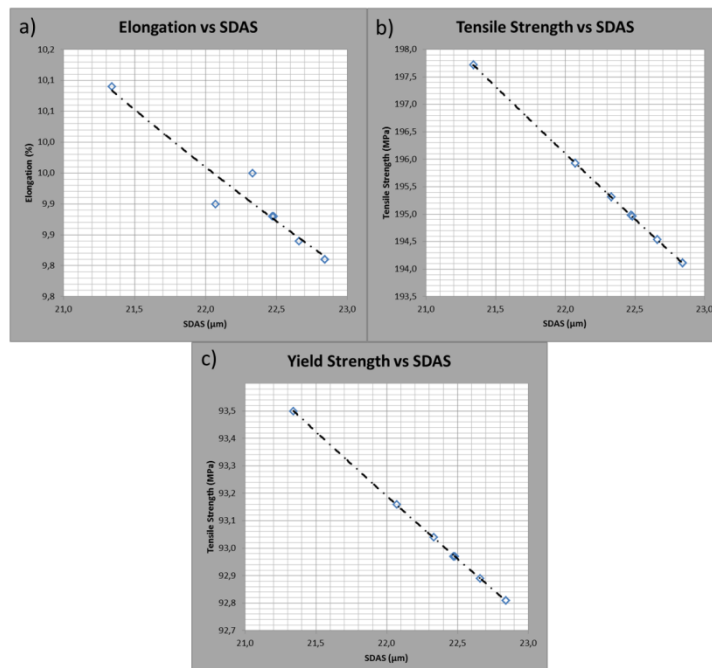


**Figure 3.28 :** a) Elongation vs SDAS b) tensile strength vs SDAS c) yield strength vs SDAS.

Cooling rate is effective on solidification time. As shown at Figure 3.29(a), higher cooling rate reduces solidification time. Short solidification time means shorter cycle time for production and more efficient production. In addition, the shorter solidification time lets more homogenous phase distribution. So the fraction of the eutectic phase will be lower shown as Figure 3.29(b).

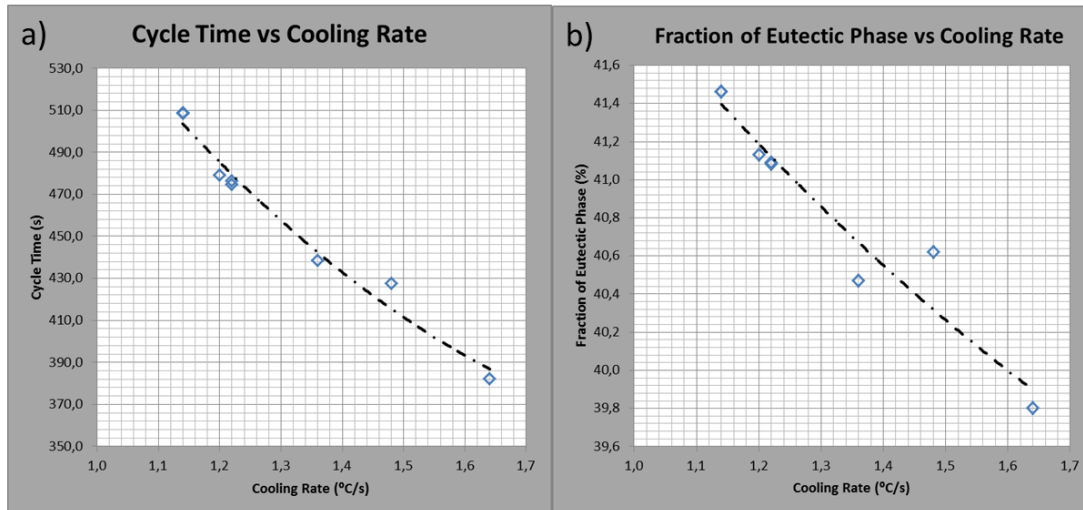


**Figure 3.29 :** a) Cycle time vs cooling rate b) fraction of eutectic phase.

According to this results cooling rate effective on SDAS and microstructure. Thus, cooling rate is effective on mechanical properties. At higher cooling rates, mechanical properties will be higher shown as Figure 3.30(a-c).

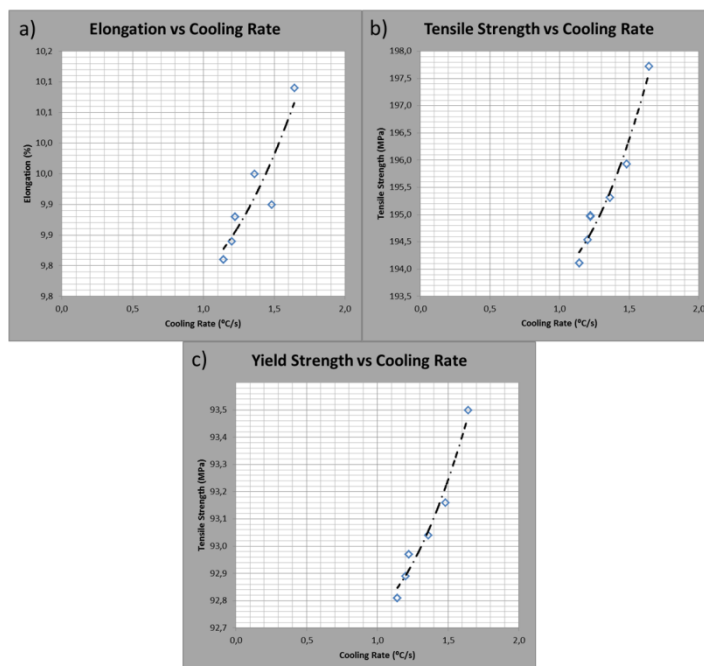


**Figure 3.30 :** a) Elongation vs cooling rate b) tensile strength vs cooling rate c) yield strength vs cooling rate.

This study shows that cooling rate is very important for microstructure and mechanical properties. However, the effect of the cooling system on microstructure and mechanical properties has not been mentioned yet. To define relationship between inlet flow rate and cooling rate Figure 3.31 is added. According to results, inlet flow rate is affecting the cooling rate and thus the mechanical properties and microstructure. Also clearly seen; as the flow rate increases, cooling rate gradually increases.

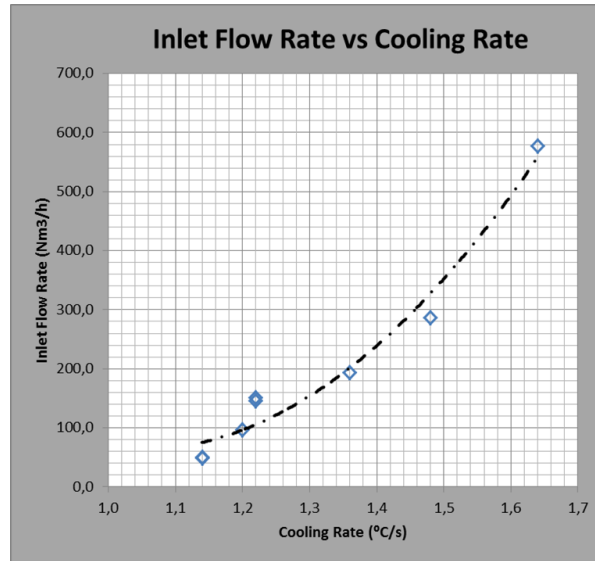


**Figure 3.31 :** Flow rate vs cooling rate.

Inlet flow rate can be defined as volumetric air consumption for cooling channels. Effective cooling channel must use less air at maximum cooling rate. At section 3.2.1, the efficiency of the cooling channel is defined with inlet flow rate. Results indicate that maximizing inlet flow rate best way to make efficient cooling system. Maximizing inlet flow rate increases the amount of air used in unit time. However, shortens the cycle time. There are recommendations on this topic in the conclusion section.

#### 4. CONCLUSION

As a result, the following conclusions can be drawn:

1. System pressure is very important for cooling efficiency. According to system pressure values between 2 bars and 6 bars, higher flow rates were obtained at 6 bar system pressure. So for this study 6 bar system pressure is the optimum pressure for cooling efficiency.
2. Considering the results, only increasing the number of outlets does not mean that a more efficient cooling system will be obtained. Also the number of inlets must be taken into consideration.
3. Increasing the number of the outlets provides a flow rate up to a certain point. However, there is a decrease in flow rate after reaching this peak point. This peak point must be determined to optimize the cooling performance.
4. While the number of outlets may increase with the increase in the total flow rate, the amount of mass flow from each outlet decreases. Considering this situation, optimization between the total inlet flow rate and the average outlet mass flow is required. In this study, proportional relation between inlet cross-sectional area and outlet section ratio is used. This parameter is named  $A_i/A_o$ .
5. In this study, the optimum  $A_i/A_o$  ratio is 0.5 for the examined cooling system when the maximum total inlet flow rate according to the  $A_i/A_o$  ratio is examined. This ratio must be examined for different cooling systems.
6. In this study, investigations showed that the  $A_i/A_o$  ratio affected the internal pressure of the cooling system. If the numbers of inlets and outlets are adjusted according to  $A_i/A_o$  ratio, system internal pressure will be at optimum value for cooling efficiency.
7. In this study, the effect of  $A_i/A_o$  ratio on average outlet mass flow was investigated. When the results were examined, it was seen that the numbers of inlets or outlets had no stable effect alone, but the  $A_i/A_o$  ratio was effective with pressure. Therefore, it is seen that when the cooling design is made, the number

of inlet should be adjusted by using the optimum  $A_i/A_o$  ratio according to the number of outlets needed.

8. In this study, the effect of flow rate on cooling rate was found to be very high. Therefore, the maximum possible flow rate is important in terms of cooling efficiency.
9. In this study, it was observed that the high cooling rate formed a finer microstructure. As a result, the cast quality and mechanic properties have increased. Ensuring optimum cooling efficiency is also important in terms of product quality.
10. Finally, the cycle time decreases at high cooling rates. As a consequence, it will be ensured in financial gains that increase production performance.



## REFERENCES

- [1] Fridlyander, I. N., Sister, V. G., Grushko, O. E., Berstenev, V. V., Sheveleva, L. M., & Ivanova, L. A. (2002). Aluminum Alloys: Promising Materials In The Automotive Industry. *Metal Science and Heat Treatment*, 44(9/10), 365–370. <https://doi.org/10.1023/a:1021901715578>
- [2] Lesuer, D. R., & Kipouros, G. J. (1995). Lightweight Materials For Transportation Applications. *The Journal of The Minerals (JOM)*, 47(7), 17. <https://doi.org/10.1007/bf03221222>
- [3] Kaufman, J. G., & Rooy, E. L. (2004). *Aluminum alloy castings properties: Properties, processes and applications (1st ed.)*. Materials Park, OH: ASM International.
- [4] Cerit, M. (2010). Numerical Simulation Of Dynamic Side Impact Test For An Aluminium Alloy Wheel. *Scientific Research and Essays*, Vol. 5(18), 2694–2701.
- [5] Campbell, J. (2011). *Complete casting handbook: Metal casting processes, techniques and design*. Oxford: Butterworth-Heinemann
- [6] KULEŞOĞLU, A. (2017). *Nano-Reinforced Aluminum Matrix Composites İzmir Katip Çelebi University, 2017* (Unpublished master's thesis).
- [7] Zhang, B., Maijer, D., & Cockcroft, S. (2007). Development Of A 3-D Thermal Model Of The Low-Pressure Die-Cast (LPDC) Process Of A356 Aluminum Alloy Wheels. *Materials Science and Engineering: A*, 464(1-2), 295–305. <https://doi.org/10.1016/j.msea.2007.02.018>
- [8] Lee, R. J. (2006). *Effect of cooling circuit duration on formation of solidification shrinkage in A356 casting automotive wheels: A thesis submitted to Auckland University of Technology in partial fulfilment of the requirements for the degree of Master of Engineering (ME), 2006* (Unpublished master's thesis).
- [9] Duan, J., Reilly, C., Maijer, D. M., Cockcroft, S. L., & Phillion, A. B. (2015). Application of Numerical Optimization to Aluminum Alloy Wheel Casting. IOP Conference Series: *Materials Science and Engineering*, 84, 012036. <https://doi.org/10.1088/1757-899x/84/1/012036>
- [10] Reilly, C., Duan, J., Yao, L., Maijer, D. M., & Cockcroft, S. L. (2013). Process Modeling Of Low-Pressure Die Casting Of Aluminum Alloy Automotive Wheels. *The Journal of The Minerals (JOM)*, 65(9), 1111–1121. <https://doi.org/10.1007/s11837-013-0677-1>
- [11] Maijer, D., Owen, W., & Vetter, R. (2009). An Investigation Of Predictive Control For Aluminum Wheel Casting Via A Virtual Process Model. *Journal of Materials Processing Technology*, 209(4), 1965–1979. <https://doi.org/10.1016/j.jmatprotec.2008.04.057>
- [12] Boschetto, A., Costanza, G., Quadrini, F., & Tata, M. (2007). Cooling Rate Inference In Aluminum Alloy Squeeze Casting. *Materials Letters*, 61(14-15), 2969–2972. <https://doi.org/10.1016/j.matlet.2006.10.048>
- [13] Zhang, L., Jiang, Y., Ma, Z., Shan, S., Jia, Y., Fan, C., & Wang, W. (2008). Effect Of Cooling Rate On Solidified Microstructure And Mechanical

- Properties Of Aluminium-A356 Alloy. *Journal of Materials Processing Technology*, 207(1-3), 107–111. <https://doi.org/10.1016/j.jmatprotec.2007.12.059>
- [14] Lee, R. J. (2006). *Effect of cooling circuit duration on formation of solidification shrinkage in A356 casting automotive wheels: A thesis submitted to Auckland University of Technology in partial fulfilment of the requirements for the degree of Master of Engineering (ME)*, 2006 (Unpublished master's thesis).
- [15] Kawahara, H. (2011). *Developments in Heat Transfer*. London, UNITED KINGDOM: InTech.
- [16] *Compressed air manual (8th ed.)*. (2015). Wilrijk: Atlas Copco Airpower NV.
- [17] Yunus A. Cengel, D., & Cimbala, J. M. (2013). *Fluid Mechanics Fundamentals and Applications*. New York, United State of America: McGraw-Hill Education.
- [18] Gao, X., & Li, R. (2019). Spray Impingement Cooling: The State of the Art. *Advanced Cooling Technologies and Applications*, . <https://doi.org/10.5772/intechopen.80256>
- [19] Marzec, K., & Kucaba-Pietal, A. (2014). Heat Transfer Characteristic Of An Impingement Cooling System With Different Nozzle Geometry. *Journal of Physics: Conference Series*, 530, 012038. <https://doi.org/10.1088/1742-6596/530/1/012038>
- [20] Incropera, F. P. (2007). *Fundamentals Of Heat And Mass Transfer*. New Jersey, United States of America: John Wiley.
- [21] Hosain, M. L., Bel Fdhila, R., & Daneryd, A. (2016). Heat Transfer By Liquid Jets Impinging On A Hot Flat Surface. *Applied Energy*, 164, 934–943. <https://doi.org/10.1016/j.apenergy.2015.08.038>
- [22] Lam, P. A. K., & Prakash, K. A. (2017). A Numerical Investigation And Design Optimization Of Impingement Cooling System With An Array Of Air Jets. *International Journal of Heat and Mass Transfer*, 108, 880–900. <https://doi.org/10.1016/j.ijheatmasstransfer.2016.12.017>
- [23] Oosthuizen, P. H., & Carscallen, W. E. (2013). *Introduction to Compressible Fluid Flow*. Florida, United States of America: CRC Press.
- [24] Greitzer, E. M., Tan, C. S., & Graf, M. B. (2004). *Internal Flow: Concepts and Applications*. Cambridge, United Kingdom: Cambridge University Press.
- [25] Mazzelli, F., Little, A. B., Garimella, S., & Bartosiewicz, Y. (2015). Computational And Experimental Analysis Of Supersonic Air Ejector: Turbulence Modeling And Assessment Of 3D Effects. *International Journal of Heat and Fluid Flow*, 56, 305–316. <https://doi.org/10.1016/j.ijheatfluidflow.2015.08.003>
- [26] Hemidi, A., Henry, F., Leclaire, S., Seynhaeve, J., & Bartosiewicz, Y. (2009). CFD Analysis Of A Supersonic Air Ejector. Part I: Experimental Validation Of Single-Phase And Two-Phase Operation. *Applied Thermal Engineering*, 29(8-9), 1523–1531. <https://doi.org/10.1016/j.applthermaleng.2008.07.003>
- [27] Besagni, G., & Inzoli, F. (2017). Computational Fluid-Dynamics Modeling Of Supersonic Ejectors: Screening Of Turbulence Modeling Approaches. *Applied Thermal Engineering*, 117, 122–144. <https://doi.org/10.1016/j.applthermaleng.2017.02.011>
- [28] Croquer, S., Poncet, S., & Aidoun, Z. (2016). Turbulence Modeling Of A Single-Phase Rnu134a Supersonic Ejector. Part 1: Numerical Benchmark.

- [29] U.S. House. (2011). *CFD Analysis of Multi-jet Air Impingement on Flat Plate* (pp. 2431-2435) (N. K. Chougule, G. V. Parishwad, P. R. Gore, S. Pagnis, & S. N. Sapali, Authors) [H.R. Doc. from Proceedings of the World Congress on Engineering 2011 Cong.]. London: Newswood Limited.
- [30] Caggese, O., Gnaegi, G., Hannema, G., Terzis, A., & Ott, P. (2013). Experimental And Numerical Investigation Of A Fully Confined Impingement Round Jet. *International Journal of Heat and Mass Transfer*, 65, 873–882. <https://doi.org/10.1016/j.ijheatmasstransfer.2013.06.043>
- [31] Fechter, S., Terzis, A., Ott, P., Weigand, B., Von Wolfersdorf, J., & Cochet, M. (2013). Experimental And Numerical Investigation Of Narrow Impingement Cooling Channels. *International Journal of Heat and Mass Transfer*, 67, 1208–1219. <https://doi.org/10.1016/j.ijheatmasstransfer.2013.09.003>
- [32] Penumadu, P. S., & Rao, A. G. (2017). Numerical Investigations Of Heat Transfer And Pressure Drop Characteristics In Multiple Jet Impingement System. *Applied Thermal Engineering*, 110, 1511–1524. <https://doi.org/10.1016/j.applthermaleng.2016.09.057>
- [33] Liu, Z., & Feng, Z. (2011). Numerical Simulation On The Effect Of Jet Nozzle Position On Impingement Cooling Of Gas Turbine Blade Leading Edge. *International Journal of Heat and Mass Transfer*, 54(23-24), 4949–4959. <https://doi.org/10.1016/j.ijheatmasstransfer.2011.07.008>
- [34] Afroz, F., & Sharif, M. (2013). Numerical Study Of Heat Transfer From An Isothermally Heated Flat Surface Due To Turbulent Twin Oblique Confined Slot-Jet Impingement. *International Journal of Thermal Sciences*, 74, 1–13. <https://doi.org/10.1016/j.ijthermalsci.2013.07.004>
- [35] Yu, P., Zhu, K., Shi, Q., Yuan, N., & Ding, J. (2017). Transient Heat Transfer Characteristics Of Small Jet Impingement On High-Temperature Flat Plate. *International Journal of Heat and Mass Transfer*, 114, 981–991. <https://doi.org/10.1016/j.ijheatmasstransfer.2017.06.112>
- [36] Moukalled, F., Mangani, L., & Darwish, M. (2015). *The Finite Volume Method in Computational Fluid Dynamics: An Advanced Introduction with OpenFOAM® and Matlab*. New York, United State of America: Springer International Publishing.
- [37] Shabani, M., & Mazahery, A. (2011). Prediction of Mechanical Properties of Cast A356 Alloy as a Function of Microstructure and Cooling Rate. *Archives of Metallurgy and Materials*, 56(3). <https://doi.org/10.2478/v10172-011-0073-1>
- [38] Zhang, L., Jiang, Y., Ma, Z., Shan, S., Jia, Y., Fan, C., & Wang, W. (2008). Effect of cooling rate on solidified microstructure and mechanical properties of aluminium-A356 alloy. *Journal of Materials Processing Technology*, 207(1-3), 107-111. <https://doi.org/10.1016/j.jmatprotec.2007.12.059>
- [39] Chen, R., Shi, Y., Xu, Q., & Liu, B. (2014). Effect of cooling rate on solidification parameters and microstructure of Al-7Si-0.3Mg-0.15Fe alloy. *Transactions of Nonferrous Metals Society of China*, 24(6), 1645-1652. [https://doi.org/10.1016/S1003-6326\(14\)63236-2](https://doi.org/10.1016/S1003-6326(14)63236-2)
- [40] Velluvakkandi, N. (2009). *Developing an effective die cooling technique for casting solidification: A thesis submitted in fulfilment of the degree of Master*

*of Engineering, School of Engineering, Auckland University of Technology, July 2009 (Unpublished master's thesis).*

- [41] Dong, Q., Choi, Y., Hong, J., & Hwang, H. (2012). Prediction of mechanical properties of Al alloys with change of cooling rate. *Overseas Foundry*, 9, 381-386.

## CURRICULUM VITAE

**Hakan YAVUZ**

### Educational Background

Degree	Department	University	Year
Postgraduate	Faculty of Economics and Administrative Sciences	Ege University	2007-2009
Undergraduate	Metallurgical and Materials Engineering	Dokuz Eylül University	2001-2006

### Work Experience

Company	Position	Year
CMS Jant & Makine A.Ş.	Mold and Process Design Specialist, R&D	2015-....
CMS Jant A.Ş.	Foundry Chief Engineer	2014-2015
Lodos Teknik A.Ş.	Aluminum Recycling and Refractory Chief Engineer	2012-2014
Lodos Teknik A.Ş.	Aluminum Recycling Plant Engineer	2011-2012
Lodos Teknik A.Ş.	Casting Simulation Engineer	2010-2011
Winsa A.Ş.	Sales Support	2008
Dirinler Döküm A.Ş.	Shift Engineer	2007

### **List of Publications;**

1. Aybarç, U., Yavuz, H., Dispınar, D., & Seydibeyoglu, M. O. (2018). The Use of Stirring Methods for the Production of SiC-Reinforced Aluminum Matrix Composite and Validation via Simulation Studies. *International Journal of Metalcasting*, 13(1), 190-200. doi:10.1007/s40962-018-0250-3

### **Conference Papers;**

1. U. Aybarç, H. Yavuz, “Alüminyum Metal Matris Kompozit Üretiminde Farklı Karıştırma Yöntemlerinin Etkisinin İncelenmesi ve Simülasyon Çalışmaları ile Karşılaştırılması”, Tüdoksad - 10. Uluslararası Döküm Kongresi, 2018
2. Y. Ercan, A. Kara, H. Yavuz, E. Çubuklusu, “Yönlü Katılaşmanın Alüminyum Alaşımlı Jantların Sertliği Üzerindeki Etkisinin Araştırılması”, 8<sup>th</sup> Aluminum Symposium, 2017
3. U. Aybarç, H. Yavuz, “Affects of Die Coating and Coating Thickness on Solidification, Material Properties and Microstructure of A356 Aluminum Alloy”, 1. Uluslararası Üniversite-Sanayi İşbirliği, Ar-Ge ve İnovasyon Kongresi, 2017
4. U. Aybarç, H. Yavuz, “Affects of Die Coating and Coating Thickness on Solidification, Material Properties and Microstructure of A356 Aluminum Alloy Effect of Mold and Casting Temperature on the Distribution of Reinforcement Material in Composite Material Production”, 1. Uluslararası Üniversite-Sanayi İşbirliği, Ar-Ge ve İnovasyon Kongresi, 2017
5. H. Yavuz, A. Kara, E. Çubuklusu, B. Çe, U. Aybarç “The Effect of Filter Type on Filling During Low Pressure Die Casting: a Numerical Study”, IMSP, 2016
6. E. Akıncı, H. Yavuz, E. Bozkurt “Alçak Basınç Döküm Teknolojisinde Kullanılan Kalıp Malzemelerinin Karşılaştırılması”, IMSP, 2016
7. H. Yavuz, E. Çubuklusu, U. Aybarç “Jant Üretiminde Kullanılan Metal Filtrelerden Düşük Fe İçerikli Alüminyum Geri Kazanımı”, 1. Uluslararası Mühendislik Mimarlık ve Tasarım Sempozyumu, 2015